UNIVERSITY OF CALIFORNIA, SAN DIEGO

Design, Development, and Use of Genetically-Encoded Fluorescent Reporters of Neural Activity

A dissertation submitted in partial satisfaction of the Requirements for the degree

Doctor of Philosophy

in

Neurosciences

by

Samuel Andrew Hires

Committee in charge:

Professor Roger Y. Tsien, Chair
Professor Jeffry Isaacson
Professor Massimo Scanziani
Professor Charles Stevens
Professor Charles Zuker

2007

The Dissertation of Samuel Andrew Hires is approved, and it is acceptable in quality and form for publication on microfilm:

Chair

University of California, San Diego

2007

Epigraph

Man is a tool-using Animal… without tools he is nothing, with tools he is all.

Thomas Carlyle

Table of Contents

List of Figures and Table

Acknowledgements

This thesis exists only through the combined efforts of a great number of people that have made a significant impact on my life and my career. I would like to acknowledge and thank them all, but this space is too limited. Foremost, I would like my parents, Sam and Sue, who have always provided strong and steadfast support openly and behind the scenes. Also, my siblings, Renee and Bryan, who are passengers beside me on the boat of life.

Certain teachers kept my passion lit during the long years of schooling. John Benson humbled my intuition with his mind-twister of "what is i^i?" Guosong Liu showed me the passion of following a scientific hypothesis. Mriganka Sur absorbed my scattered ideas and showed me how to apply them towards experimental systems.

All members of the Tsien Lab family have provided generous help when it was needed. In particular, Rob Campbell taught me molecular biology, Greg Nelson and Michael Lin participated in many useful discussions, Alice Ting provided life and career insight, Steven Adams kept me laughing, and Paul Steinbach kept me company.

I have a tremendous appreciation for the tireless work of my long-time collaborator Yongling Zhu. Also, many thanks go to Massimo Scanziani for helping me empathize with a brain slice, Chuck Stevens for entertaining my speculations, Charles Zuker for showing me what to do with data that lacks controls and Jeff Isaacson for consistently guiding me in a positive direction. Finally, I thank Roger Tsien for assembling an incredible group of performers, conducting with a soft hand, letting me play at my own pace, and sparking innumerable moments of inspiration.

Chapter One, in part, has been submitted for publication of the material as it may appear in Proceedings of the National Academy of Sciences, 2008, Hires S. Andrew; Zhu, Yongling; Tsien, Roger Y. The dissertation author was the primary author on this work.

Vita

Education

Ph. D. in Neurosciences (2001-2007)
University of California – San Diego, La Jolla, CA

B.S. in Brain & Cognitive Science (1997-2001)
Massachusetts Institute of Technology, Cambridge, MA
Minor: Biology

Research Experience

Doctoral Research - UC San Diego, La Jolla, CA (Sept 2001-Nov 2007)
Designed, created, and optimized the first genetically-encoded optical indicators of glutamate. Expressed these in cultured neurons to make the first direct optical measurements of neurotransmitter release and reuptake from electrical stimulation. Applied this with synaptophysin-2-phluorin to quantitatively measure and computationally model glutamate release, spillover and uptake in neuronal cultures with millisecond resolution.
PI: Prof. Roger Tsien (858)534-4891

Visiting Scientist - RIKEN BSI, Tokyo, Japan (July-Aug 2002)
Generated novel fluorescent proteins by screening of multi-site mutants of GFP.
PI: Dr. Atsushi Miyawaki

Doctoral Research Rotation - UC San Diego (April 2002-July 2002)
Generated chimeric mouse taste receptors via PCR-based DNA shuffling.
PI: Prof. Charles Zuker

Doctoral Research Rotation - UC San Diego (Jan 2002-April 2002)
Performed simultaneous cAMP imaging with whole-cell patch clamp recording of ganglion cells of developing rat retina using FlCRhR dyes.
PI: Prof. Marla Feller

Undergraduate Research PCLM, MIT (Feb 2000-Aug 2001)
Examined the role of metabotropic glutamate receptors in synaptogenesis with pharmacological and anti-sense RNA techniques. Developed and automated a high-throughput synaptic density analysis technique.
PI: Prof. Guosong Liu

Undergraduate Research Clinical Research Center, MIT (Winter 1999-Summer 1999)
Studied the correlation of *in vivo* serotonin levels with high carbohydrate diet preference in the rat via pharmacological manipulation and microdialysis.

PI: Prof. Richard Wurtman

Publications

Amy E. Palmer, Marta Giacomello, Tanja Kortemme, S. Andrew Hires, Varda Lev-Ram, David Baker, and Roger Y. Tsien. 2006. Ca2+ Indicators based on computationally redesigned calmodulin-peptide pairs. *Chemistry & Biology* **13**, 521–530

S. Andrew Hires, Yongling Zhu, and Roger Y. Tsien. Direct measurement of synaptic glutamate spillover and reuptake by linker optimized glutamate-sensitive fluorescent reporters. *Submitted*

Seminars

"Measuring glutamate spillover and uptake with GluSnFRs." Imaging Neurons and Neural Activity: New Methods, New Results. Cold Spring Harbor Labs, March 2007.

"Optical measurements of presynaptic strength with novel, genetically-encoded glutamate sensitive fluorescent reporters." Program No. 17.12 Washington, DC: Society for Neuroscience, 2005.

"Direct visualization of synaptic release plasticity with novel, genetically-encoded, glutamate-sensitive fluorescent reporters." UCSD Neuroscience Graduate Program Spring Retreat, April 2005.

"Direct visualization of synaptic release plasticity with novel, genetically-encoded, glutamate-sensitive fluorescent reporters." Imaging Neurons and Neural Activity: New Methods, New Results. Cold Spring Harbor Labs, March 2005.

"Exploring neuronal activity with genetically-encoded, glutamate-sensitive fluorescent reporters" UCSD All-Grad Research Symposium, January 2005.

Abstracts and Poster Presentations

S.A. Hires, Y. Zhu, C.F. Stevens, R.Y.Tsien. Dynamic optical mapping of synaptic glutamate release with genetically encoded, glutamate-sensitive fluorescent reporters. Soc. Neurosci. Abstr., Vol. 30 952.13, 2004

S.A. Hires, C. Zuker. "DNA shuffling of mammalian taste receptors" RIKEN Summer Program 2002

X. Zhao, A. Hires, G. Liu. Activation of pre- and post-synaptic metabotropic glutamate receptors is crucial for the formation of glutamatergic synapses. Soc. Neurosci. Abstr., Vol. 27, Program No. 572.14, 2001.

Awards
2001 - Merck Pre-doctoral Fellowship
2004 – Best UCSD student abstract, Fine Science Tools, Meeting of the SfN.

ABSTRACT OF THE DISSERTATION

Design, Development, and Use of Genetically-Encoded Fluorescent Reporters of Neural Activity

by

Samuel Andrew Hires

Doctor of Philosophy in Neurosciences

University of California, San Diego, 2007

Professor Roger Y. Tsien, Chair

The brain teems with bursts of fleeting activity. To deduce the meaning of its electrochemical flashes, an accurate record of their presence must first be captured. The acquisition of precise patterns of synaptic activity has been limited by the lack of tools to directly observe neurotransmitter release and propagation. This thesis

demonstrates how a new class of experimental tools, genetically-encoded fluorescent reporters, provides an experimental modality well-suited to solve this problem.

Novel reporters for optical recording of neurotransmitter release were developed. These were constructed by genetic fusion of fluorescent proteins to environmentally sensitive elements. These reporters rapidly changed their fluorescence in response to changes in neurotransmitter concentration or pH.

The most successful reporter was a sensor for the excitatory neurotransmitter glutamate. The dynamic range this reporter was strongly enhanced by a comprehensive screen of linker mutations and its affinity was tuned for measurement of synaptically released glutamate by mutagenesis of its ligand-binding pocket. This optimized reporter was genetically targeted to the extracellular surface of neurons. The release, propagation, and recycling of synaptically released glutamate in response to electrical stimulation was quantitatively determined by recording the changes in the color of the reporter's fluorescence. Functionally relevant levels of glutamate were found to spill beyond the synaptic cleft to extrasynaptic regions in an activity-dependent manner, implying that the independence of synaptic signaling is determined by the degree of neuronal excitation. These glutamate reporters were also used as a measurement of presynaptic strength in a model system of long-term potentiation.

Prototype reporters for inhibitory neurotransmission and a spectrally distinct reporter of synaptic vesicle fusion were also designed and tested, but had limited functionality. Besides the creation of a powerful new method of recording synaptic activity, the successes and failures of sensor development provide an illustrated primer to the design and optimization of future genetically-encoded fluorescent reporters.

Introduction

How does the microcircuitry of the brain process information? How is data physically encoded, and how do these physical characteristics sculpt the nature of neural computation? The accuracy of our answers to these questions is limited by the precision of the tools used to address them.

The most pressing task required to further our understanding of the brain is simply getting the relevant data out. Extraction of information from the brain presents formidable challenges. Thoughts and perceptions are ephemeral. A memory may be accessible only during rumination. Network connectivity is labyrinthine. Cell types are numerous, tightly packed and only partially characterized. The brain is thick, composed of translucent, light-scattering material and encased in a hard shell that bleeds profusely when cut. Total information density is high, but specific information patterns may be sparsely encoded. Numerous experimental techniques have been developed to circumvent these and other difficulties in the study of the brain. Despite this work, the range of currently available techniques painfully limits the classes of questions that can be adequate addressed.

To precisely understand how the circuitry of the brain encodes and processes information, it is necessary to study neural transmission at a level of fine detail. We must record the individual 'bits' of information flow with high fidelity across multiple members of a neuronal circuit. What constitutes a single bit of neural information? When a message is passed from one neuron to the next, rather than eject continuously variable amounts of neurotransmitter, a neuron releases individual vesicles filled with thousands of identical neurotransmitter molecules[1], which all concurrently excite or

inhibit the downstream neuron. Thus, a bit could be the release of a single synaptic vesicle.

The transmission of neural bits is driven by the action potential, the digital output spike of a neuron. The timing and rate of action potentials are in turn driven by the integration of positive and negative bits of synaptic input. Perhaps our recording task could be simplified by simply using action potential spikes as a relevant approximation of the information flow between neurons. The analysis of spike rates in response to sensory stimulation already has informed theories of how a fruit fly can recognize the scent of a banana[2], how a mouse knows its position in a room[3], and how an owl can hear the location of its prey[4]. In these and similar studies using single and multiunit electrical recording, correlations between stimuli and neural spike rates are observed. Then, using spike trains alone, the corresponding stimulus can be predicted with high fidelity. Althought these types of experiments identify neural correlates of sensory stimulation, they rarely explain how the correlations between spike rate and stimulus are generated.

To understand how spike codes are generated and what they mean, spikes must be understood in the context of the circuit in which they reside. Spikes cause the release of excitatory or inhibitory vesicles, dependent on the cell type. These transmitters are generally released to multiple classes of output neurons, which serve distinct functions in the microcircuit. The spatial pattern of their release is stochastic[5], and dependent on short and long-term forms of synaptic plasticity[6], local autoregulation[7] and activity-dependent feedback loops. Following synaptic release, neurotransmitter may be tightly localized to the originating synapse, or may travel to

neighboring synapses[8]. The sensitivity of efferent cells to the spike output is dependent on postsynaptic receptor expression levels[9], their phosphorylation state[10], and transmembrane regulatory proteins[11]. All of these and other factors influence the functional consequence of an action potential and must be considered as possible contributors to a circuit's computational repertoire.

An ideal method of neural recording should capture as many of these relevant variables as possible. It should have sufficient temporal and spatial resolution to detect the minimal functional bits of information, synaptic releases of neurotransmitter. It should be able to simultaneously observe the activity of multiple cells in a network, specified by cell type. To elucidate the circuit architecture, it should provide the morphology of the observed cells and where along the cell the release is occurring. It should recognize the polarity of these bits as excitatory, inhibitory or modulatory. Finally, the technique should be applicable in multiple preparations, from simple cell cultures, through brain slices and into *in vivo* applications.

Although electrical methods of recording neuronal spikes have excellent temporal resolution, can record from up to hundreds of cells simultaneously and have been validated in many preparations, including *in vivo*[3], they lack several characteristics of an ideal recording device. Identification of cell type is difficult, and cell type selection may be biased. Therefore, neurotransmitter polarity is uncertain or inferential. Morphology can be determined, but only when using intracellular recording techniques that limit simultaneous recording to only one or two neurons. Spatially resolved measurements of release patterns are impossible. Therefore, an

alternative method of recording is necessary to capture the critical details of neuronal communication.

Genetically-encoded fluorescent reporters show great promise to fill this need. These indicators are generally composed of the green fluorescent protein or color variants, which are mutated or fused to other proteins in a manner that makes the fluorescence signal sensitive to a specific change in the local environment. Theoretically, these indicators uniquely encompass all the necessary characteristics of an ideal neural activity recorder. The spatial resolution of light microscopy is sufficient to detect synapse-sized features, where individual bits are transferred. Fluorescent lifetimes are on the order of nanoseconds, producing thousands of photons per reporter molecule per second and providing high temporal resolution. High-sensitivity and high-resolution cameras allow the simultaneous acquisition of millions of pixel values per second with very low background noise, providing high acquisition bandwidth over a sizeable portion of the microcircuit. This allows simultaneous recording of tens to hundreds of cells within an imaging plane[12]. Genetic targeting can specify the cell types studied and fluorescence imaging can trace cellular morphology of all observed cells without need for post-hoc preparation. Sensors can be tuned to respond only to specific neurotransmitter types, reporting the polarity of the response. Finally, cellular and synaptic responses using genetically-encoded indicators have been recorded in culture, slice, and *in vivo*[13].

The creation and application of genetically-encoded fluorescent sensors is a rapidly developing field. Only ten years have passed since the publication of the first set of genetically-encoded fluorescent reporters, cameleons[14], which sense calcium

concentration through ligand-binding dependent changes in fluorescent resonance energy transfer between the chromophores of cyan and yellow fluorescent proteins. Since then, the response magnitude of cameleons has been dramatically enhanced[15], interference of endogenous calmodulin with cameleon signaling has been neutralized[16], and single fluorescent protein (FP) based calcium indicators, such as pericam[17] and G-CaMP[18] have been developed and optimized. The genetically-encoded strategy has been extended to make single FP sensors of vesicle fusion[19], dual FP sensors of PKA[20], PKC[21], Src[22] and Abl[22] activity, and numerous cellular metabolites[23]. Despite this progress, the genetically-encoded toolkit for specifically imaging neuronal activity remains limited. This thesis describes advances made in expanding this toolkit to major mammalian neurotransmitters and markers of synaptic release. It provides insight into generalizible rules and challenges of sensor construction. It also demonstrates the application of these new reporters to questions related to information density, memory encoding and the role of support cells in the brain.

Chapter One describes the design and development of a novel family of genetically-encoded glutamate-sensitive fluorescent reporters known as GluSnFRs. These are based on linear fusions of cyan and yellow fluorescent proteins to a glutamate periplasmic binding protein (PBP). A thorough screening strategy for optimization of this sensor in mammalian cells is detailed. This methodology is generalizable to other genetically-encoded reporters. Optimized GluSnFRs are used to quantitatively measure how much glutamate spills beyond the active zone of a synapse

following vesicle fusion. The impact of this spillover on synaptic independence and extrasynaptic signaling is investigated.

Chapter Two demonstrates how GluSnFRs can be used to measure changes in presynaptic strength. Long-term potentiation of synaptic strength is thought to be a primary mechanism by which memories are physically encoded, but the locus of its expression has been historically contentious. GluSnFR imaging is used to determine if a model long-term potentiation induction protocol causes changes in presynaptic strength as well as its reported postsynaptic effects.

Chapter Three looks at extending the GluSnFR sensor framework to GABA, the primary inhibitory neurotransmitter in the brain. Genomic data is mined for potential GABA PBPs. A candidate is selected, synthesized and used as a substrate for prototype GABASnFR sensors. Several sensor construction strategies are reported. These include modification of the affinity of GluSnFR towards GABA via mutagenesis, varying affinity and linkers of linearly fused FPs with the putative GABA PBP, and simple DNA shuffling between GluSnFR and the putative GABA PBP.

Chapter Four reports the development of a different modality of neural sensor, a pH-sensitive fluorescent protein designed to report synaptic vesicle fusion. Green versions of this pH sensor have found extensive use in studies of synaptic transmission and presynaptic neural activity. We set out to make a complementary colored version. Orange color variants of mRFP are tagged to synaptic vesicles by fusion to VAMP or synaptophysin. These are shown to have dramatic changes in fluorescent intensity in response to pH changes. These orange FPs are spectrally distinct from cyan, green and

yellow fluorescent proteins, raising the possibility of simultaneous imaging of multiple ligands or cell types. These prototypes are tested to assist in the possible dynamic localization of glutamate release from GluSnFR transfected astrocytes. The need for testing of new sensors in biologically relevant systems is reinforced by the lack of functional response of sensor prototypes in neurons and astrocytes, despite promising results in non-neuronal expression systems.

References

1. Takamori, S. et al. Molecular anatomy of a trafficking organelle. *Cell* **127**, 831-846 (2006).

2. Wilson, R. I., Turner, G. C. & Laurent, G. Transformation of olfactory representations in the Drosophila antennal lobe. *Science* **303**, 366-370 (2004).

3. Wilson, M. A. & McNaughton, B. L. Dynamics of the hippocampal ensemble code for space. *Science* **261**, 1055-1058 (1993).

4. Konishi, M. Coding of auditory space. *Annu Rev Neurosci* **26**, 31-55 (2003).

5. Katz, B. Quantal mechanism of neural transmitter release. *Science* **173**, 123-126 (1971).

6. Murthy, V. N., Sejnowski, T. J. & Stevens, C. F. Heterogeneous release properties of visualized individual hippocampal synapses. *Neuron* **18**, 599-612 (1997).

7. Chittajallu, R. et al. Regulation of glutamate release by presynaptic kainate receptors in the hippocampus. *Nature* **379**, 78-81 (1996).

8. Diamond, J. S. A broad view of glutamate spillover. *Nat Neurosci* **5**, 291-292 (2002).

9. Bredt, D. S. & Nicoll, R. A. AMPA receptor trafficking at excitatory synapses. *Neuron* **40**, 361-379 (2003).

10. Lee, H. K., Barbarosie, M., Kameyama, K., Bear, M. F. & Huganir, R. L. Regulation of distinct AMPA receptor phosphorylation sites during bidirectional synaptic plasticity. *Nature* **405**, 955-959 (2000).

11. Milstein, A. D., Zhou, W., Karimzadegan, S., Bredt, D. S. & Nicoll, R. A. TARP subtypes differentially and dose-dependently control synaptic AMPA receptor gating. *Neuron* **55**, 905-918 (2007).

12. Dombeck, D. A., Khabbaz, A. N., Collman, F., Adelman, T. L. & Tank, D. W. Imaging large-scale neural activity with cellular resolution in awake, mobile mice. *Neuron* **56**, 43-57 (2007).

13. Guerrero, G. et al. Heterogeneity in synaptic transmission along a Drosophila larval motor axon. *Nat Neurosci* **8**, 1188-1196 (2005).

14. Miyawaki, A. et al. Fluorescent indicators for Ca_2+_ based on green fluorescent proteins and calmodulin. *Nature* **388**, 882-887 (1997).

15. Nagai, T., Yamada, S., Tominaga, T., Ichikawa, M. & Miyawaki, A. Expanded dynamic range of fluorescent indicators for Ca(2+) by circularly permuted yellow fluorescent proteins. *Proc Natl Acad Sci U S A* 10554-10559 (2004).

16. Palmer, A. E. et al. Ca2+ indicators based on computationally redesigned calmodulin-peptide pairs. *Chem Biol* **13**, 521-530 (2006).

17. Nagai, T., Sawano, A., Park, E. & Miyawaki, A. Circularly permuted green fluorescent proteins engineered to sense Ca(2+). *Proc Natl Acad Sci U S A* **98**, 3197-3202 (2001).

18. Nakai, J., Ohkura, M. & Imoto, K. A high signal-to-noise Ca(2+) probe composed of a single green fluorescent protein. *Nature Biotechnology* **19**, 137-141 (2001).

19. Miesenbock, G., De Angelis, D. A. & Rothman, J. E. Visualizing secretion and synaptic transmission with pH-sensitive green fluorescent proteins. *Nature* **394**, 192-195 (1998).

20. Zhang, J., Ma, Y., Taylor, S. S. & Tsien, R. Y. Genetically encoded reporters of protein kinase A activity reveal impact of substrate tethering. *Proc Natl Acad Sci U S A* 14997-15002 (2001).

21. Violin, J. D., Zhang, J., Tsien, R. Y. & Newton, A. C. A genetically encoded fluorescent reporter reveals oscillatory phosphorylation. *Journal of Cell Biology* **161**, 899-909 (2003).

22. Ting, A. Y., Kain, K. H., Klemke, R. L. & Tsien, R. Y. Genetically encoded fluorescent reporters of protein tyrosine kinase activities in living cells. *Proc Natl Acad Sci U S A* 15003-15008 (2001).

23. Deuschle, K. et al. Construction and optimization of a family of genetically encoded metabolite sensors by semirational protein engineering. *Protein Sci* **14**, 2304-2314 (2005).

Chapter One

Optical measurement of synaptic glutamate spillover and reuptake by linker optimized glutamate-sensitive fluorescent reporters

Abstract

Genetically encoded sensors of glutamate concentration are based on fluorescence resonance energy transfer (FRET) between Cyan and Yellow Fluorescent Proteins bracketing a bacterial glutamate-binding protein. Such sensors have yet to find quantitative applications in neurons, due to poor response amplitude in physiological buffers or when expressed on the neuronal cell surface. We have improved GluSnFR, our glutamate-sensing fluorescent reporter, by systematic optimization of linker sequences and glutamate affinities. Using SuperGluSnFR, which exhibits a 6.2-fold increase in response magnitude over the original GluSnFR, we demonstrate quantitative optical measurements of the timecourse of synaptic glutamate release, spillover and reuptake in cultured hippocampal neurons with near millisecond temporal and spine-sized spatial resolution. During burst firing, functionally significant spillover persists for hundreds of milliseconds. These glutamate levels appear sufficient to prime NMDA receptors, potentially effecting dendritic spike initiation and computation. Stimulation frequency-dependent modulation of spillover suggests a mechanism for non-synaptic neuronal communication.

Introduction

Glutamate is the primary excitatory neurotransmitter in the brain, and precise measurement of its spatiotemporal pattern of synaptic release and propagation would provide insight into diverse brain processes, including synaptic crosstalk, cerebral ischemia, and mechanisms of learning and memory. In hippocampal slices, synaptic

glutamate spillover to the dendrite and neighboring synapses induces homeostatic regulation of glutamate release through extrasynaptic mGluR activation[1], limits synaptic independence[2], lengthens EPSC durations[3], and permits heterosynaptic LTP/LTD[4]. Spillover is a primary means of chemical neurotransmission between mitral cells in the rat olfactory bulb[5] and between climbing fibers and molecular layer interneurons in cerebral cortex[6]. Estimates of glutamate concentration and dynamics in synaptic, extrasynaptic and extracellular compartments have been made by NMDAR antagonist displacement[7], glutamate uptake inhibitor application[2], whole "sniffer" cells[8], outside-out "sniffer" patch electrodes[9,10], patch recording of astrocyte synaptically-evoked transporter currents (STCs)[11], enzymatically-coupled electrochemical probes[12], enzymatically-coupled metabolite imaging[13], and other methods. While each method provided a new perspective on glutamate action, all were hampered by a lack of resolution in the spatial or temporal domains due to single-site measurement, reliance on partially coupled or confounded currents, desensitizing receptors, or indirect and slow secondary cascades.

Recently, the glutamate reporters GluSnFR (glutamate-sensing fluorescent reporter; SAH, YZ, Stevens and RYT 2004, Society for Neuroscience Abstracts) and FLIPE (fluorescent indicator protein for glutamate)[14] were constructed by linear genetic fusions of the glutamate periplasmic binding protein GltI (also known as ybeJ) with enhanced cyan fluorescent protein (ECFP) and a yellow fluorescent protein, Citrine[15] or Venus[16]. These reporters provide a sensitive optical readout of glutamate concentration *in vitro* by fluorescence resonance energy transfer (FRET)-dependent changes in the CFP/YFP emission ratio. When expressed on the surface of

hippocampal neurons, synaptic glutamate release was detectable (Hires SA, Zhu Y, Stevens CF, and Tsien RY, SFN Abstracts 2004)[14]. However, quantitative measurements of rapid glutamate transients have been hampered by the low signal to noise ratio of these sensors when used in physiological buffers and by suboptimal glutamate affinity.

Intramolecular FRET reporter responses have been dramatically improved by restricting the rotational freedom of the chromophores, adjusting their orientation by linker variation and alternative fluorescent protein substitution[17,18,19]. Therefore, to maximize GluSnFR response magnitude for neuronal measurements, we performed a comprehensive, mammalian cell based screen of linker truncations of linearly fused constructs, as well as circularly permuted fluorescent protein substitution. To optimize sensor affinity, we rationally mutated GltI residues known to coordinate ligand binding. We have identified a greatly improved variant of GluSnFR, SuperGluSnFR, which exhibits 44% change in emission ratio upon glutamate binding with a dissociation constant (K_d) of 2.5 μM when expressed on the extracellular surface of neurons.

We have used SuperGluSnFR to directly measure the timecourse of glutamate propagation following synaptic release. We demonstrate that sub-micromolar glutamate persists along the dendritic surface for hundreds of milliseconds following coordinated synaptic release. Spillover concentration is strongly modulated by stimulation number and frequency. Active uptake and buffering by neuronal and glial glutamate transporters appears insufficient to prevent extrasynaptic NMDA receptor activation following bursts of synaptic release. Furthermore, uptake transporter

capacity may regulate the dependence of extrasynaptic glutamate signaling on action potential frequency and provide an avenue for non-synaptic neuron and astrocyte communication.

Results

The initial construct design of GluSnFR consisted of the mature length GltI domain bracketed by a C-terminal truncated ECFP (AA1-228) and full-length Citrine (Fig. 1.1). Later experiments anchored GluSnFRs to the extracellular surface of mammalian cells by fusion to the truncated PDGFR domain in the pDisplay vector (Fig. 1.1). Minimal linkers encoded by a single restriction site were used to maximize inter-domain rigidity. This first GluSnFR was designated $GluSnFR_{0N0C}$, where the subscript indicates the number of amino acids truncated from the N- and C-terminus of the mature GltI PBP prior to FP fusion. When dilute purified $GluSnFR_{0N0C}$ in 50mM Tris buffer was excited at 420nm, its emission spectrum showed two peaks corresponding to CFP and YFP emissions, whose ratio was modestly sensitive to glutamate (Fig. 1.2). Trypsin digestion extinguished the 526nm YFP peak and raised the 476nm CFP peak by 15.2%, indicating a FRET efficiency of 13.2% (Fig. 1.3). Application of increasing glutamate in 50mM Tris buffer increased the emission ratio from ~0.66 to ~0.77, with a maximum ratio change (ΔR_{max}) of 18% and apparent K_d of ~150nM (Fig. 1.4). Replacing Tris buffer with HBSS reduced ΔR_{max} to 7% (Fig. 1.4). Addition of NaCl to Tris buffer caused a concentration-dependent reduction in ΔR_{max} to 0% in 50mM Tris + 1M NaCl (Fig. 1.5). Substitution of 100mM Na-gluconate or KCl for 100mM NaCl displayed an identical reduction of dynamic range, indicating a

general effect of buffer ionic strength rather than substrate interactions with a specific ion (data not shown). Since neurons require buffers with ionic strength of ~0.15, observed ΔR_{max} in mammalian cell systems had been limited to ~10%[14].

Glutamate-dependent ratio changes were partially reversible by glutamate deamination following addition of glutamate-pyruvate transaminase and 10mM pyruvate to the cuvette (Fig. 1.6). Titrations with aspartate and glutamine gave K_ds of ~700nM and ~30μM respectively, consistent with fluorescently labeled GltI[20]. Application of 1mM serine, arginine and sucrose had no effect (data not shown).

The high glutamate affinity (150nM K_d) of $GluSnFR_{0N0C}$ containing wild-type GltI might cause partial saturation of the sensor at background glutamate levels in neuronal systems, limiting dynamic range. Furthermore, native PBPs have k_{on} rates of ~10^8 M^{-1} s^{-1} [21] implying a k_{off} of ~15 s^{-1} for this GluSnFR that would significantly slow the response decay to brief impulses of glutamate. We reduced the glutamate affinity by rational, site-directed mutagenesis of key glutamate binding residues[20]. We generated a range of glutamate K_d from 150nM to 700μM (T93A, E26A and E26D were 300nM; S73T was 2.5μM; R25K was 20μM; E26R was 700μM). Mutants are numbered from start of the mature GltI product. We preferred the S73T affinity for neuronal measurements.

To maximize response magnitude, we screened a linker-truncation library of GluSnFRs on the surface of mammalian cells in HBSS. GluSnFRs with N- and C-terminal truncations of GltI(S73T) (Fig. 1.7) were fused to pDisplay (Fig. 1.1), which expressed spatially uniformly on the extracellular surface of mammalian cells (Fig. 1.7). Constructs were scored by efficiency of membrane targeting and ratio change

between zero and saturating [glutamate] (Fig. 1.7). The best mutant, $GluSnFR_{8N5C}$(S73T), had a dramatically lower glutamate-free CFP/YFP ratio and a 44% average ΔR_{max} (n=18), a 6.2-fold improvement over the 7.1% average of $GluSnFR_{0N0C}$ (Figs. 1.8, 1.9). We refer to this construct as SuperGluSnFR. *In vitro* tests of soluble SuperGluSnFR demonstrated ΔR_{max} of 46% and 34% in 50mM Tris and Ringer's solution, respectively (Fig. 1.2). The slightly lower ΔR_{max} in Ringer's in solution vs. on cell surface may be due to the increased conformational freedom of free solution. Glutamate titration curves of SuperGluSnFR expressed on HEK293 or HeLa cells demonstrated a 2.5μM apparent K_d and 1.0 Hill coefficient (Fig. 1.10).

To test the selectivity of SuperGluSnFR for glutamate, a panel of glutamate receptor agonists and antagonists consisting of 2,3-dihydroxy-6-nitro-7-sulfamoylbenzo(*F*)quinoxaline (NBQX), 2-amino-5-phosphonovaleric acid (APV), α-amino-3-hydroxy-5-methylisoxazole-4-propionic acid (AMPA), *N*-methyl-D-aspartic acid (NMDA), kainic acid (KA), (+/-)-*trans*-1-amino-1,3-cyclopentane dicarboxylic acid (ACPD), and (RS)-α-methyl-4-carboxyphenylglycine (MCPG) was sequentially applied to SuperGluSnFR transfected HEK293 cells. No tested compound directly induced a ratio change or reduced the ΔR_{max}. However, 300μM NMDA, 25μM ACPD and 250μM MCPG each caused a small reduction in ratio change from 2.5μM glutamate (Fig. 1.11). Addition of 100μM DL-*threo*-β-benzyloxyaspartate (TBOA) or 1mM γ-aminobutyric acid (GABA) had no effect (data not shown).

We used SuperGluSnFR to detect glutamate on the surface of cultured dissociated hippocampal neurons. Following transfection, protein was localized on the

extracellular surface of the neuron with even distribution across dendritic spines and shaft and significant intracellular fluorescence confined to the soma or occasional tiny inclusions in the dendritic shaft (Fig. 1.12). The glutamate affinity of SuperGluSnFR in neurons was determined by bath changes of Ringer's solution (2mM Ca^{2+}, 1.3mM Mg^{2+}, 25μM NBQX and 50μM APV) with increasing glutamate from 0 to 100μM, and was identical to the affinity in HEK293 cells (Fig. 1.10). Background glutamate levels in the bath were negligible, but inclusion of 100μM TBOA in the titration buffer was required to prevent local depletion of glutamate by astrocyte-mediated uptake (Fig. 1.24).

We tested the ability of SuperGluSnFR to resolve electrically evoked glutamate transients with high spatial resolution. A brief train of 10 field stimulations was delivered at 30Hz while a small segment of SuperGluSnFR expressing dendrite was imaged at high (150x) magnification. Each pulse in the train was designed to evoke a single action potential across all neurons[22]. During burst stimulation, a rapid, transient increase in CFP/YFP ratio was observed across all areas of the dendrite (Fig. 1.13). Addition of 100μM TBOA increased the peak response and dramatically prolonged the recovery towards baseline glutamate levels (Fig. 1.13), indicating a glutamate-specific response. Lowering extracellular calcium to 0.1mM and raising magnesium to 5mM reversibly abolished responses to field stimulation, indicating the glutamate source was synaptic release (data not shown).

The average area of an active zone in hippocampal culture has been estimated at 0.027μm^2[2,23] contributing to <2% of the total dendritic surface area. Furthermore, the high speed of intersynaptic glutamate diffusion (D = 0.76μm^2/ms) has been predicted

to produce a relatively smooth glutamate distribution for timescales above 5ms[24]. Even if a significant proportion of the functional synapses are made directly on the dendritic shaft, the GluSnFR signal, particularly when integrated over 33ms intervals, should primarily represent glutamate levels arising from synaptic spillover and pooling.

Since spike number may affect the spatial distribution of spillover, we reduced the stimulus to a single AP. The signal to noise ratio was insufficient to resolve individual responses without significant spatial averaging. Therefore, we averaged thirty single AP stimulations. This response also had very broad spread across dendrites, indicating that spillover affects spines and extrasynaptic areas to a similar extent (Fig. 1.14). Although the trial-averaged spread was homogeneous, due to the stochastic nature of synaptic release (~0.3 vesicles/synapse at 2mM Ca^{++}, 1.3mM Mg^{++})[25], there may have been a greater heterogeneity on individual trials that we were unable to resolve due to signal/noise or camera speed.

We assessed the temporal resolution of SuperGluSnFR by high-speed imaging (770fps) of glutamate transients evoked by a single AP. Twenty-seven CFP/YFP traces of single AP stimulation on a single neuron's dendrite were averaged and corrected by a fit bleach curve of a stimulation free trace (Fig. 1.15). Individual responses were clearly resolvable (Fig. 1.15). The trial-averaged ratio was converted to estimated glutamate concentration (Fig. 1.15) using titration curves (Fig. 1.10). The 20-80% rise time was 6.6ms, peak glutamate concentration was 720nM and the time to half decay was 40ms from peak (Fig. 1.15).

For SuperGluSnFR to accurately report glutamate spillover decay timecourse, the rate of ligand unbinding, k_{off}, must exceed the rate of decay of ligand at the neuronal surface. We were uncertain how increasing the sensor K_d to 2.5μM would affect the kinetics, so we estimated them using a numerical model of glutamate release and uptake. Total release amount and GluSnFR binding constants were allowed to vary while holding other parameters fixed. Glutamate release was assumed to be instantaneous and homogeneous with minimal buffering from GluSnFR. Since the FRET ratio is a sub-linear function of glutamate concentration (Fig. 1.10), spatial averaging may underestimate the concentration of the initial portion (<5ms) of the heterogeneously distributed synaptic release transient. Asynchronous release, or buffering by GluSnFR itself would also lower the apparent rates. Thus, the best-fit parameters of $k_{on} = 3.0 \times 10^7\ M^{-1}s^{-1}$ and $k_{off} = 75\ s^{-1}$ (Fig. 1.16) serve only as a lower bound. Even at this lower bound, SuperGluSnFR kinetics are sufficiently rapid to capture the essential waveform of spillover glutamate beyond the first 10ms following synaptic release.

To determine how active glutamate reuptake regulates spillover, we imaged glutamate during a set of six field stimulation conditions. Trains of 1AP, 10AP-15Hz and 10AP-30Hz were delivered in Ringer's with or without 100μM TBOA (Fig. 1.17). TBOA increased the peak glutamate concentration during stimulation and greatly slowed the decay back to baseline. In the single AP case, TBOA increased the average peak [glutamate] at 67ms from 270nM to 440nM and the time to half decay from 90ms to 140ms (Fig. 1.18). Peak glutamate levels, particularly for the single AP cases, are likely underestimates due to the camera's broad temporal integration window. In

the 10AP cases, glutamate levels reached an apparent steady state after 4AP of stimulation with active uptake, while they continued to rise throughout the entire TBOA stimulation. TBOA raised peak [glutamate] from 540 to 1200nM and 830 to 1320nM, while half decay increased from 160 to 650ms and 140 to 390ms for 15 and 30Hz respectively. Doubling stimulation frequency from 15Hz to 30Hz gave a 60% enhancement of peak [glutamate] with active uptake, while only a 10% enhancement with uptake blocked. Thus active reuptake may serve multiple purposes, to recycle glutamate and to permit AP frequency dependent signaling by modulation of spillover concentration.

To explore the effect of our measured glutamate transients on NMDA receptor activation, we made a simple numerical model of glutamate dynamics for 2 seconds following onset of field stimulation (Figs. 1.19-22, Table 1). Following a single action potential, only 1.4% of NR_{2A}, 2.4% of NR_{2B}, 3.7% of NR_{2D} receptors were doubly bound by glutamate (Fig. 1.21). However, the prolonged spillover from a burst of 10AP at either 15 or 30Hz caused a sustained activation of 20 or 22% NR_{2A}, 36 or 34% NR_{2B}, and 50 or 45% of NR_{2D} receptors, respectively.

In order to measure glutamate dynamics in different spatial compartments, including the synaptic cleft, we attempted to target GluSnFR to the synapse. The final four C-terminal amino acid residues of synaptic targeted proteins bind to specific PDZ-domains of PSD-95, conferring synaptic or perisynaptic localization. Therefore, constructs were generated appending the last 4 to 10 amino acids of the C-terminal domain of the synaptic membrane proteins neurexin, neuroligin, $NMDAR_{1\text{-}4}$, $NMDAR_{2A}$, and $mGluR_5$, as well as two PDZ binding domains, -ETQV and –VSNL,

previously shown to target channelrhodopsin-2 to the synaptic cleft (Gradinaru V, et. al, SFN Abstracts 2006), to the C-terminal end of the PDGFR of GluSnFR. All constructs expressed extracellularly on the membrane of transfected HEK293 cells and responded to application of glutamate. When transfected into neurons, GluSnFRs with the neurexin, NR_{2A}, and $mGluR_5$ PDZ binding domains expressed homogenously over the plasma membrane. In contrast, constructs using the neuroligin, $NR_{1\text{-}4}$, -ETQV and –VSNL PDZ binding domains showed some diffuse expression of GluSnFR on the plasma membrane, but also dense, punctate localizations at areas that resembled synapses. However, these puncta had abnormally high CFP/YFP ratios and were unresponsive to application of glutamate, possibly due to intracellular retention at these sites.

Discussion

Sensor Optimization

FRET sensor optimization is an area of active research, with numerous recent reports on improved fluorescent proteins, FRET pairs, substrate and linker mutations and screening techniques. Optimization of GluSnFR provides a cautionary example of the delicate sensitivity of FRET reporters to their constituents. The fitness landscape of GluSnFR linkers was far more peaked than we expected. A single construct, $GluSnFR_{8N5C}$, of the 176 tested was far superior to all others (Fig. 1.7). Although there was general improvement in sensor response as linkers were truncated, the process was non-monotonic, limiting the effectiveness of this rational strategy of sensor design. We attempted systemic substitution of fluorescent proteins (FPs) and circularly

permuted FPs to improve response, including the fluorescent protein variants ECFP-A206K, Cerulean[26], CyPet, YPet[27], Venus[16] and cpVenus (145, 157, 173, 195). Surprisingly, all substitutions of improved components to linker-optimized GluSnFRs reduced either the quality of the reporter's surface expression or response magnitude. This is likely due to linker sequences being already highly tuned for the specific chromophore orientations and subtle electrostatic interactions of the GltI domain and the FP pair.

We inserted ECFP into the putative transmembrane loops of GltI, similar to FLI[81]PE reported by Deuschle et al[17]. When expressed as a purified protein, FLI[81]PE has a two-fold ratio-change to glutamate, but this and all tested ECFP insertion mutants fail to express properly on the surface of mammalian cells. Incorporation of superfolding GFP[28] mutations into the inserted ECFP (sfECFP) improved folding and trafficking of many insertion mutants. However, our best-case ΔR_{max} of sfECFP-inserted GluSnFRs was only 4% when expressed on cell surface (data not shown). Further improvements of sensor response may be possible by FP substitution or insertion, but will require a re-screening of many linker combinations for that pair.

Screening of single circularly permuted fluorescent protein insertions into GltI may produce a single wavelength glutamate sensor analogous to camgaroos[18]. A single-FP GluSnFR could be of practical use in more challenging preparations, such as 2-photon *in vivo* imaging, or when quantitative calibration is not a priority.

SuperGluSnFR represents a major improvement over other optical indicators of glutamate. No previous membrane-tethered PBP-based FRET reporter has achieved greater that 10% FRET ratio change for glutamate or any other substrate. Another

recently reported glutamate sensor, EOS[29], requires purification of recombinant protein, followed by thiol-mediated dye labeling and cell surface immobilization through biotinylation. The apparent glutamate off-rate of EOS is on the order of hundreds of milliseconds. In contrast, SuperGluSnFR is genetically expressed, allowing cell-specific or subcellular targeting, has been quantitatively calibrated, and has adequate response size, sensitivity and kinetic rates to resolve single action potentials. Future versions of SuperGluSnFR may be genetically-targeted to the active zone by fusion to full-length synaptic proteins or targeting motifs, raising the possibility of direct comparison of synaptic vs. extrasynaptic glutamate dynamics following synaptic release. For synaptic targeting, a GluSnFR variant with lower glutamate affinity, such as R25K or E26, would likely be useful to prevent sensor saturation at the higher concentration ranges found in the synaptic cleft.

Functional Significance

Measurements of glial synaptic transporter currents (STCs) indicate that the bulk of synaptically released glutamate is rapidly buffered and internalized by glutamate transporters. Estimates of spillover glutamate timecourse using STCs, primarily mediated by EAAT2 in the hippocampus, have provided an evolving range of estimates of clearance time in the low tens of milliseconds[30]. Recently, deconvolution analysis using partially blocked STC timecourses has suggested that the true clearance rate of glutamate is faster than the STC decay rate, with an exponential τ_{decay} of 5.8ms in P12-14 and 0.75ms in adult hippocampal slices[31]. Despite this rapid rate of STC decay, spillover in the Schaffer collateral pathway of hippocampal slice is thought to prolong NMDAR-mediated EPSCs by tens to hundreds of milliseconds in a

stimulus intensity-dependent manner[3]. Possible mechanisms include increased activation of extrasynaptic NR_{2B} and NR_{2D} subunit containing receptors[32] or cooperative action of pooled spillover from neighboring synapses[2]. Furthermore, extended activation of NMDARs can trigger dendritic calcium spikes in the basal dendrites of cortical and CA1 pyramidal neurons[33,34]. Priming of the NMDARs by residual glutamate has been suggested as the activation mechanism, but direct measurements of these glutamate transients have not been made.

SuperGluSnFR imaging may reconcile the discrepancy between STC estimates of millisecond glutamate clearance rates and prolonged NMDAR activation. Following bursts of electrical stimulation, our imaging shows long, slowly decaying glutamate transients persist across both dendritic spines and shaft. These are of sub-micromolar concentration, but are sufficient to dramatically enhance NMDAR activation for hundreds of milliseconds in a stimulus strength-dependent manner (Fig 5d). These glutamate transients may be missed in STC recordings as STCs are confounded by a small, slowly decaying potassium conductance, which is difficult to perfectly compensate[30]. Given the estimated EAAT2 glutamate K_d of 18μM[35], transporter currents at sub-micromolar extracellular glutamate concentrations are probably small enough to be obscured by errors associated with the potassium conductance. Although SuperGluSnFR measurements are insensitive to the first few milliseconds of spillover, due to sensor kinetics and heterogeneous initial glutamate distribution, their calibration, sensitivity, and spatial resolution provide a valuable complement to the fine temporal resolution of STCs.

The ease of imaging SuperGluSnFR in a reduced culture preparation forced some tradeoffs in potential physiological relevance. Spillover decay timecourse may vary from culture to brain slice, due to differences in the density of synapses, transporters and buffering agents, temperature, neuropil geometry, and access to bath. We drove synaptic release with spatially broad field stimulations to heterogeneous circuits, which caused simultaneous release from many synaptic neighbors likely leading to pooling of extrasynaptic glutamate release. *In vivo*, neuronal activity is generally sparser and glutamate uptake may be more efficient, so spillover and NMDAR priming may be more temporally and spatially constrained. Nonetheless, our imaging results in culture are congruent with numerous observations of the functional consequences of spillover in slice[2,3,33,34]. Direct observation of glutamate propagation with GluSnFRs in slice models[36] or via 2-photon imaging and/or microendoscopy[37] *in vivo* would more directly address the extent and significance of glutamate spillover.

Steady-state spillover concentration during burst stimulation is strongly modulated by stimulation frequency (Fig. 1.17). This suggests that non-synaptically connected neurons or astrocytes may be able to estimate the firing rate of neighboring neurons by the degree of activation of high-affinity extrasynaptic glutamate receptors. This could allow induction of a measured amount of heterosynaptic LTD[4], homeostatic regulation[1] or vasoregulation[38]. These effects would be sensitive to modulation of glutamate uptake by changes in astrocyte membrane potential, internal glutamate concentration, or other means.

Linker-optimized GluSnFRs may also be adapted for a number of other neuronal applications beyond measuring synaptic spillover. The selectivity of

GluSnFRs for true glutamate over standard glutamatergic agonists and antagonists should facilitate dissection of feedback loops where GluRs modulate release or uptake. SuperGluSnFR is currently being used in studies of glutamate release from astrocytes. GluSnFRs could be used as a calibration tool to assess the propagation of glutamate in uncaging or iontophoresis experiments, as a specific marker of presynaptic modulation in studies of LTP or LTD or in mapping the functional connectivity of the brain. More clinically relevant uses may include GluSnFR imaging in the screening of drug candidates for glutamate release, transporter or receptor modulation, or in models of glutamate excitotoxicity in cerebral ischemia.

Materials and Methods

Sensor construction and *in vitro* characterization

Genomic DNA from *E. coli* was isolated by chemical lysis and cartridge purification. GltI was amplified from the genomic DNA by PCR and subcloned into the bacterial expression vector pRSET$_B$ (Invitrogen). To make GluSnFR$_{0N0C}$-pRSET$_B$, cDNA corresponding to the mature peptide of GltI was ligated into the AKAR2-pRSET$_B$ PKA reporter[39] at the *Sph*I and *Sac*I sites between ECFP and Citrine, replacing the reporter's central phosphorylation and binding sites. This construct was expressed in bacteria, extracted by chemical lysis (B-PER II, Pierce), purified by 6-His Ni-NTA gel column filtration (Qiagen) and subjected to three days of sequential dialysis to remove remaining contaminants. Spectroscopy was performed as previously described[40]. Ligand-induced ratio changes were assayed by progressive glutamate addition to an albumin-coated quartz cuvette containing 10 nM GluSnFR in 50mM Tris or HBSS (pH = 7.40). For mammalian cell surface expression, the five *Sph*I and two *Sac*I sites were removed from an empty pDisplay vector (Invitrogen) by multisite mutagenesis[41]. An ECFP-GltI fragment and Citrine fragment were amplified from GluSnFR$_{0N0C}$-pRSET$_B$ by PCR with new *Bgl*II and *Pst*I restriction sites flanking the N- and C-terminal of the combined fragment. These were combined by triple ligation into the modified pDisplay vector (Invitrogen) between the *Bgl*II and *Pst*I sites to make GluSnFR$_{0N0C}$-pDisplay.

Library construction and screening

Affinity mutations were made in GltI-pRSET$_B$ with the QuikChange site-directed mutagenesis kit (Qiagen), transferred to GluSnFR$_{0N0C}$-pRSET$_B$ by digestion

and ligation at the *Sph*I and *Sac*I sites and assayed *in vitro* as above. $GltI_{S73T}$ was incorporated into $GluSnFR_{0N0C}$-pDisplay by digestion and ligation at *Sph*I and *Sac*I sites. Glutamate affinity of this mammalian expression construct was assayed by bath changes of HBSS with increasing [glutamate] on transfected HEK293 and HeLa cells.

Preliminary large truncations of the N- and C- terminus of GltI indicated that proper expression was unlikely with deletions beyond the first putative α-helix element of the N and C-termini (data not shown). Therefore, the library was limited to 176 combinations of deletions of 0-15 amino acids of the N-terminal and 0-10 of the C-terminal of GltI. Primers for 0-15 AA truncations of the N-terminus and 0-10 AA of the C-terminus of mature GltI protein were combined in 96-well format PCR. Truncation combinations were amplified with Phusion polymerase (NEB) and purified with 96-well PCR cleanup cartridges (Qiagen). All product lengths were confirmed on an analytical agarose gel, digested with *Sph*I and *Sac*I, ligated into the $GSFR_{0N0C}$-pDisplay vector, replacing the full-length GltI domain, and plated on selective media. Two colonies of each transformation were cultured and miniprepped in 96-well format. Proper insert length was checked for all by analytical restriction digests.

HEK293 or HeLa cells were seeded on 96-well culture plates, grown for one day, and transfected with one of the 176x2 minipreps. Two days after transfection, response changes to glutamate were measured by thorough bath exchanges with glutamate-free and 100μM [glutamate] HBSS. Repeated optical measurements were made on selected fields in each well with a 20x air objective and a motorized stage. A random library sample and all large responders were confirmed to have the correct genetic sequence. 0N0C, 8N0C and 8N5C truncations were selected for further

confirmatory imaging in transfected HEK293 cells on 12mm coverslips in a Warner imaging chamber with a 40x oil objective.

Neuronal culture preparation and stimulation

Dissociated hippocampal cell culture was prepared as described[43]. Briefly, rats were sacrificed on postnatal day 0-1, hippocamppi dissected, dissociated and plated at 25,000 cells/coverslip on 18mm coverslips coated with a monolayer of purified hippocampal astrocytes. Cultures were grown for 7-8 DIV, transfected with SuperGluSnFR via calcium phosphate precipitation[44], allowed to mature to 14-17 DIV and assayed. Highly expressing neurons with clear plasma membrane expression were selected for optical measurements. Great care was taken to minimize light exposure and bleaching throughout the experiment. Neurons were imaged with a mercury arc lamp with 0.33%-1.5% neutral density transmission and 420/20 excitation filters. The emission beam was split with a DualView (Optical Insights) with a CFP/YFP filter set (OI-05-EX), recorded at 30fps by a Hamamatsu EB-CCD camera (C7190-53), digitally recombined and ratioed with SimplePCI (CImaging). High-speed single AP imaging was performed with a Cascade 128+ (Roper) camera in 3x3 binning mode and Metafluor 6.1 (UIC). Spatially resolved ratio changes were calculated using custom MATLAB processing routines.

Field stimulation was delivered by a Grass stimulator (SD9) to a custom chamber, similar to Warner Instruments RC-21BRFS, with custom control software. Stimulator settings were 0.3ms, 70-80V biphasic pulse per action potential. All neuronal manipulations were done at room temperature in Ringer's solution with 2mM [Ca^{++}], 1.3mM [Mg^{++}], supplemented with 25μM NBQX and 50μM APV to block

recurrent excitation from glutamate perfusion or release. For uptake regulation experiments (Fig. 1.17), four traces of each 1AP and 2 traces of each 10AP condition were obtained in 8 neurons, converted to glutamate concentration, then averaged. Glutamate decays were poorly fit by single exponentials, so times to half decay are reported (Fig. 1.18). To block active reuptake, 100μM TBOA was selectively added to the bath. To simplify diffusion modeling, stimulations were performed in a still bath rather than under continuous perfusion.

Neuronal glutamate calibration

Optical glutamate titration curves were generated by bath changes of a broad range of [glutamate] in Ringer's solution. Absolute CFP/YFP emission ratio changes were normalized to the maximum change. A variable-slope dose response fit was performed on the average normalized change to find the apparent K_d for glutamate. Later experiments used only the 0 and 100μM [glutamate] condition to find ΔR_{max}. 100μM ligand is predicted to bind only 97.5% of a substrate of 2.5μM K_d, so use of this value may cause a 2.5% systemic overestimate of glutamate concentrations. For electrical stimulation, pixel intensities of ROIs in the CFP and YFP emission were averaged, background subtracted, then ratioed. To correct for inter-trial changes in sensor bleach levels and autofluorescence, pre-stimulus ratios were multiplicatively scaled to the [glu] free calibration ratio for that cell. To correct for a partially-reversible bleach component (0.5-2% of absolute ratio per trial), ratios were corrected by a linear fit of the pre-stimulus bleach rate, which closely matched non-stimulus bleach curves for the combination of light intensities and exposure times. Following these corrections, average extracellular [glutamate] (glu_{ex}) was calculated with the

formula $K_d*((R_{free}-R)/(R-R_{sat}))*(CFP_{free}/CFP_{sat})$, where K_d is 2.5μM, R equals the current YFP/CFP emission, R_{free} and R_{sat} are YFP/CFP emission in zero and 100μM glutamate, and CFP_{free} and CFP_{sat} are CFP emission in zero and 100μM glutamate[42].

Sensor calibration

Because GluSnFRs are ratiometric indicators, background-subtracted responses should be independent of indicator concentration. However, when expressed on the surface of mammalian cells, baseline SuperGluSnFR FRET ratios and R_{max} are variable (Fig. 1.8), depending on cell type, reporter expression level, autofluorescence background and reporter bleaching. Therefore, to make quantitative measurements of [glutamate], each cell's R_{max} must be determined by calibration with at least two known glutamate concentrations with synaptic responses normalized to this R_{max}. We used 0 and 100μM glutamate, because application of greater than 100μM glutamate to neurons, even in the presence of GluR antagonists, often caused dramatic changes in intracellular autofluorescence.

Typical ratio bleaching curves for the light intensities we used had a fast exponential drop in the first several hundred milliseconds of illumination followed by a near linear, partially dark-reversible bleaching of ~0.5 to 2% absolute ratio over the next several seconds. Over multiple illuminations, the slope of these two components evolved significantly. Thus, a bi-exponential fit of a single canonical bleach curve was inadequate to reliably characterize the bleach rate, while multiple interleaved bleaching curves caused an unacceptable loss of signal by the end of each experiment. Therefore, after discarding the initial fast component, we scaled the ratio by a linear fit of the prestimulus bleach rate for each trace. This method provided reliable correction

for the first two seconds following each stimulus, with increasing divergence at longer timepoints.

Determination of background glutamate concentration

In neuronal cultures without TBOA in the bath solution, glutamate titrations of SuperGluSnFR gave a curve with apparent K_d of 8.9μM and a Hill coefficient of 1.5 (Fig. 1.10). We formulated two hypotheses for the discrepancy between this curve and the HEK293/HeLa titration curves. First, micromolar levels of background glutamate may exist near the surface of neurons in equilibrium between spontaneous glutamate release, reuptake and diffusion. *In vivo* microdialysis has estimated background glutamate levels in the extracellular fluid of the cerebellum at 2.0μM, although these levels may be overestimates due to probe-induced tissue damage[45]. Similar background glutamate would raise the response floor, increasing the apparent sensor K_d and Hill coefficient (Fig. 1.10). Alternatively, the astrocyte uptake capacity may outpace the diffusion of glutamate from the bath onto the culture surface, causing surface depletion of neurotransmitter following glutamate application.

To test the first hypothesis, we rapidly perfused Ringer's with 1μM glutamate directly onto SuperGluSnFR expressing neurons during continuous FRET ratio monitoring. This induced a rapid increase in CFP/YFP ratio, indicating the pipette location was appropriate to induce GluSnFR responses and also providing an upper bound to the background [glutamate]. Perfusion of glutamate-free Ringer's from the same unmoved pipette had no effect on the CFP/YFP ratio, indicating background glutamate levels were below the level of detection of SuperGluSnFR (Fig 1.23).

Using a numerical model of glutamate diffusion and uptake we checked if local depletion by transporter uptake was sufficient to explain the shifted titration curve. The concentration timecourse after bath exchange of varying levels of glutamate was calculated assuming no significant spontaneous release from neurons and astrocytes. Model equations were as in Supplementary Table 1, with glutamate added homogenously throughout the bath at $t=0$. Following glutamate applications, the model showed significant depletion of glutamate near the coverslip surface (Fig. 1.24) that was proportionally greater for smaller bath concentrations. By lowering the uptake rate (k_2) or transporter concentration (U_{max}) such that the total maximum uptake rate was 40,000 molecules $s^{-1}/\mu m^2$ coverslip, we were able to qualitatively fit the TBOA-free neuronal titration curve with locally depleted glutamate levels at the 30 second timepoint (Fig. 1.10). This indicated transporters were sufficient to rapidly deplete surface glutamate levels following bath application.

Glutamate dynamics and receptor modeling

Electrically-evoked glutamate release was modeled as an instantaneous injection of homogeneously distributed glutamate (1.5μM, equivalent to 0.192 vesicles/μm^3 @ 4700 glutamates/vesicle) in the neuronal plane for the first AP of each stimulation. For each successive AP, a decreasing amount of glutamate was injected, estimated by a double exponential association fit of synaptopHluorin fluorescence increases for 30Hz and 15Hz 10AP field stimulations (data not shown). The tenth action potential injected 43% and 47% of the first for the respective 30Hz and 15Hz cases. Additional asynchronous release was not considered. To account for the interlaced filtering effects of the Hamamatsu camera, model glutamate concentration

was integrated with a 33.3ms time window and averaged with a 33.3ms delayed duplicate trace.

Following release, glutamate diffused through the neuropil region, became transiently bound by SuperGluSnFR, glutamate transporters or NMDA receptors, became bound and internalized by transporters, or diffused into the bath (Table 1.1). Glutamate diffusion was modeled as 1-dimensional diffusion from the release plane using the central difference approximation for space discritization and Euler's method for time discritization. Step intervals were 3.3μs and 250nm and total simulation duration was 2 seconds. Shorter intervals did not improve macroscopic fit properties. GluSnFR, transporter and NMDAR location was assumed to be homogeneous within the neuronal plane. Diffusion rate (D = 0.76μm^2/ms), and reuptake and GluSnFR binding equations were adapted from Barbour and Hausser[24]. Since the culture neuropil was heterogeneous with unknown geometries and bath exposure, tortuosity and extracellular volume reduction parameters were omitted.

Glutamate transporters were considered as a single species with rate constants (k_1 = 10^7 M^{-1}s^{-1}, k_{-1} = 86 s^{-1}, k_2 = 14 s^{-1})[46]. Maximum free binding concentration (U_{max} = 10 μM) was set at somewhat less than literature estimates for hippocampal slice[47]. With TBOA in the bath, U_{max} was set to zero. For the NMDA receptors, off rates and K_d values were derived from the equation K_d=(√2-1) EC_{50}, assuming the EC_{50} ($EC_{50:2A}$=1.7μM, $EC_{50:2B}$=0.8μM, $EC_{50:2D}$=0.4μM)[48,49] reflects two independent glutamate binding events (k_1 =5x10^6 M^{-1}s^{-1}, , $k_{-1:2A}$ = 3.52 s^{-1}, $k_{-1:2B}$ = 1.66 s^{-1}, $k_{-1:2D}$ = 0.83 s^{-1}). Total NMDAR binding sites were 300nM equally distributed between NR_{2A}, NR_{2B} and NR_{2D} subtypes. We used the lower bound rate constants of SuperGluSnFR

(k_1 = 3x10^7 M^{-1}s^{-1}, k_{-1} = 75 s^{-1}). GluSnFR concentration was estimated at ~200 molecules/μm^2 coverslip (eq. to 127nM homogeneously distributed in the neuropil) by calibrating pixel intensities to thin optical chambers filled with known concentrations of purified SuperGluSnFR (data not shown). Vesicle release rates were roughly estimated with synaptopHluorin imaging (data not shown) and adjusted to fit the rising phase of the average 1AP, 10AP-15Hz and 10AP-30Hz in TBOA GluSnFR traces. The model captured the essential timecourse of spillover rise and decay, although the degree of frequency-dependent facilitation in the active uptake case was consistently lower in the model (Fig. 1.19). This discrepancy was perhaps due to the dramatic simplification of the spatial distribution of release and transporters. No significant glutamate accumulated in the far end of the model chamber within 2 seconds indicating use of a closed-boundary condition model was accurate for these timescales (Fig. 1.20).

Although the glutamate release kinetics are constrained by the TBOA records, glutamate transporter kinetic estimates vary significantly[35,50], and our estimate of the concentration of transporters in the culture system is imprecise. Therefore, we perturbed the model to assess the system's parametric sensitivity. Increasing [SuperGluSnFR] from 200 molecules/μm^2 coverslip to 1500 molecules/μm^2 (1μM) had a negligible effect on the modeled glutamate transients, indicating buffering by the sensor had little impact on the observed responses (Fig. 1.22). A three-fold increase in either transporter k_2 or U_{max} caused a precipitous drop in spillover glutamate during stimulation, while decreasing either caused a reciprocal increase in spillover (Fig. 1.22). Therefore, the model was most sensitive to the total internalization capacity of

glutamate by transporters. Our data do confirm that previously published estimates in a simple uptake model can reproduce our quantitative optical measurements of spillover glutamate dynamics. Furthermore, it suggests that the magnitude of glutamate spillover is highly sensitive to total uptake capacity.

Synaptic targeting

Constructs for synaptically targeted expression were made by overlap extension PCR. For neurexin, neuroligin, $NMDAR_{1\text{-}4}$, $NMDAR_{2A}$, and $mGluR_5$, reverse PCR primers coding the last ten amino acids of each protein sandwiched by the complement to the C-terminal tail of PDGFR and a *NotI* site were paired with a forward PDGFR primer. For -ETQV and –VSNL, only a four amino acid sandwich was used. Using these primer pairs, fragments consisting of truncated PDGFR with PDZ binding domain tail were generated by PCR. These fragments were digested with *PstI* and *Not I* and ligated into $GluSnFR_{8N0C}$ or SuperGluSnFR:pDisplay, replacing the existing truncated PDGFR.

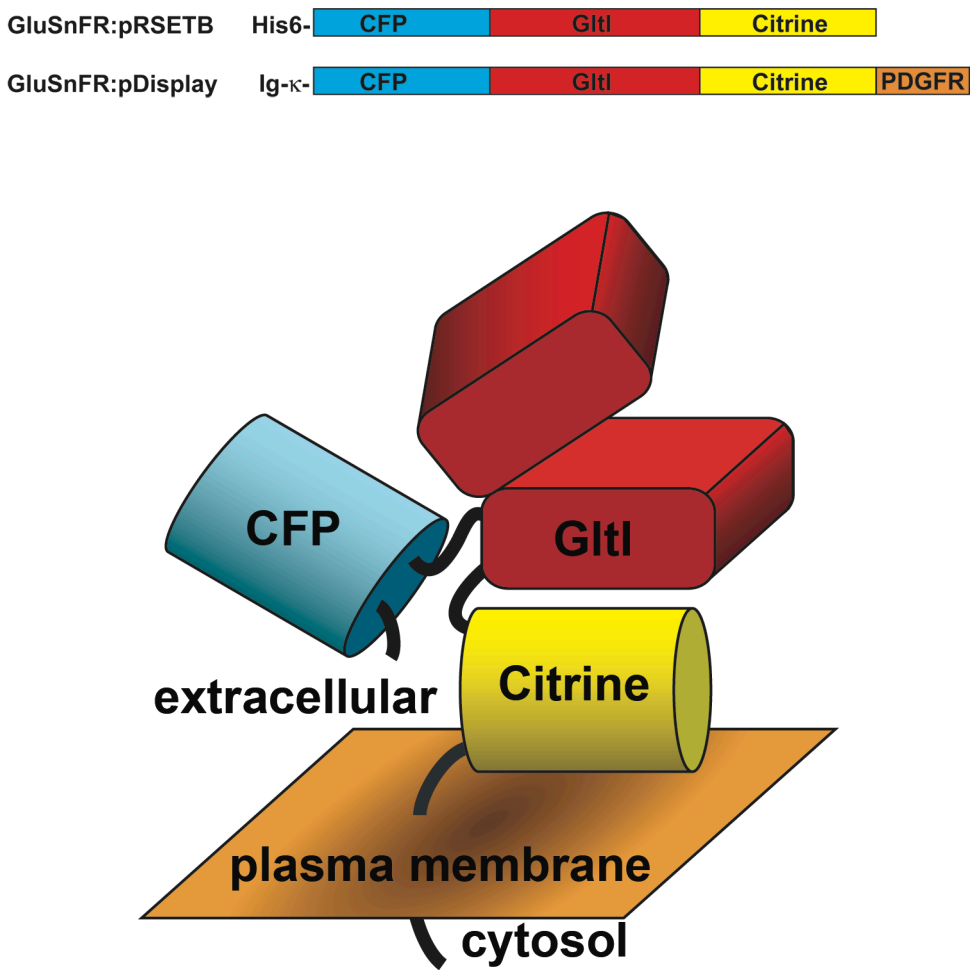

Figure 1.1 - Genetic construction of GluSnFR for protein purification (*top*, *above*) or mammalian cell surface display (*top*, *below)*. His6 is a hexahistidine protein purification tag. Ig-κ is a murine Ig κ-chain V-J2-C signal peptide. Schematic of surface displayed GluSnFR in ligand-free state (*bottom*).

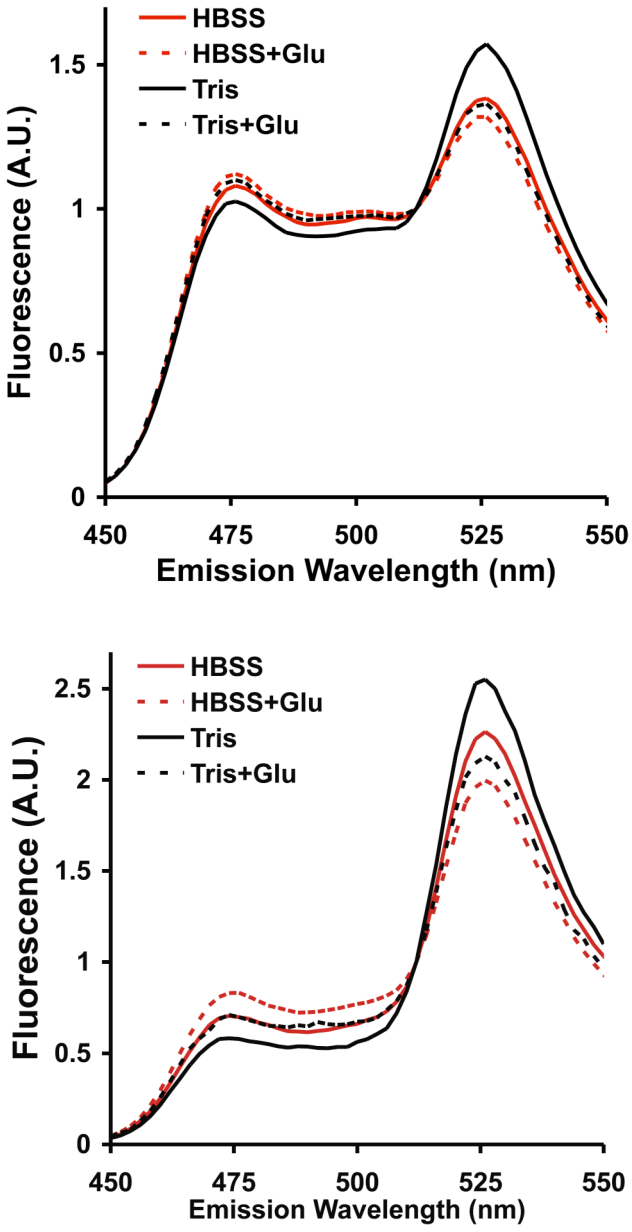

Figure 1.2 – *In vitro* emission spectra changes of soluble GluSnFR$_{0N0C}$ (*top*) or soluble GluSnFR$_{8N5C}$ (*bottom*) to 1mM glutamate in 50mM Tris buffer (*black*) or HBSS (*red*).

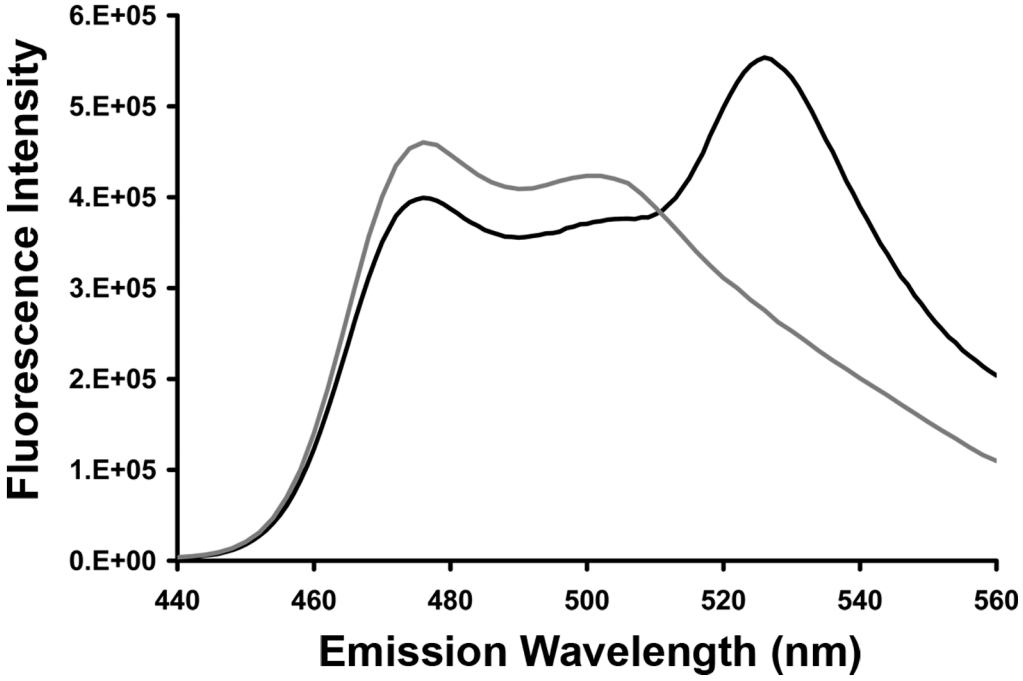

Figure 1.3 - Emission spectrum of soluble $GluSnFR_{0N0C}$ before and after digestion with trypsin. Excitation of 420nm.

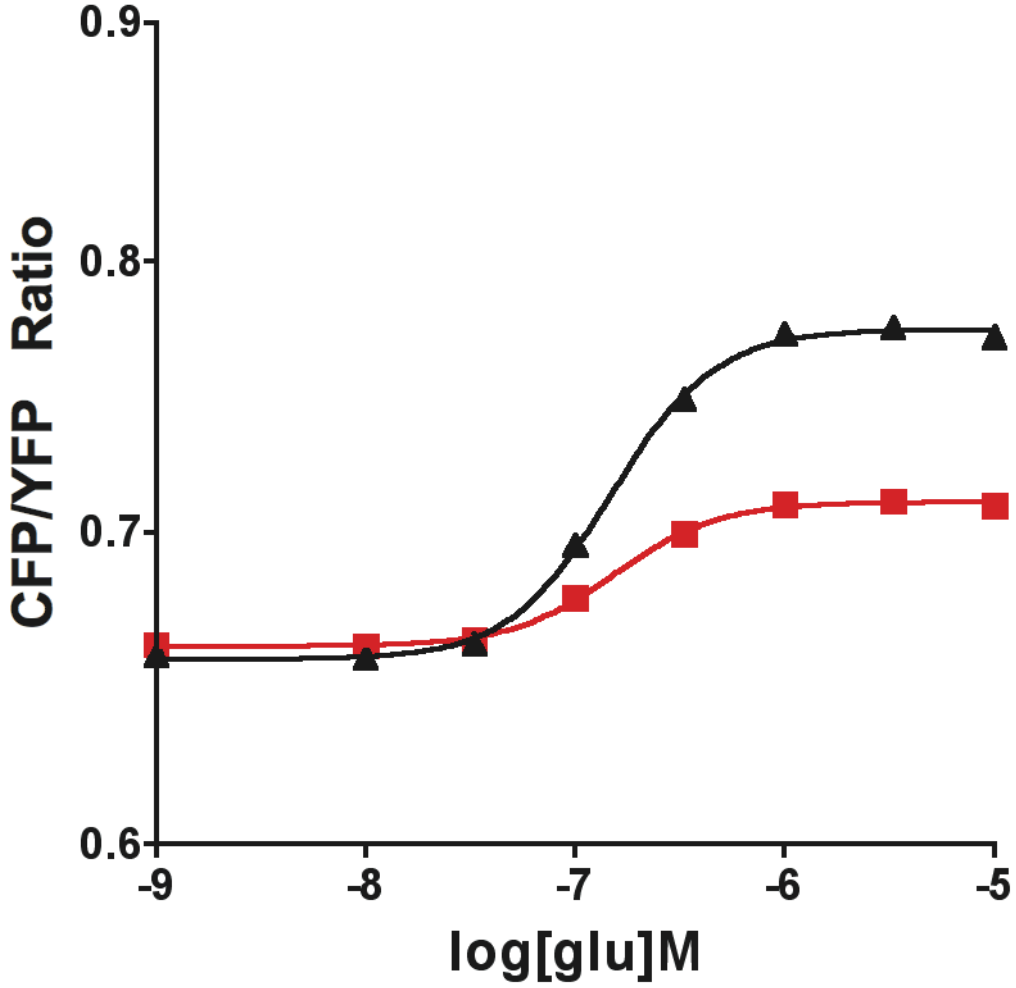

Figure 1.4 - Titration curves of soluble GluSnFR$_{0N0C}$ in 50mM Tris (*black triangle*) or HBSS (*red square*).

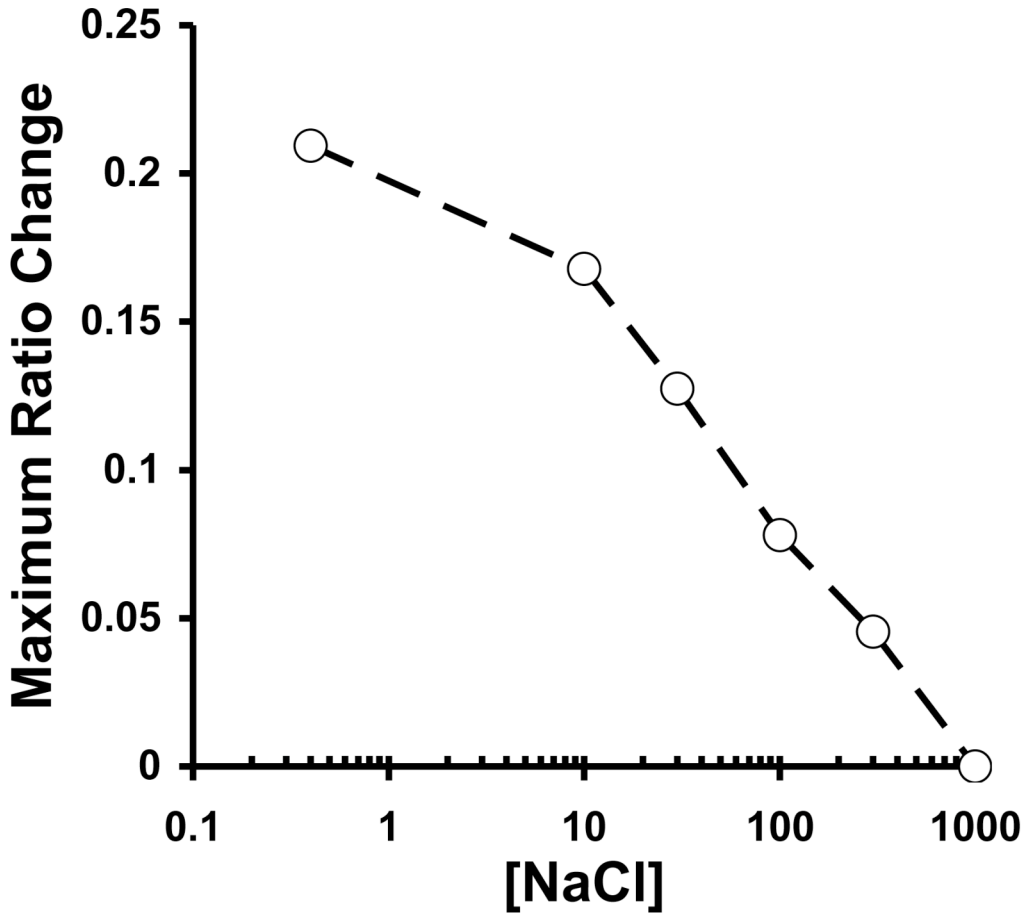

Figure 1.5 - Maximum ratio change of $GluSnFR_{0N0C}$ (*circle*) decreases with increasing ionic strength of buffer.

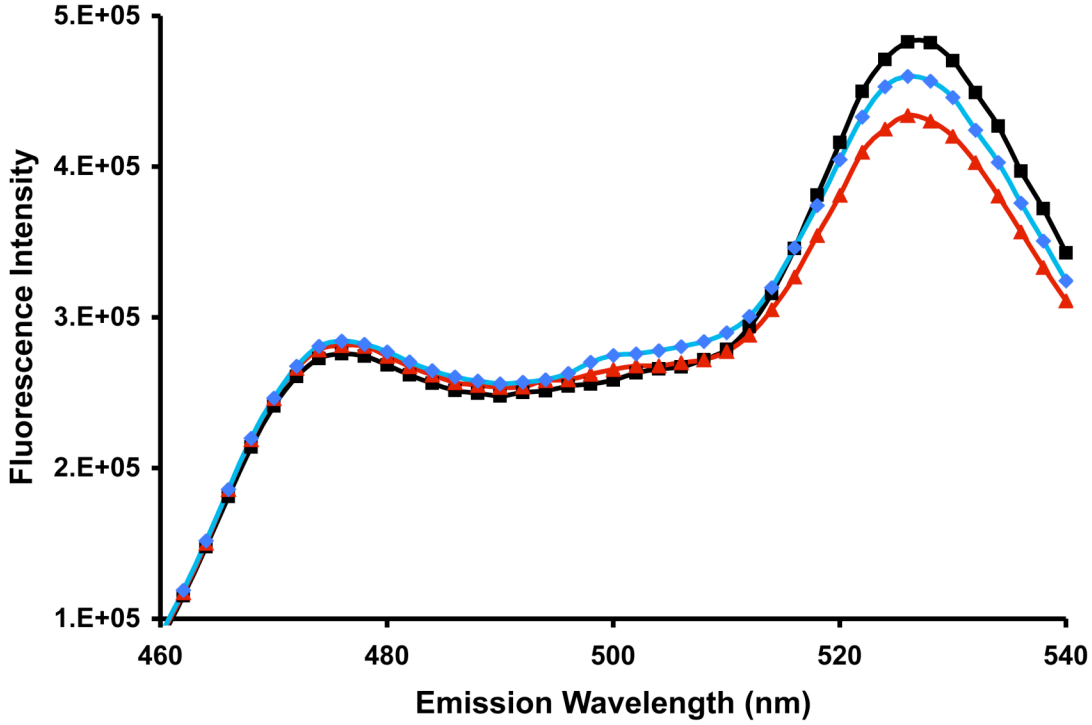

Figure 1.6 - Partial reversal of glutamate binding by conversion of glutamate to α-ketoglutarate. Glutamate-free (*black square*), *plus* 333nM [glutamate] (*red triangle*), after 10 minutes with enzyme (*blue diamond*).

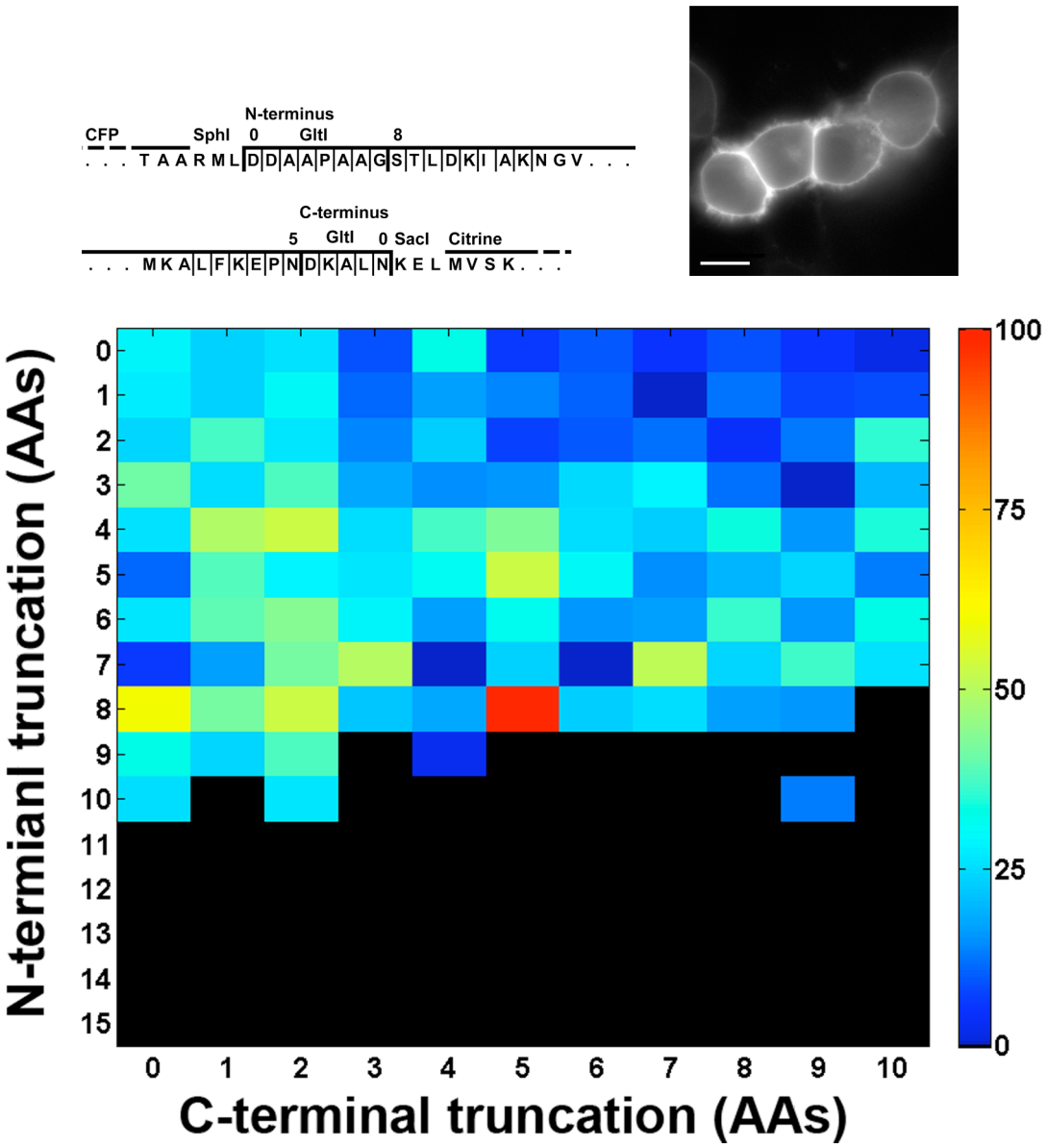

Figure 1.7 - Optimization of GluSnFR response on mammalian cell surface. Amino acid sequence of GltI N- (*top left, above*) and C-terminal (*top left, below*) truncations between CFP and Citrine. Truncation sites are indicated with thin vertical lines. The truncations for the original GluSnFR$_{0N0C}$ and best responding construct GluSnFR$_{8N5C}$ are noted in bold lines. FRET channel showing clean extracellular membrane expression on transfected HEK293 cells (*top right*). Scale bar indicates 10 microns**.** Map of the truncation combination to response magnitude (*bottom*). Color indicates the percent of maximal ratio change relative to GluSnFR$_{8N5C}$. Black indicates improper construct folding.

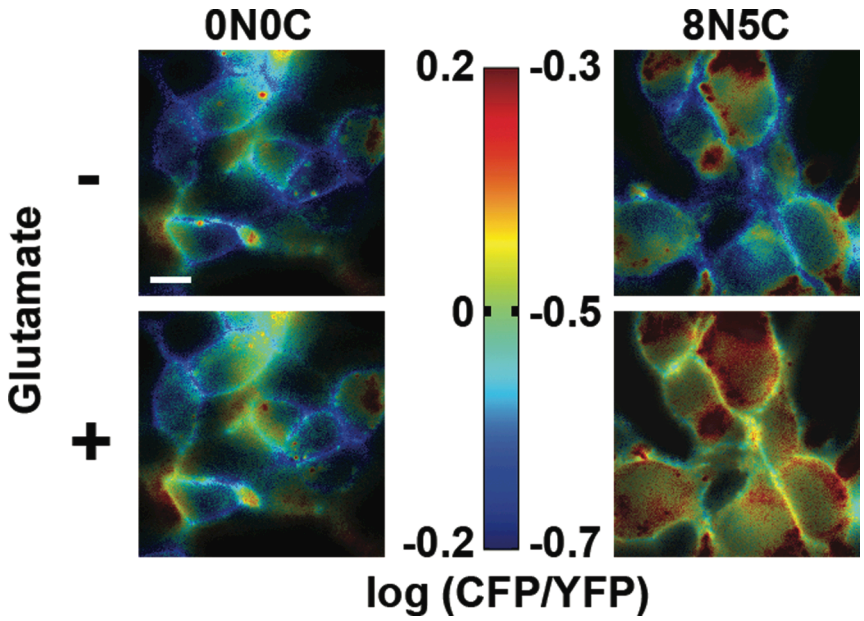

Figure 1.8 –HEK293T cells transfected with the non-optimized GluSnFR$_{0N0C}$ (*left*) or the best responder GluSnFR$_{8N5C}$ (*right*). Colorbar values encompass the same range of relative CFP/YFP change for both constructs. Scalebar is 10 microns.

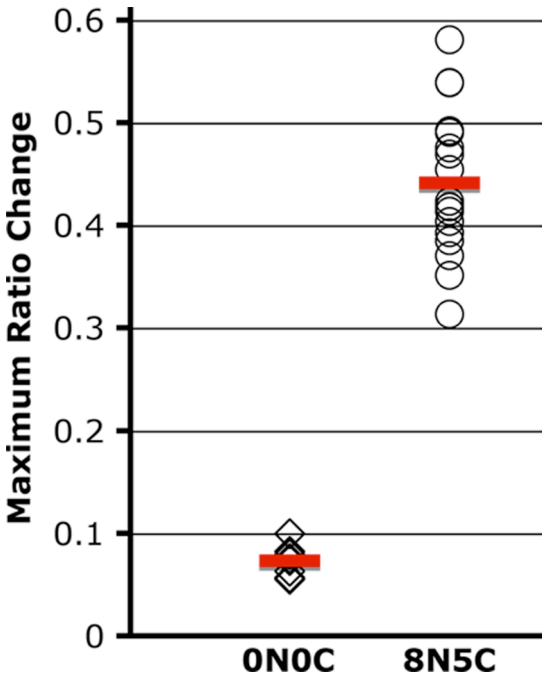

Figure 1.9 - Ratio change between glutamate free and 100uM glutamate solutions of HBSS for $GluSnFR_{0N0C}$ (n=9 fields), and $GluSnFR_{8N5C}$ (n=18).

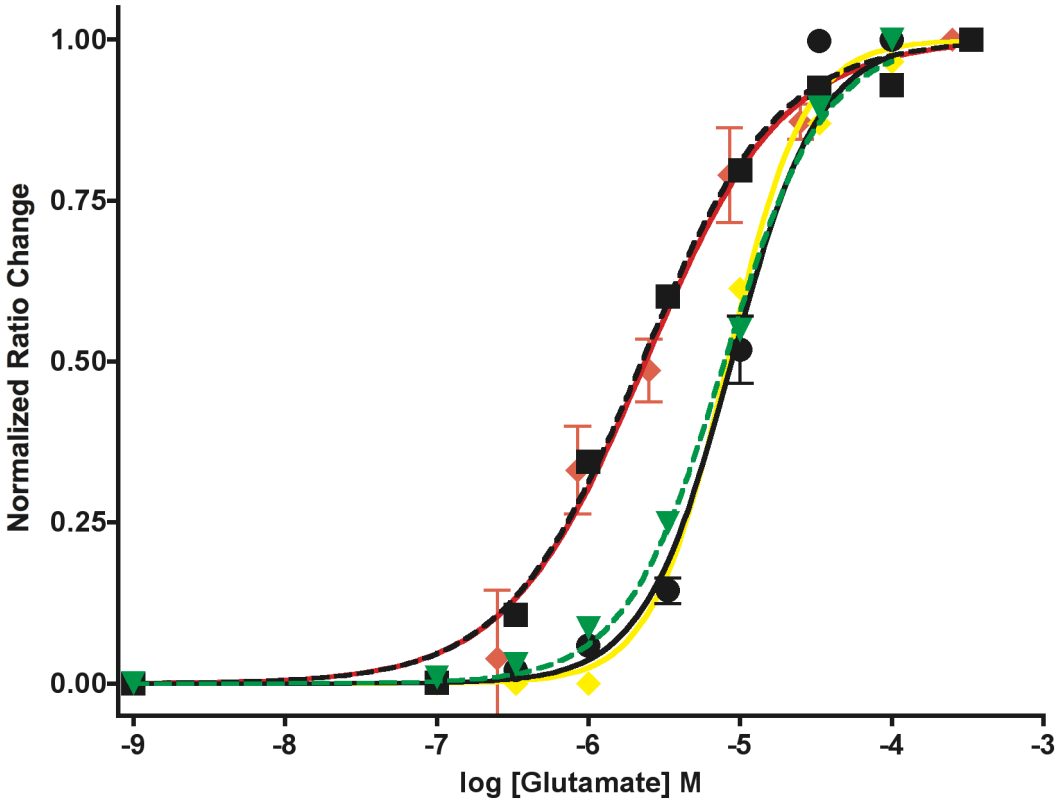

Figure 1.10 - Glutamate titration curves of HEK/HeLa cells in Ringer's (*squares, black dashed)*, neurons in Ringer's (*circles, black solid*), neurons adjusted with 2µM background glutamate (*triangle, yellow*), modeled apparent titration curves at 30 s after glutamate bath exchange (*green triangle, dotted*), and neurons in Ringer's plus 100µM TBOA (*diamonds, red*).

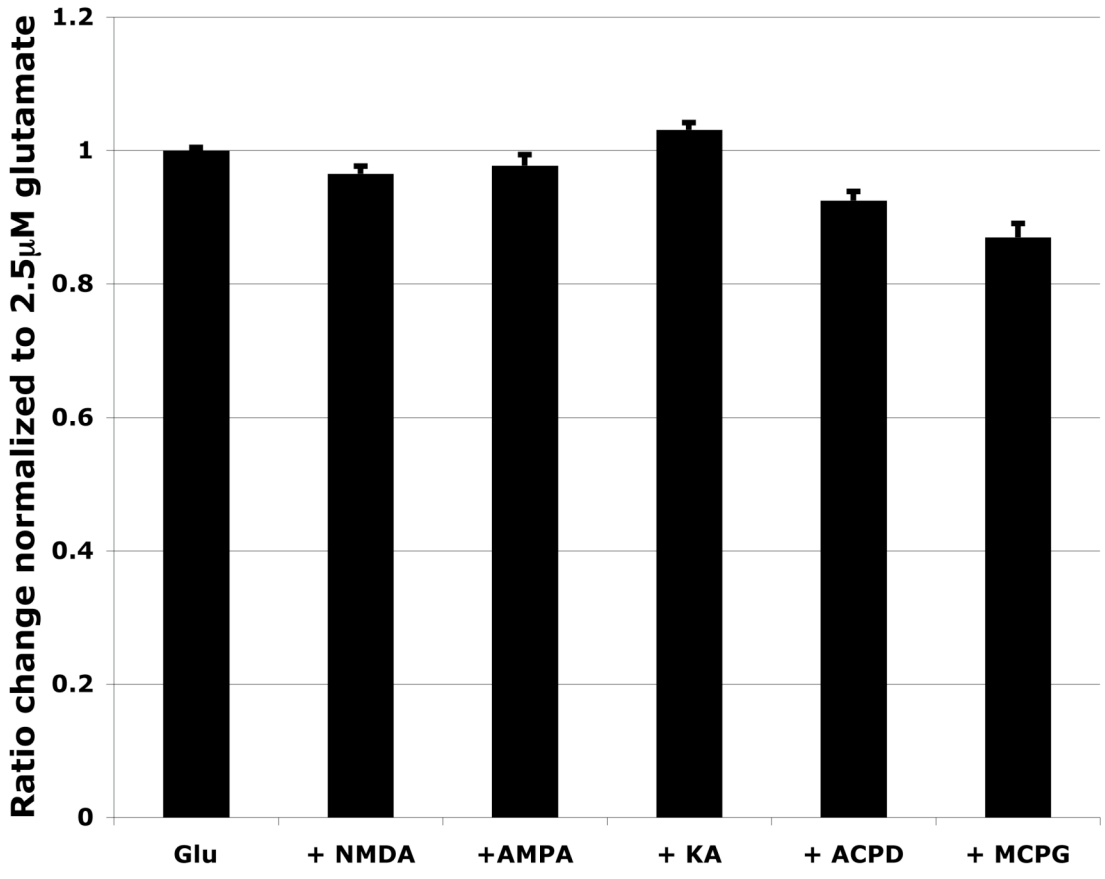

Figure 1.11 - Responses of GluSnFR to 2.5μM glutamate in the presence of 300μM NMDA, 100μM AMPA, 100μM KA, 25μM ACPD and 250μM MCPG normalized to the response to 2.5μM glutamate alone (n=4 fields per condition).

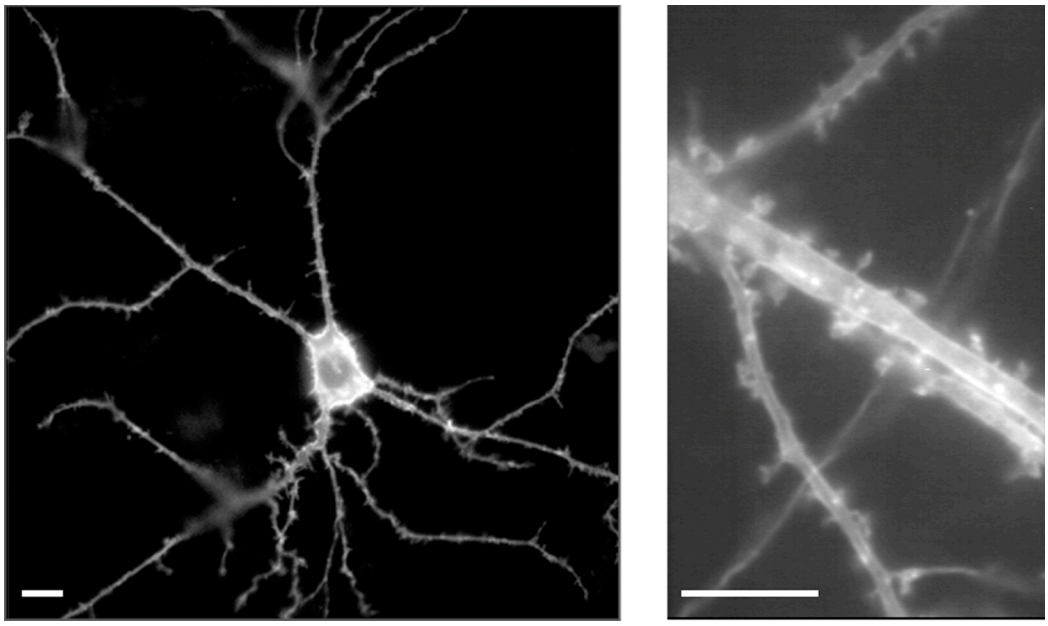

Figure 1.12 - FRET channel of SuperGluSnFR expressing neurons. Scale bars indicate 10 microns.

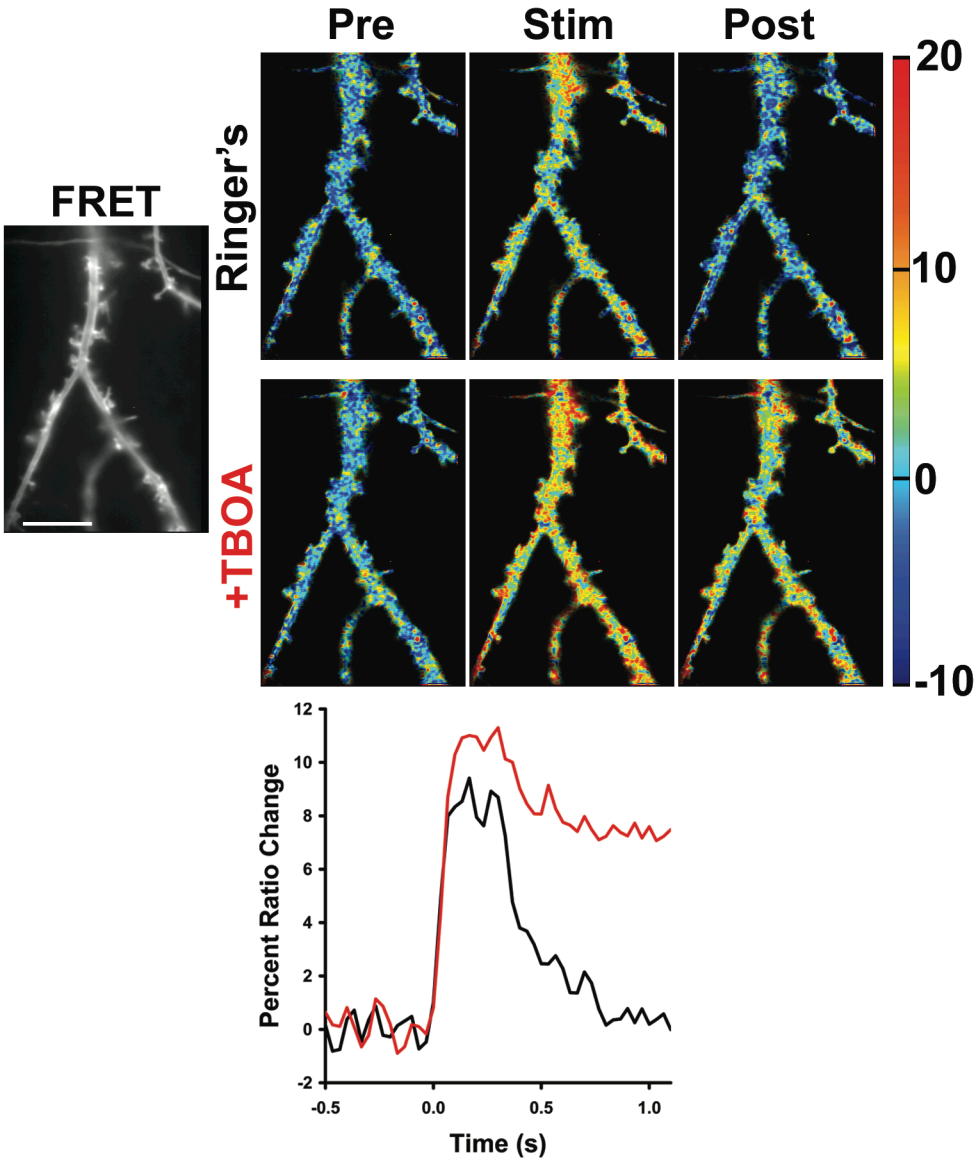

Figure 1.13 - Spatial resolution of glutamate measurement following synaptic release. FRET channel of SuperGluSnFR expressed on the dendritic surface imaged at 150x (*far left*). Scale bar = 10 microns. (*top*) Spatially resolved percent ratio change before (*left*), during (*middle*) and after (*right*) a 10AP, 30Hz field stimulus in Ringer's (*above*) and with 100µM TBOA added (*top*, *below*). Images are intensity-modulated, temporal averages of 10 frames indicated by bars above the traces in *4b*, spatially filtered with a 5 pixel wide (466nm eq.) 2-dimensional wiener filter to reduce noise. (*bottom*) Averaged ratio change across the total surface of the expressing neuron in *3a* in Ringer's (*black*) or with TBOA (*red*).

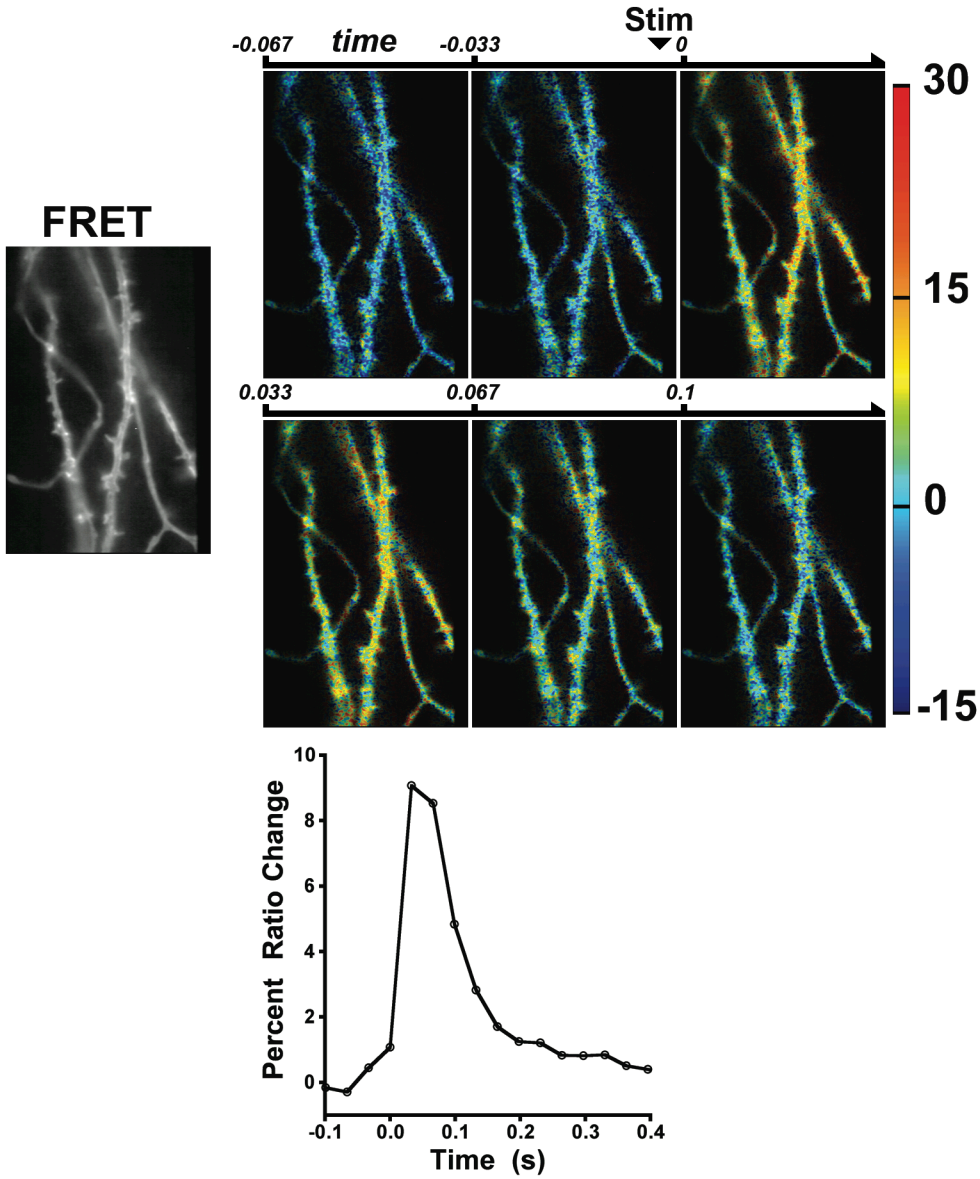

Figure 1.14 - Spatially resolved ratio change to average of 30 single AP stimuli. (*far left)* FRET as in *Figure 1.13*. Sequential frames of response *(top, above left* to *below right*) (33ms/frame). 1AP stimulation occurs with slight jitter between frame 2 and 3. Timecourse of spatially averaged dendritic response (*bottom*).

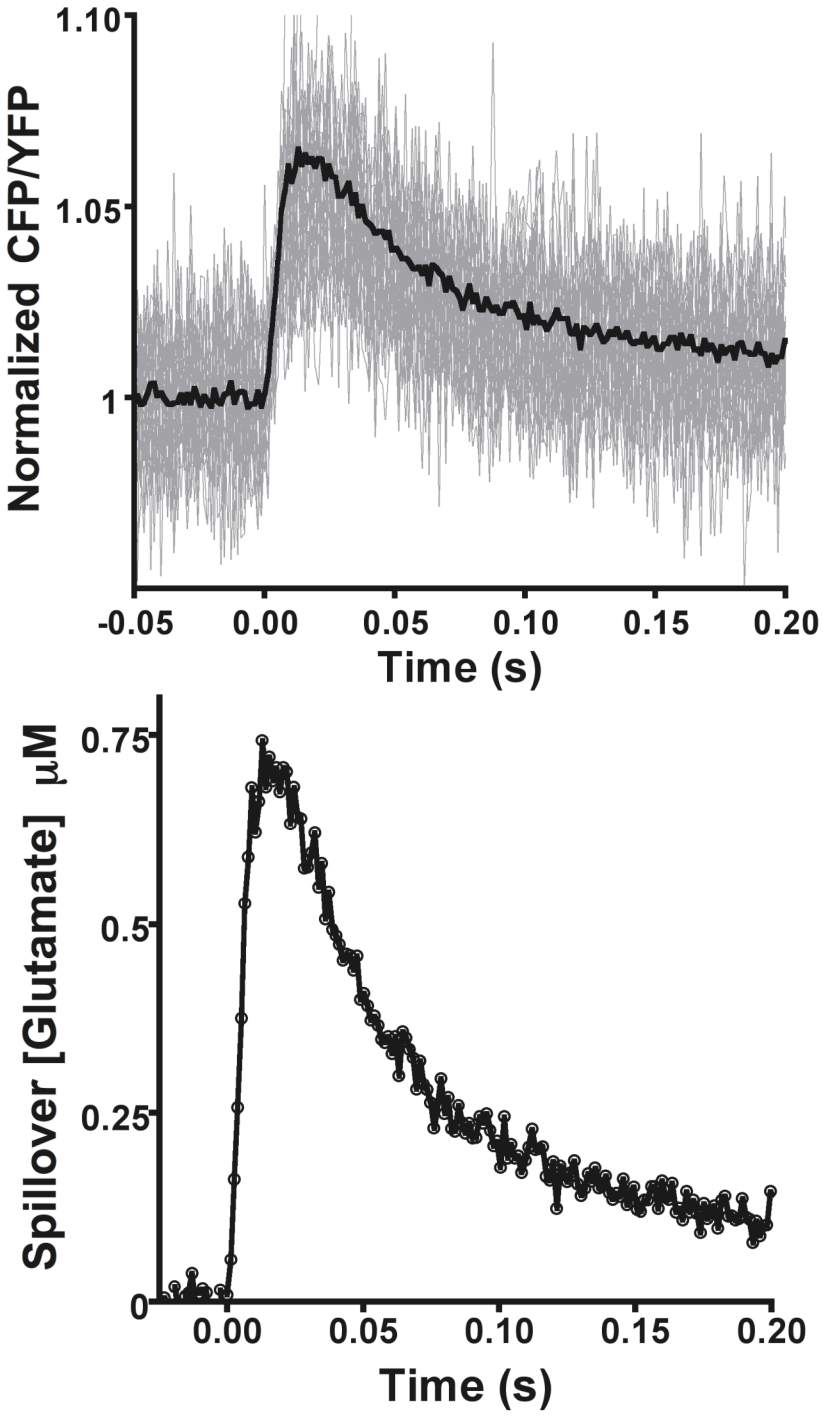

Figure 1.15 - Temporal resolution of SuperGluSnFR response. (*top*) Normalized CFP/YFP emission ratio of a SuperGluSnFR expressing dendritic arbor during single action potential field stimulus. Individual traces in *gray*, average in *black* (n=27). (*bottom*) Corresponding glutamate concentration measurements following calibration.

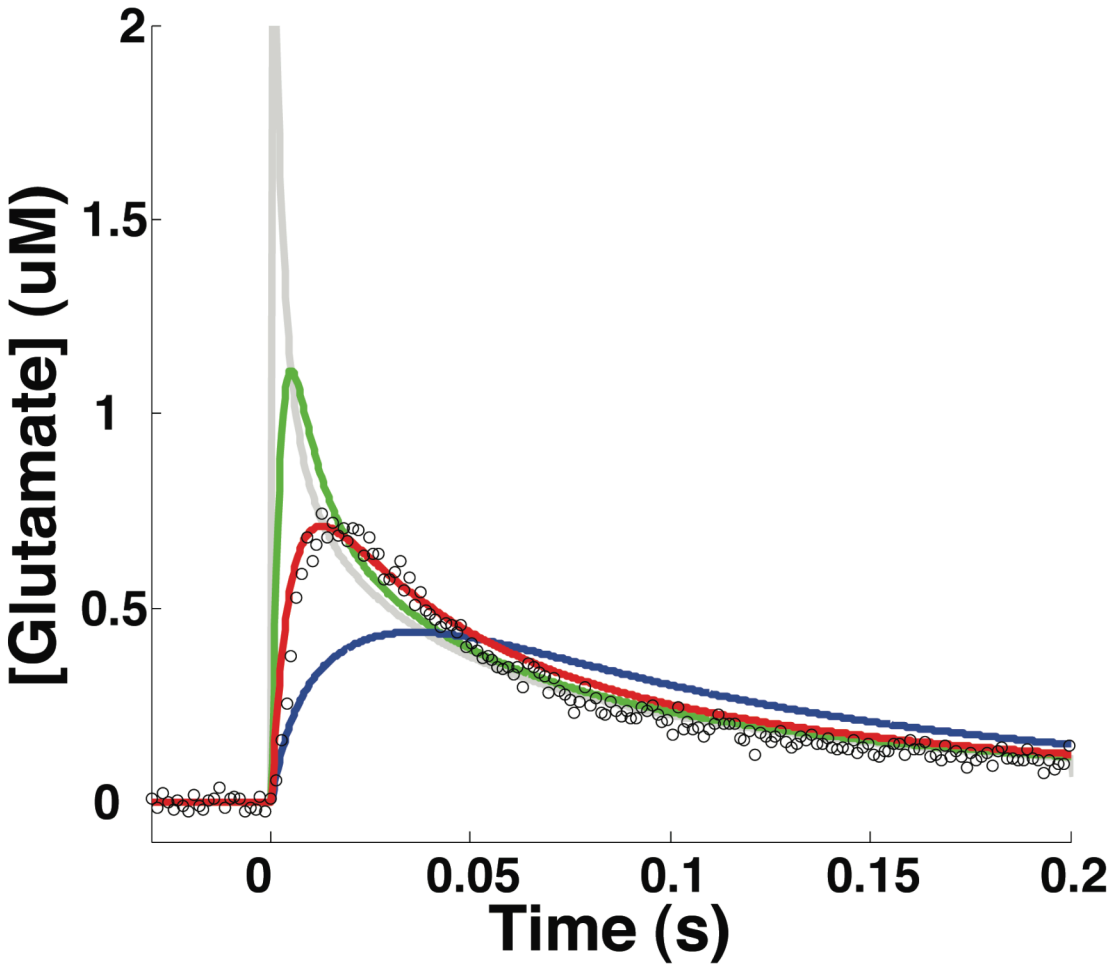

Figure 1.16 - Predicted SuperGluSnFR response to a homogeneously injected transient of 3μM [glutamate] (*gray*) with k_{on} and k_{off} of $9x10^7$ M^{-1} s^{-1} and 225 s^{-1} (*green*), $3x10^7$ M^{-1} s^{-1} and 75 s^{-1} (*red*), and $1x10^7$ M^{-1} s^{-1} and 25 s^{-1} (*blue*). Measured SuperGluSnFR response (*black circles*).

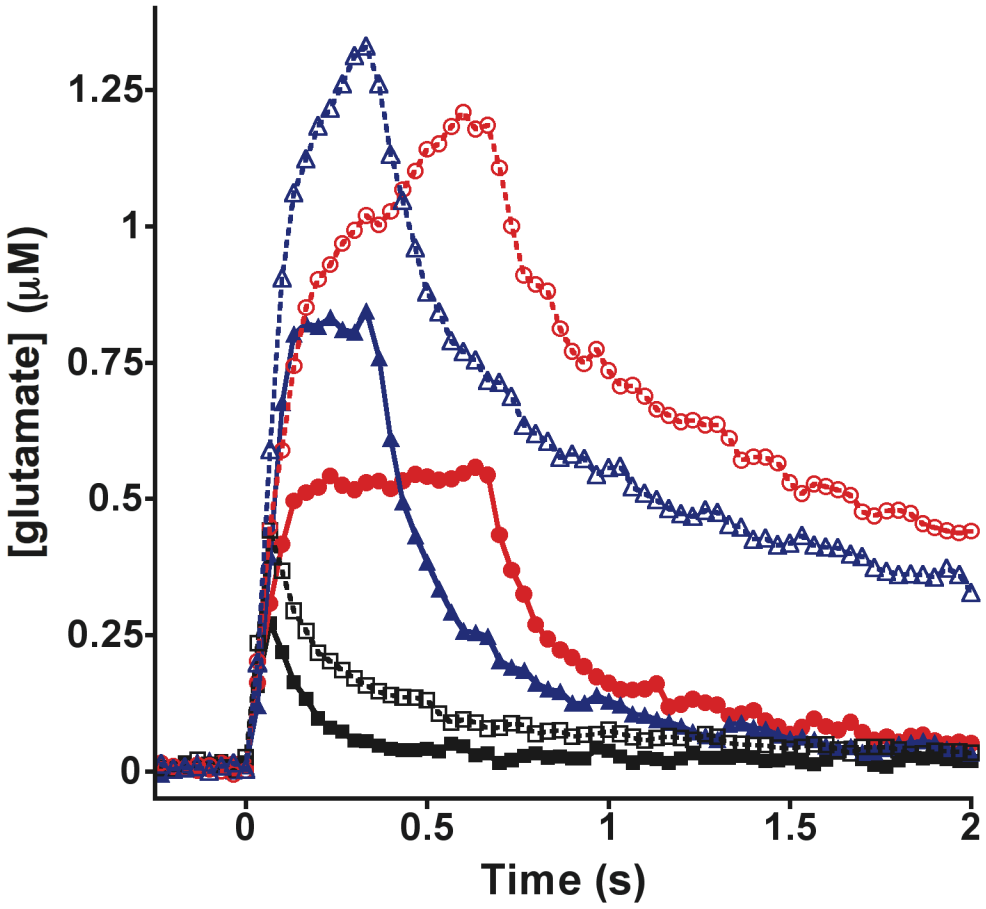

Figure 1.17 - Timecourse of glutamate release and uptake. Average responses to single AP (*black squares*), 10AP-15Hz (*red circles*) and 10AP-30Hz (*blue triangles*) field stimulation in Ringer's solution (*solid*) or with 100µM TBOA added (*open, dotted*) to block active glutamate uptake.

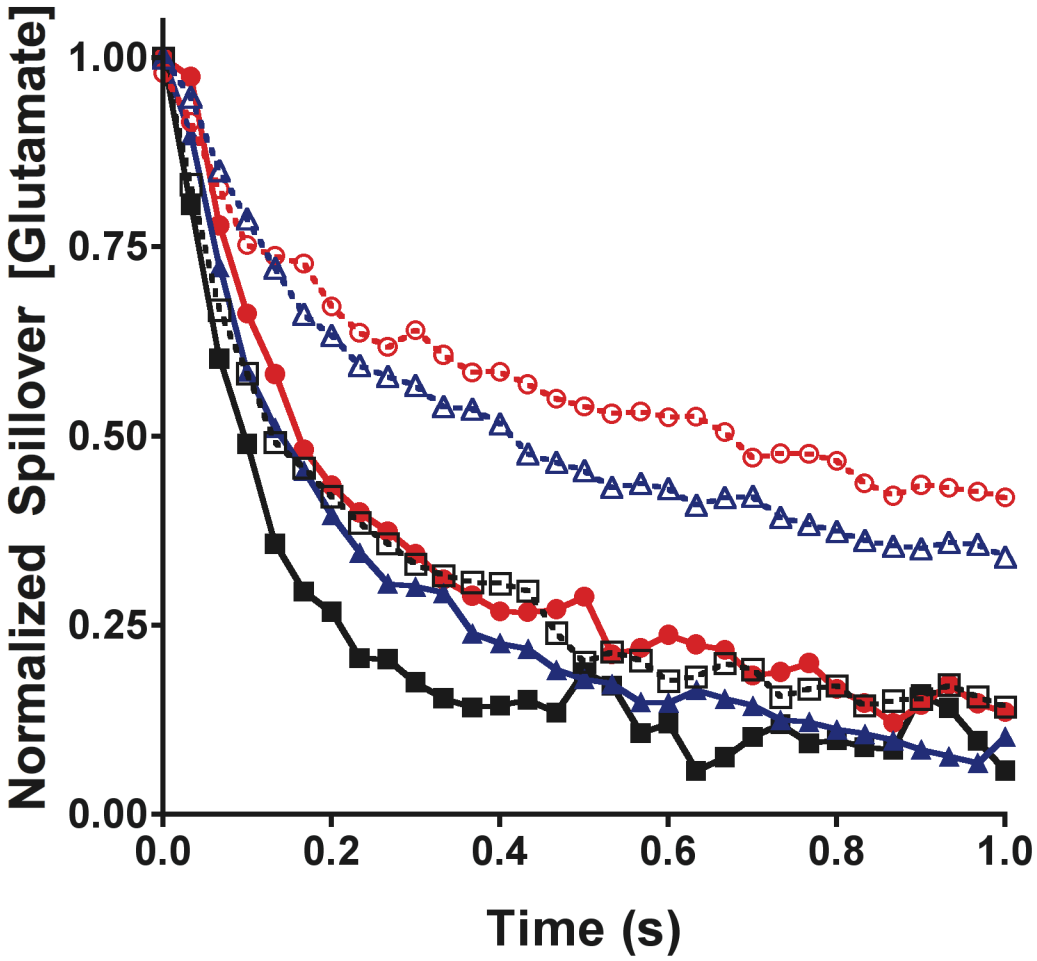

Figure 1.18 - The decay phase of *Figure 1.17* scaled to the maximum height to highlight the relative glutamate clearance rate. Colors indicate a single AP (*black squares*), 10AP-15Hz (*red circles*) and 10AP-30Hz (*blue triangles*) field stimulation in Ringer's solution (*solid*) or with 100μM TBOA added (*open, dotted*).

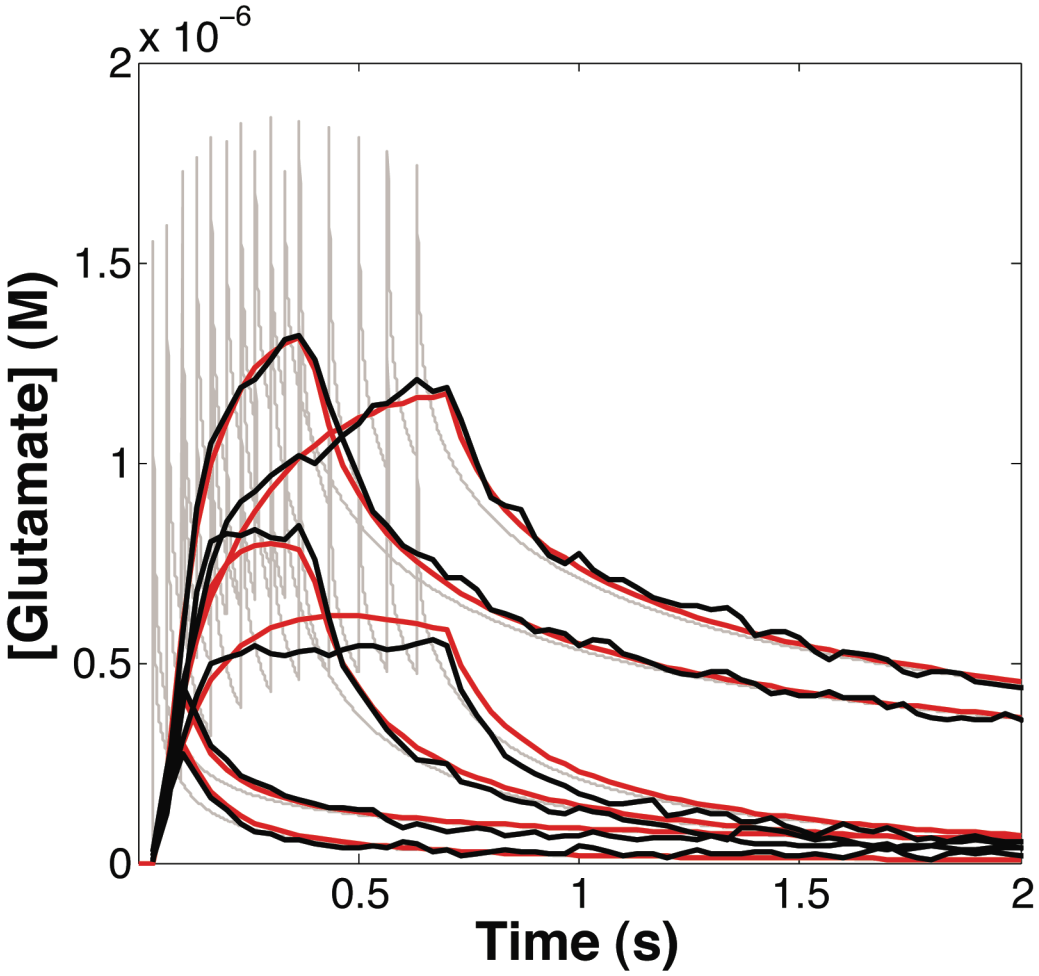

Figure 1.19 - Model of glutamate release, diffusion and reuptake. Glutamate levels in the plane of the neurons. Average SuperGluSnFR responses to field stimulation in Ringer's solution or in 100μM TBOA (*black*). Model of instantaneous glutamate levels in plane of neurons (*gray*). Model glutamate filtered by the camera integration (*red*).

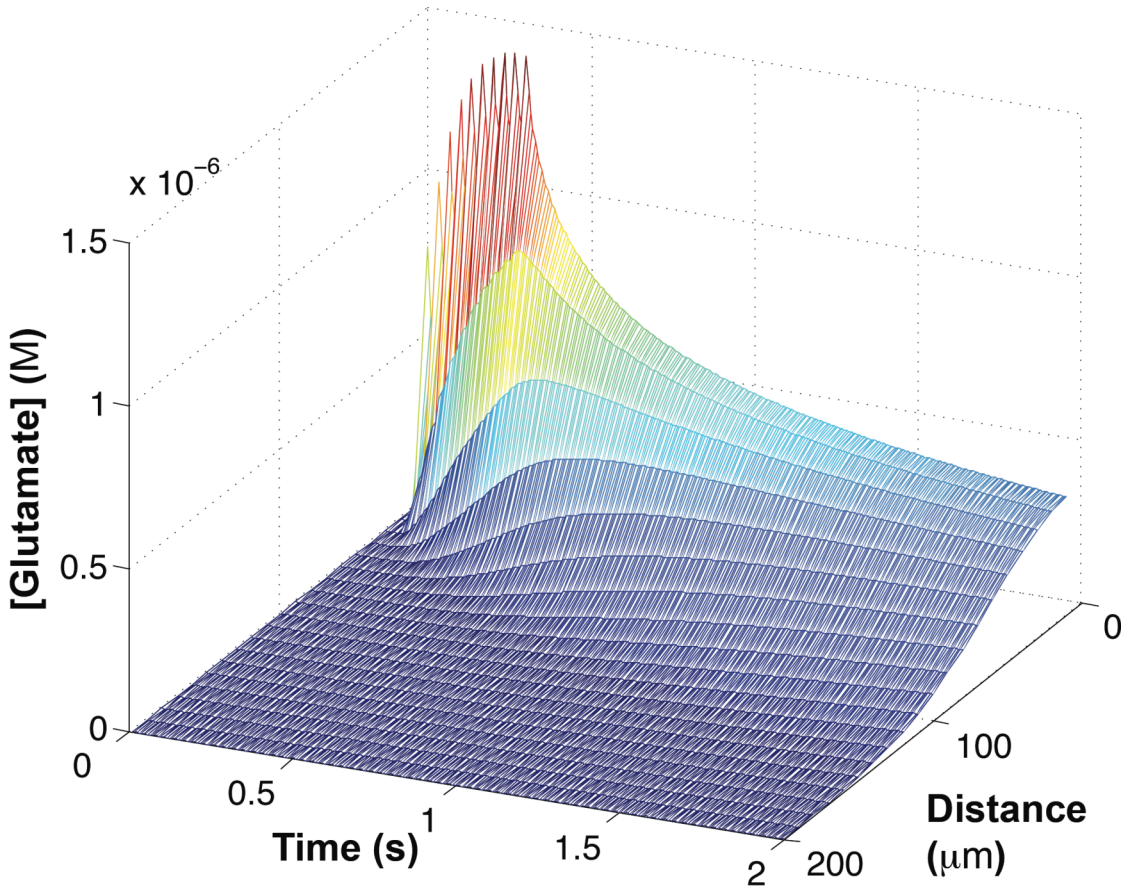

Figure 1.20 - Spatio-temporal profile of model glutamate following 10AP 30Hz stimulation in Ringer's with TBOA. Distance is measured from coverslip surface.

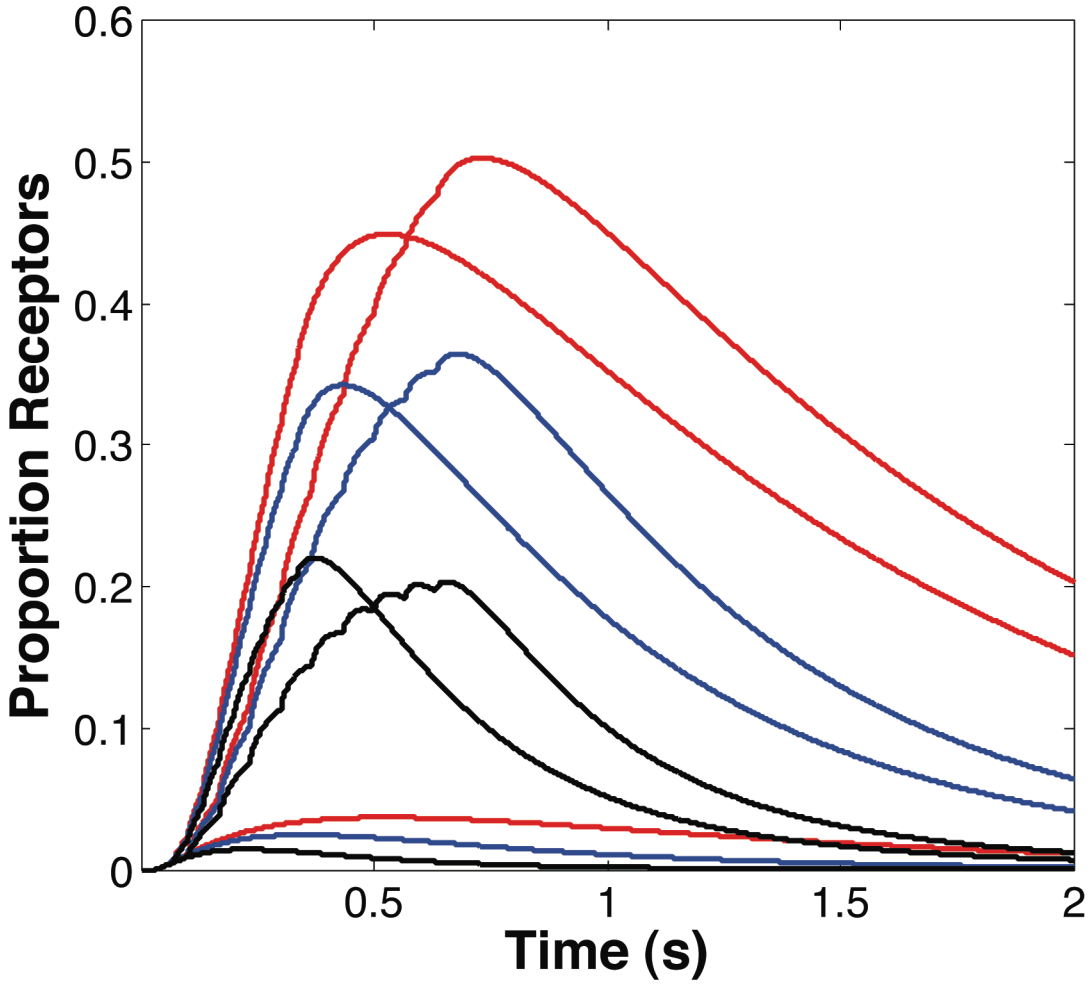

Figure 1.21 - Model of glutamate double-bound NR_{2A} (*black*), NR_{2B} (*blue*) and NR_{2D} (*red*) NMDA receptors in response to 1AP, 10AP-15Hz and 10AP-30Hz stimulation in Ringer's.

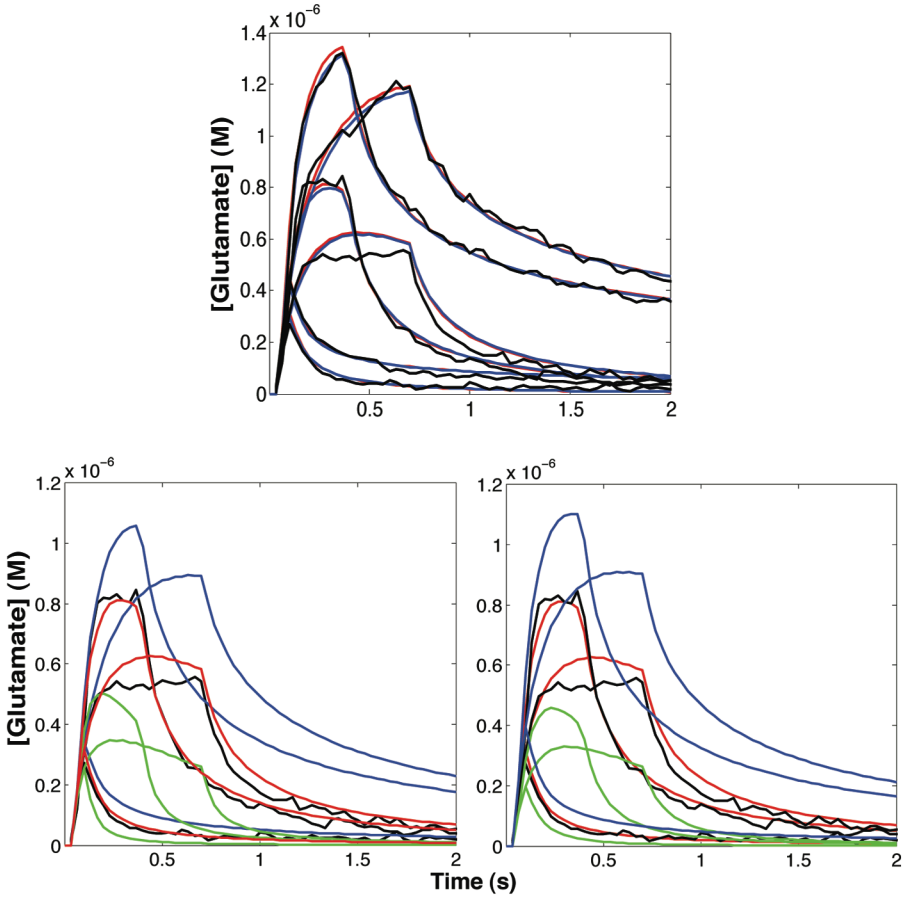

Figure 1.22 - Model Robustness Analysis. (*top*) Increasing [GluSnFR] from 200 (*red*) to 1500 (*blue*) molecules/μm^2 coverslip had no effect on modeled GluSnFR response. (*bottom left*) Varying the glutamate transporter internalization rate between 42 (*green*), 14 (*red*) and 4.3 (*blue*) molecules s^{-1} had a profound effect on spillover glutamate. (*bottom right*) Varying effective transporter concentration between 3.3μM (*blue*), 10μM (*red*) and 30μM (*green*) had a similar effect as *bottom right*.

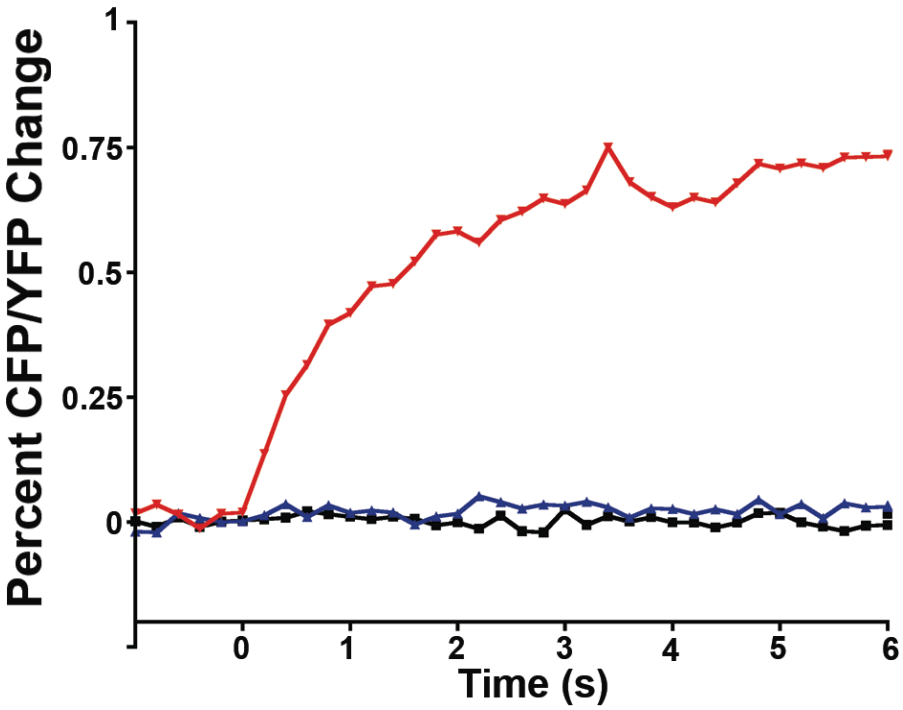

Figure 1.23 - Perfusion of GluSnFR neuron with 1μM [glutamate] (*red*), glutamate-free Ringer's (*blue*), vs. no perfusion (*black*).

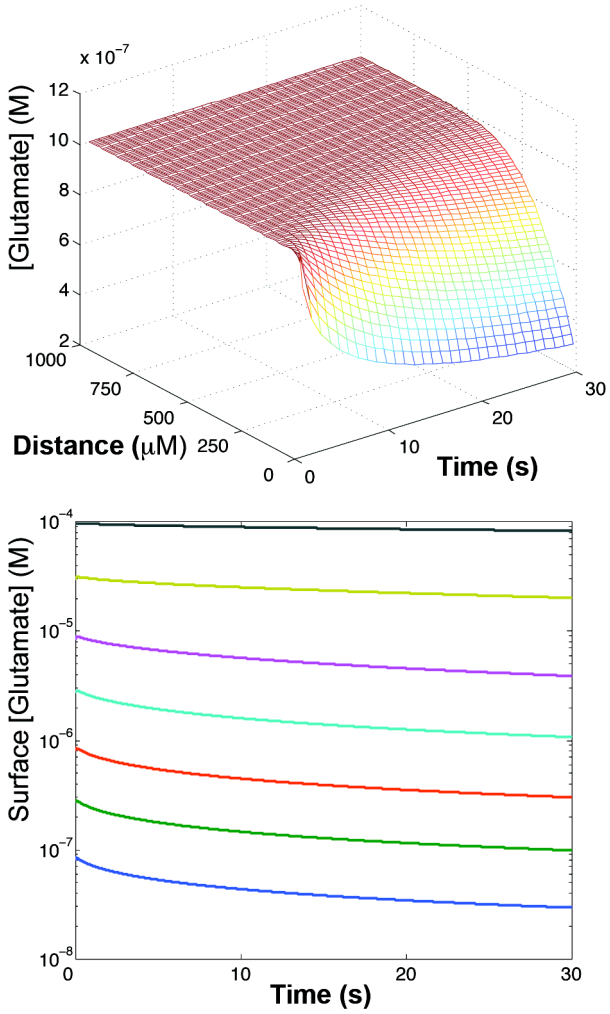

Figure 1.24 – (*top*) Modeled glutamate depletion following bath application of 10μM glutamate. Depletion is rapid and significant within the first 100μM from the neuronal plane. (*bottom*) Glutamate depletion at the coverslip surface for various initial concentrations of applied glutamate. Relative depletion is greater for smaller initial [glutamate] due to the decreased diffusive flux into the neuron-astrocyte plane.

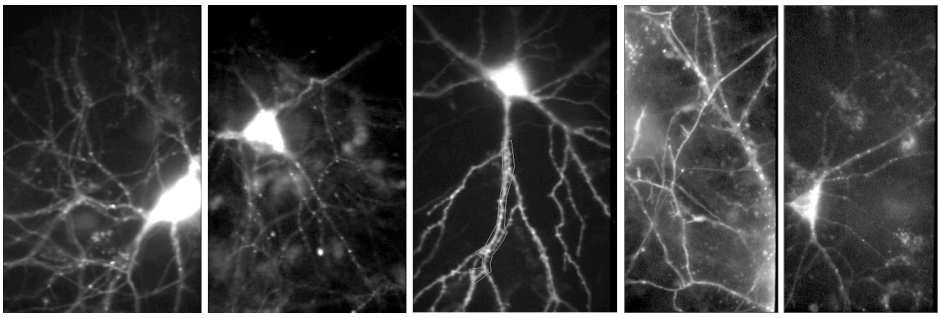

Figure 1.25 - Prototype synaptic targeting strategies – FRET emission of GluSnFR-pDisplay with C-terminal residues of neuroligin, $NMDAR_{1\text{-}4}$, $mGluR_5$, -ETQV, and –VSNL. All have diffuse expression with all but $mGluR_5$ showing punctate concentration of GluSnFR at sites resembling synapses.

Table 1.1 - State transitions and differential equations governing the glutamate diffusion, binding, and uptake model. Glutamate is modeled as one-dimensional diffusion from a homogeneous thin source. In the equations, *glu* is the extracellular glutamate; glu_{in} is intracellular glutamate; D is the diffusion coefficient; *t* is time; *x* is distance, U, G, $N_{2A,}$ N_{2B} and N_{2D} are the unliganded concentrations of glutamate transporters, GluSnFR, NMDA NR_{2A}, NR_{2B} and NR_{2D} receptors; U_{max}, G_{max}, $N_{2A:max,}$ $N_{2B:max}$ and $N_{2D:max}$ are the total concentration of transporters, GluSnFR, NR_{2A}, NR_{2B} and NR_{2D} receptors. Rate constants k_1, k_{-1} and k_2 are different for each reaction species. All components are homogeneously distributed in the neuronal plane.

$$\frac{\partial[glu]}{\partial t} = D\left\{\frac{\partial^2[glu]}{\partial x^2}\right\} + \left[k_{-1}(U_{\max} - U) - k_1 U[glu]\right] + \frac{dG}{dt} + \frac{dN_{2A}}{dt} + \frac{dN_{2B}}{dt} + \frac{dN_{2D}}{dt}$$

$$\frac{dU}{dt} = (k_{-1} + k_2)(U_{\max} - U) - k_1 U[glu] \qquad U + glu \underset{k_{-1}}{\overset{k_1}{\rightleftharpoons}} U : glu \xrightarrow{k_2} glu_{in} + U$$

$$\frac{dG}{dt} = k_{-1}(G_{\max} - G) - k_1 G[glu] \qquad G + glu \underset{k_{-1}}{\overset{k_1}{\rightleftharpoons}} G : glu$$

$$\frac{dN_{2A}}{dt} = k_{-1}(N_{2A:\max} - N_{2A}) - k_1 N_{2A}[glu] \qquad N_{2A} + glu \underset{k_{-1}}{\overset{k_1}{\rightleftharpoons}} N_{2A} : glu$$

$$\frac{dN_{2B}}{dt} = k_{-1}(N_{2B:\max} - N_{2B}) - k_1 N_{2B}[glu] \qquad N_{2B} + glu \underset{k_{-1}}{\overset{k_1}{\rightleftharpoons}} N_{2B} : glu$$

$$\frac{dN_{2D}}{dt} = k_{-1}(N_{2D:\max} - N_{2D}) - k_1 N_{2D}[glu] \qquad N_{2D} + glu \underset{k_{-1}}{\overset{k_1}{\rightleftharpoons}} N_{2D} : glu$$

References

1. Scanziani, M., Salin, P. A., Vogt, K. E., Malenka, R. C. & Nicoll, R. A. Use-dependent increases in glutamate concentration activate presynaptic metabotropic glutamate receptors. *Nature* **385**, 630-634 (1997).

2. Arnth-Jensen, N., Jabaudon, D. & Scanziani, M. Cooperation between independent hippocampal synapses is controlled by glutamate uptake. *Nat Neurosci* **5**, 325-331 (2002).

3. Lozovaya, N. A., Kopanitsa, M. V., Boychuk, Y. A. & Krishtal, O. A. Enhancement of glutamate release uncovers spillover-mediated transmission by N-methyl-D-aspartate receptors in the rat hippocampus. *Neuroscience* **91**, 1321-1330 (1999).

4. Vogt, K. E. & Nicoll, R. A. Glutamate and gamma-aminobutyric acid mediate a heterosynaptic depression at mossy fiber synapses in the hippocampus. *Proc Natl Acad Sci U S A* **96**, 1118-1122 (1999).

5. Isaacson, J. S. Glutamate spillover mediates excitatory transmission in the rat olfactory bulb. *Neuron* **23**, 377-384 (1999).

6. Szapiro, G. & Barbour, B. Multiple climbing fibers signal to molecular layer interneurons exclusively via glutamate spillover. *Nat Neurosci* **10**, 735-742 (2007).

7. Clements, J. D., Lester, R. A., Tong, G., Jahr, C. E. & Westbrook, G. L. The time course of glutamate in the synaptic cleft. *Science* **258**, 1498-1501 (1992).

8. Pasti, L., Zonta, M., Pozzan, T., Vicini, S. & Carmignoto, G. Cytosolic calcium oscillations in astrocytes may regulate exocytotic release of glutamate. *J Neurosci* **21**, 477-484 (2001).

9. Copenhagen, D. R. & Jahr, C. E. Release of endogenous excitatory amino acids from turtle photoreceptors. *Nature* **341**, 536-539 (1989).

10. Allen, T. G. The 'sniffer-patch' technique for detection of neurotransmitter release. *Trends Neurosci* **20**, 192-197 (1997).

11. Diamond, J. S., Bergles, D. E. & Jahr, C. E. Glutamate release monitored with astrocyte transporter currents during LTP. *Neuron* **21**, 425-433 (1998).

12. Pomerleau, F., Day, B. K., Huettl, P., Burmeister, J. J. & Gerhardt, G. A. Real time in vivo measures of L-glutamate in the rat central nervous system using

ceramic-based multisite microelectrode arrays. *Ann N Y Acad Sci* **1003**, 454-457 (2003).

13. Innocenti, B., Parpura, V. & Haydon, P. G. Imaging extracellular waves of glutamate during calcium signaling in cultured astrocytes. *J Neurosci* **20**, 1800-1808 (2000).

14. Okumoto, S. et al. Detection of glutamate release from neurons by genetically encoded surface-displayed FRET nanosensors. *Proc Natl Acad Sci U S A* **102**, 8740-8745 (2005).

15. Griesbeck, O., Baird, G. S., Campbell, R. E., Zacharias, D. A. & Tsien, R. Y. Reducing the environmental sensitivity of yellow fluorescent protein. mechanism and applications. *J Biol Chem* 29188-29194 (2001).

16. Nagai, T. et al. A variant of yellow fluorescent protein with fast and efficient maturation for cell-biological applications. *Nat.Biotechnol*. 87-90 (2002).

17. Deuschle, K. et al. Construction and optimization of a family of genetically encoded metabolite sensors by semirational protein engineering. *Protein Sci* **14**, 2304-2314 (2005).

18. Lakowicz, J. R. *Principles of Fluorescence Spectroscopy* (Kluwer Academic/Plenum Publishers, New York, 1999).

19. Baird, G. S., Zacharias, D. A. & Tsien, R. Y. Circular permutation and receptor insertion within green fluorescent proteins. *Proc Natl Acad Sci U S A* **96**, 11241-11246 (1999).

20. Nagai, T., Yamada, S., Tominaga, T., Ichikawa, M. & Miyawaki, A. Expanded dynamic range of fluorescent indicators for Ca(2+) by circularly permuted yellow fluorescent proteins. *Proc Natl Acad Sci U S A* 10554-10559 (2004).

21. Diamond, J. S. Deriving the glutamate clearance time course from transporter currents in CA1 hippocampal astrocytes: transmitter uptake gets faster during development. *J Neurosci* **25**, 2906-2916 (2005).

22. de Lorimier, R. M. et al. Construction of a fluorescent biosensor family. *Protein Sci* **11**, 2655-2675 (2002).

23. Miller, D. M. r., Olson, J. S., Pflugrath, J. W. & Quiocho, F. A. Rates of ligand binding to periplasmic proteins involved in bacterial transport and chemotaxis. *J Biol Chem* **258**, 13665-13672 (1983).

24. Murthy, V. N., Sejnowski, T. J. & Stevens, C. F. Heterogeneous release properties of visualized individual hippocampal synapses. *Neuron* **18**, 599-612 (1997).

25. Murthy, V. N., Schikorski, T., Stevens, C. F. & Zhu, Y. Inactivity produces increases in neurotransmitter release and synapse size. *Neuron* **32**, 673-682 (2001).

26. Schikorski, T. & Stevens, C. F. Quantitative ultrastructural analysis of hippocampal excitatory synapses. *J Neurosci* **17**, 5858-5867 (1997).

27. Barbour, B. & Hausser, M. Intersynaptic diffusion of neurotransmitter. *Trends Neurosci* **20**, 377-384 (1997).

28. Wadiche, J. I., Arriza, J. L., Amara, S. G. & Kavanaugh, M. P. Kinetics of a human glutamate transporter. *Neuron* **14**, 1019-1027 (1995).

29. Lehre, K. P. & Danbolt, N. C. The number of glutamate transporter subtype molecules at glutamatergic synapses: chemical and stereological quantification in young adult rat brain. *J Neurosci* **18**, 8751-8757 (1998).

30. Kutsuwada, T. et al. Molecular diversity of the NMDA receptor channel. *Nature* **358**, 36-41 (1992).

31. Ikeda, K. et al. Cloning and expression of the epsilon 4 subunit of the NMDA receptor channel. *FEBS Lett* **313**, 34-38 (1992).

32. Rizzo, M. A., Springer, G. H., Granada, B. & Piston, D. W. An improved cyan fluorescent protein variant useful for FRET. *Nat Biotechnol* **22**, 445-449 (2004).

33. Nguyen, A. W. & Daugherty, P. S. Evolutionary optimization of fluorescent proteins for intracellular FRET. *Nat Biotechnol* **23**, 355-360 (2005).

34. Pedelacq, J. D., Cabantous, S., Tran, T., Terwilliger, T. C. & Waldo, G. S. Engineering and characterization of a superfolder green fluorescent protein. *Nat Biotechnol* **24**, 79-88 (2006).

35. Diamond, J. S. & Jahr, C. E. Synaptically released glutamate does not overwhelm transporters on hippocampal astrocytes during high-frequency stimulation. *J Neurophysiol* **83**, 2835-2843 (2000).

36. Lozovaya, N. A. et al. Extrasynaptic NR2B and NR2D subunits of NMDA receptors shape 'superslow' afterburst EPSC in rat hippocampus. *J Physiol* **558**, 451-463 (2004).

37. Arriza, J. L. et al. Functional comparisons of three glutamate transporter subtypes cloned from human motor cortex. *J Neurosci* **14**, 5559-5569 (1994).

38. Schiller, J., Major, G., Koester, H. J. & Schiller, Y. NMDA spikes in basal dendrites of cortical pyramidal neurons. *Nature* **404**, 285-289 (2000).

39. Ariav, G., Polsky, A. & Schiller, J. Submillisecond precision of the input-output transformation function mediated by fast sodium dendritic spikes in basal dendrites of CA1 pyramidal neurons. *J Neurosci* **23**, 7750-7758 (2003).

40. Redish, A. D. et al. Independence of firing correlates of anatomically proximate hippocampal pyramidal cells. *J Neurosci* **21**, RC134 (2001).

41. Csicsvari, J., Hirase, H., Czurko, A. & Buzsaki, G. Reliability and state dependence of pyramidal cell-interneuron synapses in the hippocampus: an ensemble approach in the behaving rat. *Neuron* **21**, 179-189 (1998).

42. Behrens, C. J., van den Boom, L. P., de Hoz, L., Friedman, A. & Heinemann, U. Induction of sharp wave-ripple complexes in vitro and reorganization of hippocampal networks. *Nat Neurosci* **8**, 1560-1567 (2005).

43. Flusberg, B. A., Jung, J. C., Cocker, E. D., Anderson, E. P. & Schnitzer, M. J. In vivo brain imaging using a portable 3.9 gram two-photon fluorescence microendoscope. *Opt Lett* **30**, 2272-2274 (2005).

44. Takano, T. et al. Astrocyte-mediated control of cerebral blood flow. *Nat Neurosci* **9**, 260-267 (2006).

45. Zhang, J., Ma, Y., Taylor, S. S. & Tsien, R. Y. Genetically encoded reporters of protein kinase A activity reveal impact of substrate tethering. *Proc Natl Acad Sci U S A* 14997-15002 (2001).

46. Heim, R. & Tsien, R. Y. Engineering green fluorescent protein for improved brightness, longer wavelengths and fluorescence energy transfer. *Current Biology* **6**, 178-182 (1996).

47. Sawano, A. & Miyawaki, A. Directed evolution of green fluorescent protein by a new versatile PCR strategy for site-directed and semi-random mutagenesis. *Nucleic Acids Research* E78 (2000).

48. Bekkers, J. M. & Stevens, C. F. Excitatory and inhibitory autaptic currents in isolated hippocampal neurons maintained in cell culture. *Proc Natl Acad Sci U S A* **88**, 7834-7838 (1991).

49. Jiang, M., Deng, L. & Chen, G. High Ca(2+)-phosphate transfection efficiency enables single neuron gene analysis. *Gene Ther* **11**, 1303-1311 (2004).

50. Grynkiewicz, G., Poenie, M. & Tsien, R. Y. A new generation of Ca_2+_ indicators with greatly improved fluorescence properties. *J Biol Chem* **260**, 3440-3450 (1985).

51. Benveniste, H., Drejer, J., Schousboe, A. & Diemer, N. H. Elevation of the extracellular concentrations of glutamate and aspartate in rat hippocampus during transient cerebral ischemia monitored by intracerebral microdialysis. *J Neurochem* **43**, 1369-1374 (1984).

Acknowledgements

Chapter One, in part, has been submitted for publication of the material as it may appear in Proceedings of the National Academy of Sciences, 2008, Hires S. Andrew; Zhu, Yongling; Tsien, Roger Y. The dissertation author was the primary author on this work. Yongling Zhu participated in many of the neuronal experiments, participated in numerous discussions on experimental direction and design and put forth the majority of the effort preparing and maintaining the neuronal cultures.

Chapter Two

Application of GluSnFR imaging to studies of Long-Term Potentiation

Abstract

Long-term potentiation of synaptic strength (LTP) is the leading candidate mechanism for the physical encoding of learning and memory. The localization of LTP to the pre- or postsynaptic side of the synapse has been a subject of much debate. Since the quantity of glutamate release in response to an electrical stimulus is the physical correlate of presynaptic strength, glutamate imaging could provide a direct measurement of presynaptic strength. We attempt to optically detect LTP of glutamate release in hippocampal cell culture. A chemical LTP induction paradigm using brief application of glycine in magnesium-free bath solution causes presynaptic potentiation of 37% of neurons tested. This potentiation is blocked by the NMDA receptor antagonist AP5. Limited electrophysiological recording shows the LTP induction technique causes a consistent increase in miniEPSC size, but a reduction in frequency. These results validate GluSnFR as a useful tool in the study of long-term potentiation

Introduction

Although individual thoughts may be ephemeral, storage of these thoughts requires a long-lasting physical change in the brain's microcircuitry. The mechanisms underlying physical encoding of learning and memory have been a source of speculation, study and dispute for over a century[1]. One of the most promising candidate mechanisms for the encoding of learning is the phenomenon of long-term potentiation (LTP), an activity-dependent strengthening of synaptic efficacy. LTP can be rapidly induced, is protein-synthesis dependent, and provides a mechanism of cellular change based on the association of cause and effect[2]. It satisfies the Hebbian

theory that, “When an axon of cell A is near enough to excite a cell B and repeatedly or persistently takes part in firing it, some growth process or metabolic change takes place in one or both cells such that A's efficiency, as one of the cells firing B, is increased.”[3] Recently, *in vivo* behavioral tests have shown that inhibitory avoidance training mimics and occludes LTP induction in brain slices of trained animals[4], supporting its physiological relevance.

The possible mechanisms of synaptic strengthening during LTP include, but are not limited to, an increase in presynaptic vesicle release probability[5,6], an increase in postsynaptic AMPA receptor surface expression[7] and changes in AMPAR subtype expression or phosphorylation state[8]. Evidence has been presented for the locus of LTP expression on the presynaptic[9,10] or postsynaptic[11] side of hippocampal synapses in cell culture and of Schaffer collateral synapses in slice[8]. However, the relative contributions of each component have been difficult to conclusively separate by electrophysiological recording due to the need to measure glutamate release indirectly as current through postsynaptic receptors or transporters. Direct imaging of glutamate release with GluSnFRs would isolate the presynaptic component and allow quantification of the relative contributions of pre and postsynaptic processes to LTP.

Results

Although more removed from the *in vivo* environment than hippocampal slice, dissociated cell culture provides excellent access for optical imaging and GluSnFR gene introduction. However, electrical induction of LTP in dissociated culture is difficult to achieve, likely due to heterogeneity of cultured cell types and their

connectivity. Therefore we used a chemical LTP induction paradigm adapted from Lu et al[12]. Their primary method was a 3-minute application of 100μM glycine in a [Mg^{2+}]-free Ringer's solution, in the continuous presence of 1μM strychnine, 20μM bicuculline and 0.5μM TTX. This was reported to induce a long lasting, NMDAR-dependent potentiation of spontaneous mini EPSC amplitude and frequency. This increase in amplitude indicates an increase in postsynaptic strength. The increase in frequency could be caused by increases in presynaptic release probability, but could also be due to postsynaptic strengthening of subthreshold synapses, raising these above the noise floor. The method was reported to cause insertion of AMPARs into the postsynaptic membrane, but the study did not exclude simultaneous presynaptic potentiation.

To assess if the glycine LTP also caused an increase in presynaptic release, we measured the responses of $GluSnFR_{8N0C}$ and VAMP-pHluorin before and after glycine application. Initial experiments using a slightly modified induction protocol gave promising responses. Since we needed to see electrically evoked synaptic release, we omitted TTX from the bath. We also included strychnine only in the glycine-containing LTP induction solution. For GluSnFR imaging, trains of 20 action potentials at 20Hz were recorded before and at intervals after glycine application. $GluSnFR_{8N0C}$ responses consistently showed a dramatic increase, peaking at 10 minutes after glycine washout, and then decayed slowly over the next 20 minutes, remaining above the pre-glycine baseline (Fig. 2.1). SynaptopHluorin responses were also enhanced to a more modest extent relative to the pre-glycine control (Fig. 2.2). However, the potentiation of GluSnFR response was not blocked by including 50μM

of the NMDAR antagonist AP5 to the bath solution (Fig. 2.3). This NMDAR independent potentiation was contrary to results reported in the initial publication of the technique[12]. Co-application of the use-dependent NMDAR channel blocker MK-801 with glycine also did not block the potentiation.

Following these promising, but confusing results, we switched our gene introduction method from calcium phosphate transfection to viral transformation. calcium phosphate transfection had given inconsistent and low yields of transfected neurons. In some cases, less that one neuron per coverslip had sufficient expression of GluSnFR following calcium phosphate transfection. Lentivirus[13] and a modified Sindbis virus[14] with reduced toxicity were constructed containing the $GluSnFR_{8N0C}$:pDisplay coding sequence. Sindbis gave much higher fluorescence upon infection relative to lentivirus, required only 24 hours to reach high expression, and could consistently transduce the majority of neurons without acute cell death. However, experiments with Sindbis virus transfection failed to show increases in GluSnFR responses to glycine application. As a positive control, we tried an alternative chemical LTP induction protocol of 15 minutes bath application of Sp-cAMPS to $GluSnFR_{8N0C}$, which was reported to strongly potentiate presynaptic release[15,16]. This also failed to generate significant potentiation at 30, 60 and 90 minutes post-application.

We were concerned that despite the reduced toxicity of the Sindbis strain we were using, the hijacking of cellular protein synthesis machinery by the virus still might interfere with LTP expression. Therefore, we returned to calcium phosphate as the gene delivery method, but used a newly published, modified protocol[17]. This

method gave more consistent, higher yields of high expressing cells typically between 5-10% of plated neurons. Back in this system, we performed several control experiments for glycine LTP. Most significantly, we separated the strychnine application from the glycine pulse. To our disappointment, a 3-minute pulse of 0.5μM strychnine potentiated the GluSnFR response and occluded potentiation from subsequent application of glycine (Fig. 2.4). Since strychnine is a blocker of extrasynaptic GABA receptors, we reasoned its presence in the bath sensitized the circuitry, leading to reverberant network excitation. Unlike in glutamate spillover experiments, we did not include NBQX or APV in the solutions for fear of blocking the glycine-mediated induction. Perhaps the continued potentiation that we saw was due to incomplete washout of strychnine from the bath.

We changed our LTP induction protocol to more closely resemble the method reported by Lu et al. Rather than include strychnine only with the glycine pulse, we maintained it with bicuculline in the bath at all times. To reduce possible activity-dependent depression or run-down of the response, the test stimulus of 20AP @ 20Hz was reduced to 10AP @ 20Hz. We then tested glutamate responses at 2-minute intervals before LTP induction and at 2-10 minute intervals for 40 minutes after induction. Only a subset of neurons showed a presynaptic potentiation. Of 27 cells tested, 10 showed a long-lasting increase in electrically-evoked ratio change of 10% or more. The majority of other neurons remained unchanged, with several actually losing apparent presynaptic strength (Fig. 2.5). Although the LTP response was less reliable than our initial experiments, it was properly behaved. Bath changes mimicking the LTP application, but without glycine (n=8), or with glycine and 50μM AP5

together (n=5) both failed to show any potentiation (Fig. 2.5). Of the neurons that potentiated following glycine application, the average potentiation was a 40% increase that lasted for at least 40 minutes (Fig. 2.6). However, if all glycine-applied neurons were averaged, no significant potentiation was seen (Fig. 2.6). The full timecourse is truncated as experiments were stopped after 30 minutes if no potentiation was observed. Responses tended to run down, due to sensor bleaching or other means. Cultures that had no glycine applied, or had AP5 applied concurrently with glycine were reduced to around 80% of initial response following 50 minutes of imaging and stimulation (Fig. 2.7).

In order to corroborate our measurements of presynaptic LTP and to check if the glycine-induced cells underwent a postsynaptic potentiation, we attempted to do whole cell-patch clamp of GluSnFR expressing neurons with simultaneous imaging of optical glutamate responses. Our first goal was to observe the same glycine-induced potentiation of mini EPSCs as reported in the literature. Unfortunately, following dozens of attempts to patch cultured neurons, only three were able to be held for 30 minutes or more with steady access resistance through perfusion of regular bath and LTP-inducing solutions. Of these three cells, each showed a long-lasting increase in spontaneous mini EPSC amplitude following application (Fig. 2.8). However, unlike published reports, we saw a decrease rather than increase in miniEPSC frequency (Fig. 2.9). With the small sample size and inconsistency with published results, our electrophysiology data was inconclusive.

Since chemical LTP induction was unreliable in our hands and the physiological relevance of dissociated neuronal culture was low, pilot experiments

using organotypic hippocampal slices were performed. After three days of incubation following initial brain slicing, organotypic cultures were infected with $GluSnFR_{8N0C}$ virus and incubated overnight. Although culture and infection conditions were sub-optimal, several GluSnFR expressing neurons could be found. Puffing of 100μM glutamate onto the surface of the neuron produced a transient 8% increase in CFP/YFP ratio, without background subtraction (Fig. 2.10). This demonstrated that the increased difficulty of imaging in organotypic slices would not prevent them from being used as an improved system for assessing the presynaptic component of LTP.

Discussion

The results of chemical LTP induction were mixed. In the Lu publication, 100% of recorded cells that maintained steady holding currents and access resistance were reported to undergo long-term potentiation. However, other groups have found this glycine LTP induction stimulus to be ineffective[18]. We saw only 37% of induced cells undergo a long lasting potentiation of the glutamate response. If chemical LTP in culture were to continue as the experimental paradigm, a number of improvements must be made. Given the relatively small margin of the optical glutamate response size above the noise floor, more precise measurement of the glutamate response would raise the confidence that presynaptic LTP occurred in a subset of neurons. Since SuperGluSnFR (8N5C) has an 80% greater ratio change to a given glutamate concentration than $GluSnFR_{8N0C}$, use of SuperGluSnFR would greatly increase the signal to noise ratio. Reducing light intensity and the number of APs in a test stimulus,

while increasing the number of stimuli per timepoint would also increase the precision of the glutamate response measurement.

In the early studies, the anomalously large potentiation following transient strychnine application may have been due to a persistent enhancement of recurrent excitation. Future experiments must apply test pulses only in the presence of NBQX and AP5 to prevent recurrent excitation from distorting the direct glutamate response size. As an additional positive control, 50μM forskolin could be applied in conjunction with IBMX or rolipram, phosphodiesterase inhibitors. This treatment was reported to induce large (100-200%) presynaptic potentiation (sEPSC and mEPSC frequency, eEPSC amplitude) in hippocampal slices[6] and slice cultures[19].

If glycine-mediated LTP of mini EPSCs can be convincingly demonstrated using whole-cell patch clamp, then field stimulation-evoked responses should be tested. In the absence of TTX, short action potential trains could be delivered by a bipolar stimulating electrode lowered into the chamber while responses are electrically and optically recorded. Measurement of the covariance of the optical and electrical signals could segregate the pre- and postsynaptic LTP components. Recording baseline from a SuperGluSnFR neuron held in voltage clamp would begin in Ringer's solution containing 2mM Ca^{++}, 1.3mM Mg^{++}, strychnine, bicuculline, NBQX and AP5 for 10 minutes, with test electrical stimuli every two minutes. Then, LTP inducing Mg^{++}-free Ringer's with 100μM glycine would be washed in for 3 minutes. After 5 minutes of washout to the original bath, spontaneous mini EPSCs would be recorded continuously and evoked release will be recorded at two-minute intervals until the cell is lost. Comparison of miniEPSC amplitude, evoked optical and electrical responses

could determine the relative contribution of release probability and postsynaptic sensitivity to the potentiation of the evoked EPSC.

Measuring presynaptic LTP by GluSnFR imaging of acute hippocampal slices is attractive because this retains closer ties to the *in vivo* preparation and can be induced by classical electrical stimulation paradigms. However, it also presents significant additional challenges of imaging and gene expression. Preliminary studies testing the response of $GluSnFR_{8N0C}$ under two-photon excitation were not promising. The sensor's signal/noise ratio and resistance to bleaching was significantly impaired, presumably due to direct excitation of the citrine chromophore, imperfect filter sets and higher energy photochemistry. This may be improved by using SuperGluSnFR instead. Rather than using two-photon excitation, confocal imaging of the Schaffer collateral synapse may result in slower bleaching rates. However, the best imaging solution may be to use conventional wide-field epifluorescence microscopy over a large section of the CA1 region that has undergone focal *in utero* electroporation of SuperGluSnFR[20]. This would gather the signal from tens to hundreds of GS6 expressing cells, increasing signal/noise while preventing possible toxic effects of viral expression. Alternatively, organotypic hippocampal cultures could be prepared and SuperGluSnFR introduced by gene gun, electroporation or virus. However, culturing slices may increase the difficulty of LTP induction

Conventional tetanic stimulation of the stratum radiatum[21] and CA1 field recording would be used to induce and quantify total LTP. Changes in the optical response to CA3 stimulation would quantify the presynaptic component of LTP. Performing paired electrical field recording and optical imaging of the mossy fiber

area of hippocampus before and after tetanic stimulation could provide a positive control for optical detection of presynaptic long-term potentiation, as its presence at that synapse is not disputed[22].

Materials and Methods

Neuronal preparation and imaging

Dissociated hippocampal neuronal preparation and optical imaging was performed as in Chapter One. $GluSnFR_{8N0C}$:pDisplay with the S73T affinity mutation was introduced to cells by three primary methods. The first was calcium phosphate transfection following the protocol of Greenberg[23]. Secondly, we applied 1μL of $GluSnFR_{8N0C}$ Sindbis virus to 18mm coverslips. We later used an improved calcium phosphate precipitation method that yielded significantly high transfection efficiency[17]. The critical difference between calcium phosphate protocols was the incubation of coverslips in media preequilibrated to a 10% CO_2 environment to dissolve precipitate prior to washing and replacement in the original culture media.

Organotypic hippocampal cultures were prepared similarly to as previously described[24]. After 3 days, small volumes of $GluSnFR_{8N0C}$ Sindbis virus were focally injected into the CA1 region using glass microelectrodes attached to a 1mL syringe. Cells were imaged on a Zeiss Axioskop upright microscope with a 40x Olympus dipping objective, custom beam splitter with CFP/YFP filter sets (Optical Insights), and a PentaMAX CCD camera (Princeton Instruments). Neurons were bathed in Ringer's and perfused with 100μM glutamate to assess GluSnFR function.

Virus production

To make the $GluSnFR_{8N0C}$ Sindbis virus, a pSinrep5 vector containing the nsP2 ser mutant and helper plasmids were acquired from Andres Jeromin. The coding sequence $GluSnFR_{8N0C}$:pDisplay was subcloned into this mutant pSinRep5 vector. Recombinant Sindbis virus was generated according to the manufacturer's instructions

(Invitrogen). Briefly, RNA was transcribed from pSinrep5 and the DH-BB helper using the mMessage Machine kit (Ambion). These two RNAs were electroporated into BHK-21 cells (ATCC), and recombinant virus particles were harvested 48h after electroporation. Titer experiments on dissociated neurons showed that 1μL of non-concentrated viral media per 18mm coverslip was ideal for transforming a majority of neurons with high expression and low toxicity. Experiments on dissociated cultures were performed 20-28h post-infection.

Electrophysiology and LTP induction

Whole-cell patch recordings of neurons were made 14-17 days after plating. Patch electrodes had a tip resistance of 3-6MΩ. Recordings were performed at room temperature. The series resistance varied from 8-15MΩ, which was uncompensated. Cells with significant drift in series resistance were discarded. Electrical traces were sampled at 20kHz and recorded using pClamp10 (Molecular Devices). The patch electrode solution contained 140mM CsCl, 2.5mM EGTA, 2mM $MgCl_2$, 10mM HEPES, 2mM TEA and 4mM ATP (pH 7.30). In field stimulation experiments, the bath solution contained 140mM NaCl, 2mM $CaCl_2$, 5mM KCl, 25mM HEPES, 33mM glucose, 1μM strychnine and 20μM bicuculline (pH 7.4), with osmolarity of 325-335 mOsm. During initial experiments, strychnine was only included in the glycine LTP induction solution. For mini recording experiments, the bath was supplemented with 0.5μM TTX. To induce LTP, cells were perfused for three minutes with bath solution supplemented with 100μM glycine. Spontaneous miniEPSCs were identified and averaged by hand using custom MATLAB routines.

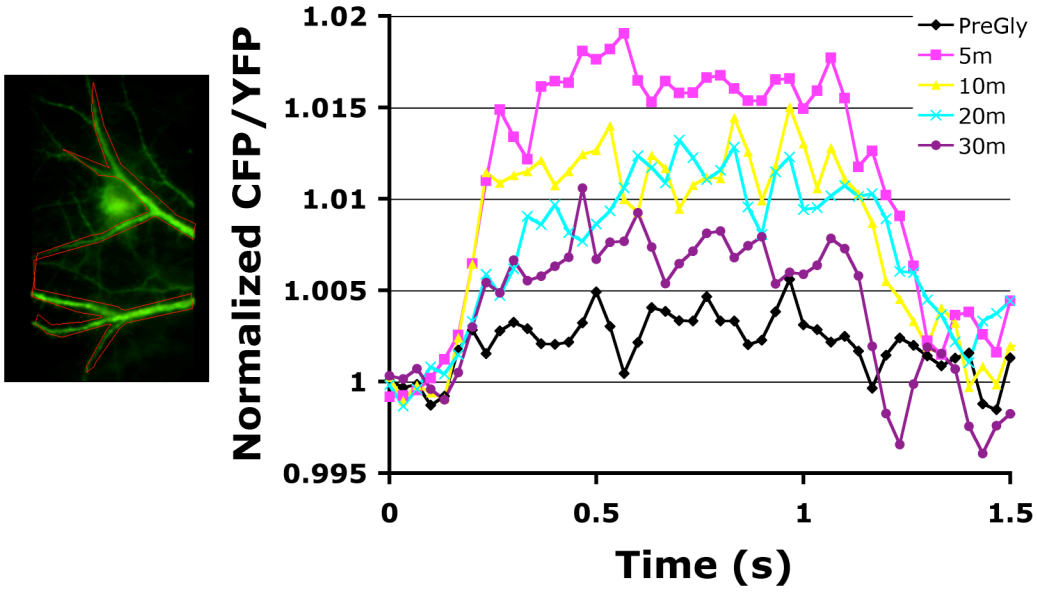

Figure 2.1 – Early attempts of LTP induction. GluSnFR$_{8N0C}$ responses to 20 action potential field stimulation at 20Hz, before and after a 3-minute glycine LTP induction protocol.

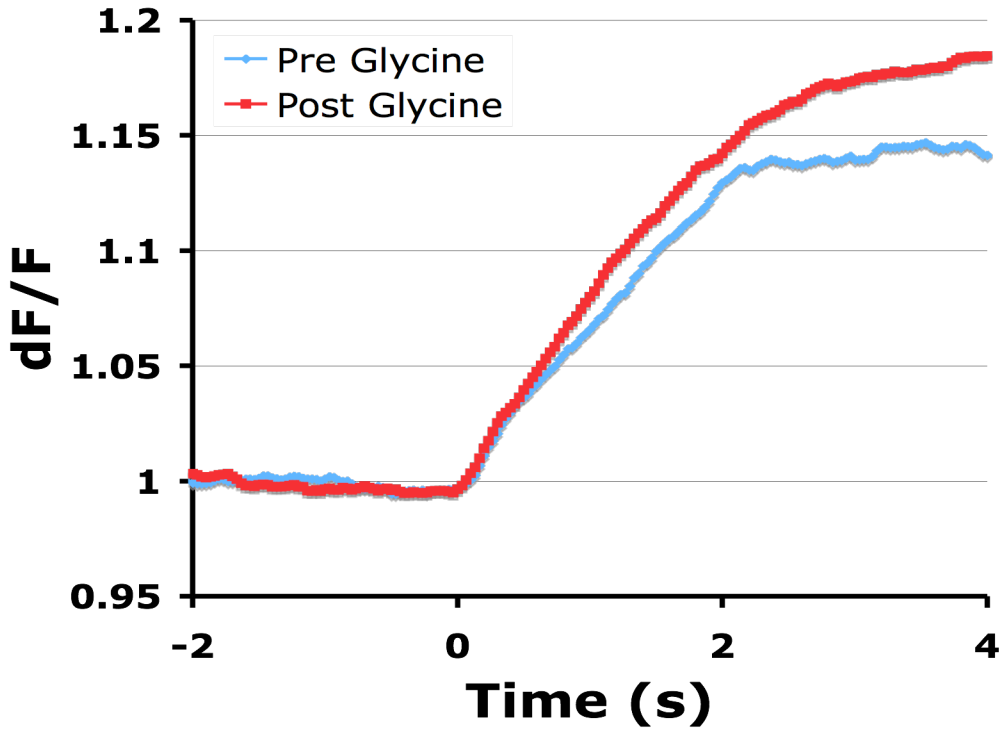

Figure 2.2 – Vesicle turnover is potentiated by glycine LTP induction. SynaptopHluorin response to four seconds of field stimulation at 20Hz before and after application of 100µM glycine

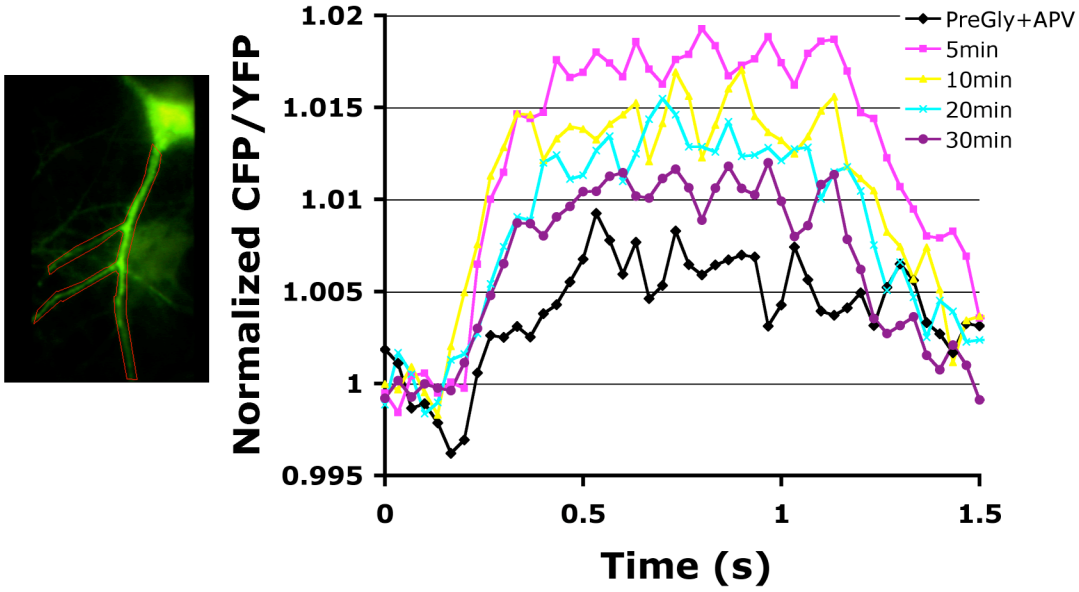

Figure 2.3 – Potentiation from the glycine LTP induction protocol appears NMDAR independent. Co-application of 50µM APV with glycine fails to block glutamate potentiation. Field stimulations are 20AP at 20Hz.

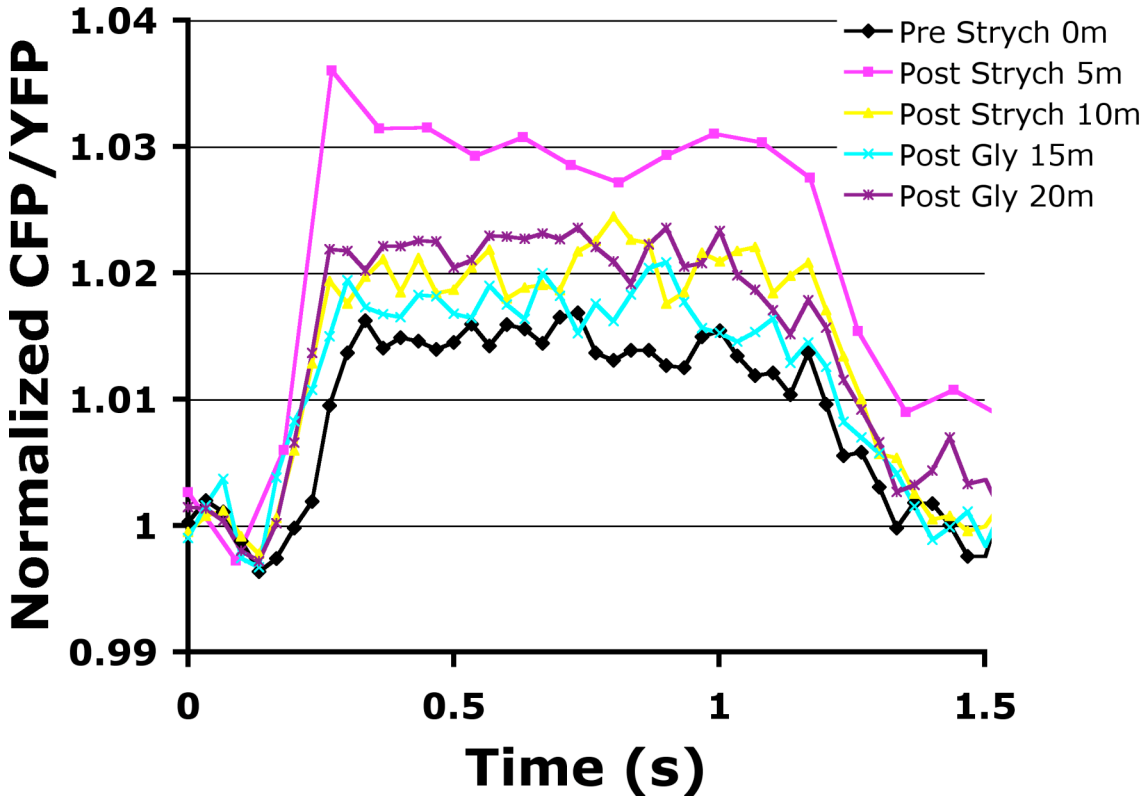

Figure 2.4 – Application of 0.5µM strychnine alone mimics and occludes glycine LTP induction. Applications of field stimulations are 20AP at 20Hz. Addition of 100µM glycine following strychnine potentiation fails to further increase response magnitude.

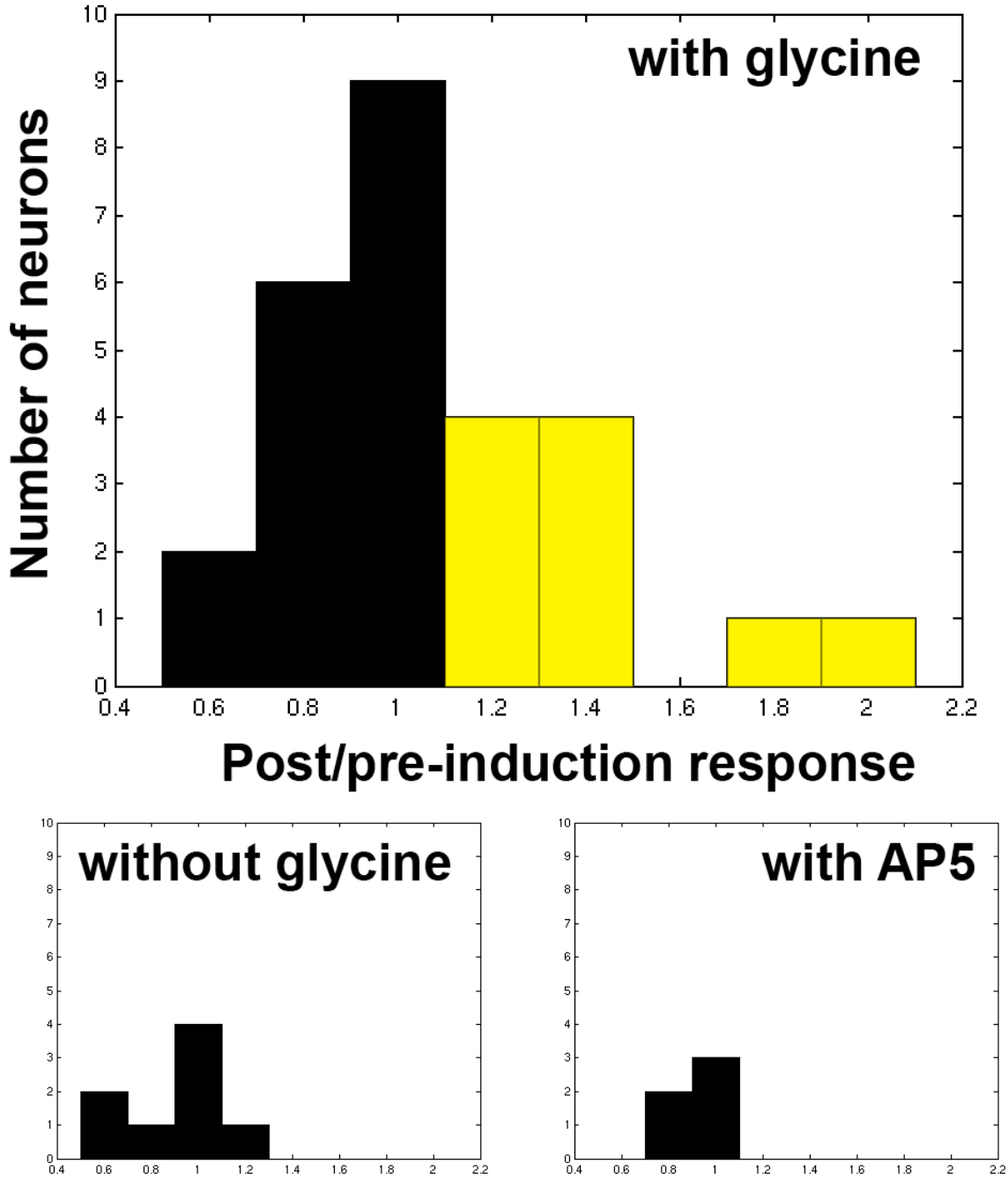

Figure 2.5 – Only glycine application with functional NMDARs induces LTP. The average post-induction glutamate response is compared to the average pre-induction response. (*above*) Ten of 27 neurons potentiate following glycine application. Mock glycine application (*below left*) or concurrent application of AP5 with glycine (*below right*) blocks potentiation.

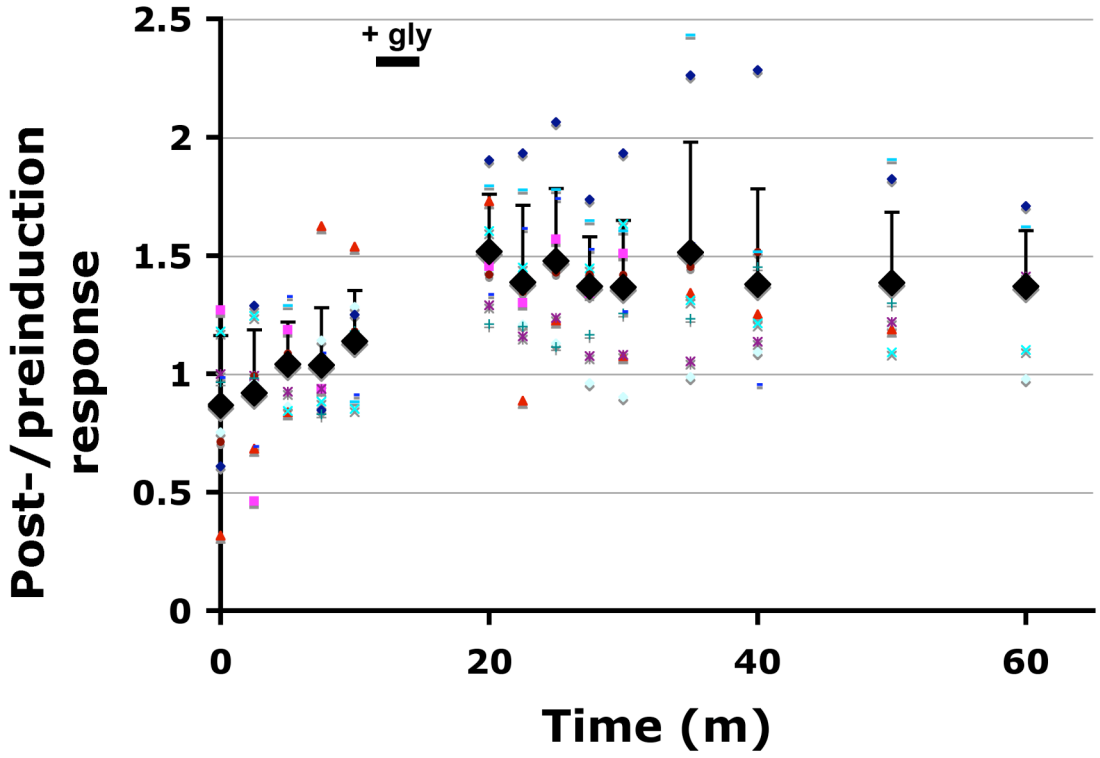

Figure 2.6 – The timecourse of glutamate response potentiation of the ten neurons that show a long lasting response noted in yellow in *Figure 2.5*. Average of all ten responses (*black*). Black bars indicate standard deviation. Individual neuron responses (*colors*).

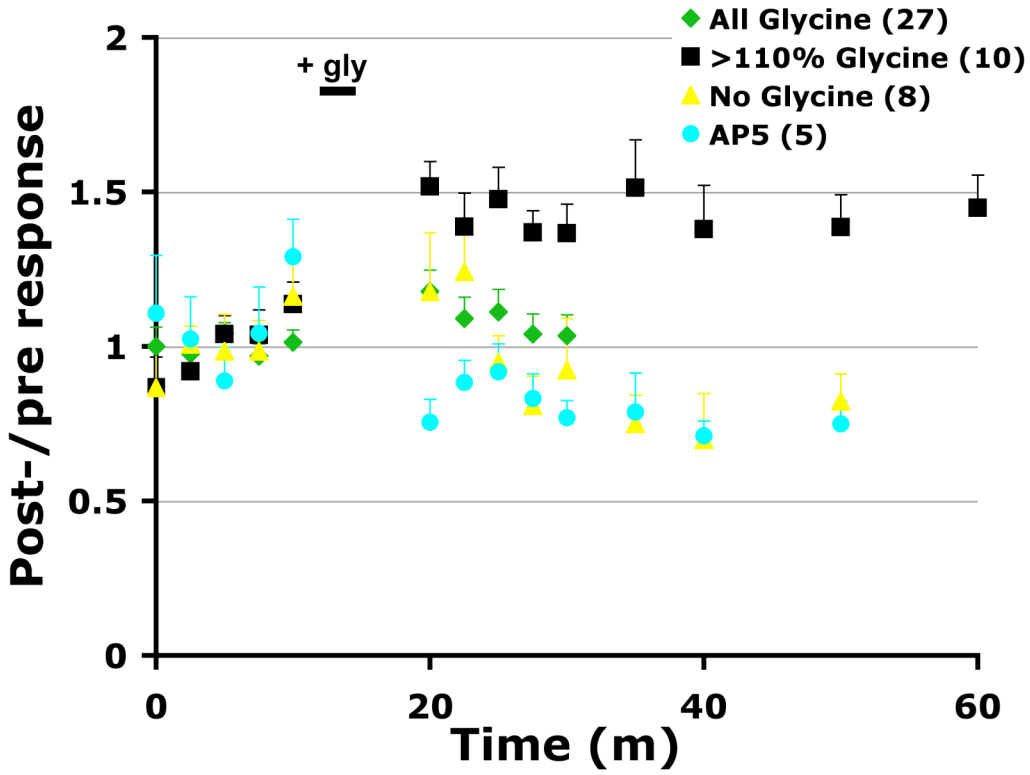

Figure 2.7 – Timecourse of three stimulation conditions. The average of glutamate responses to neurons following glycine application (*green*), of only those that potentiated (*black*), of neurons following mock glycine perfusion (*yellow*) and of neurons with the NMDA receptors blocked with AP5 (*cyan*).

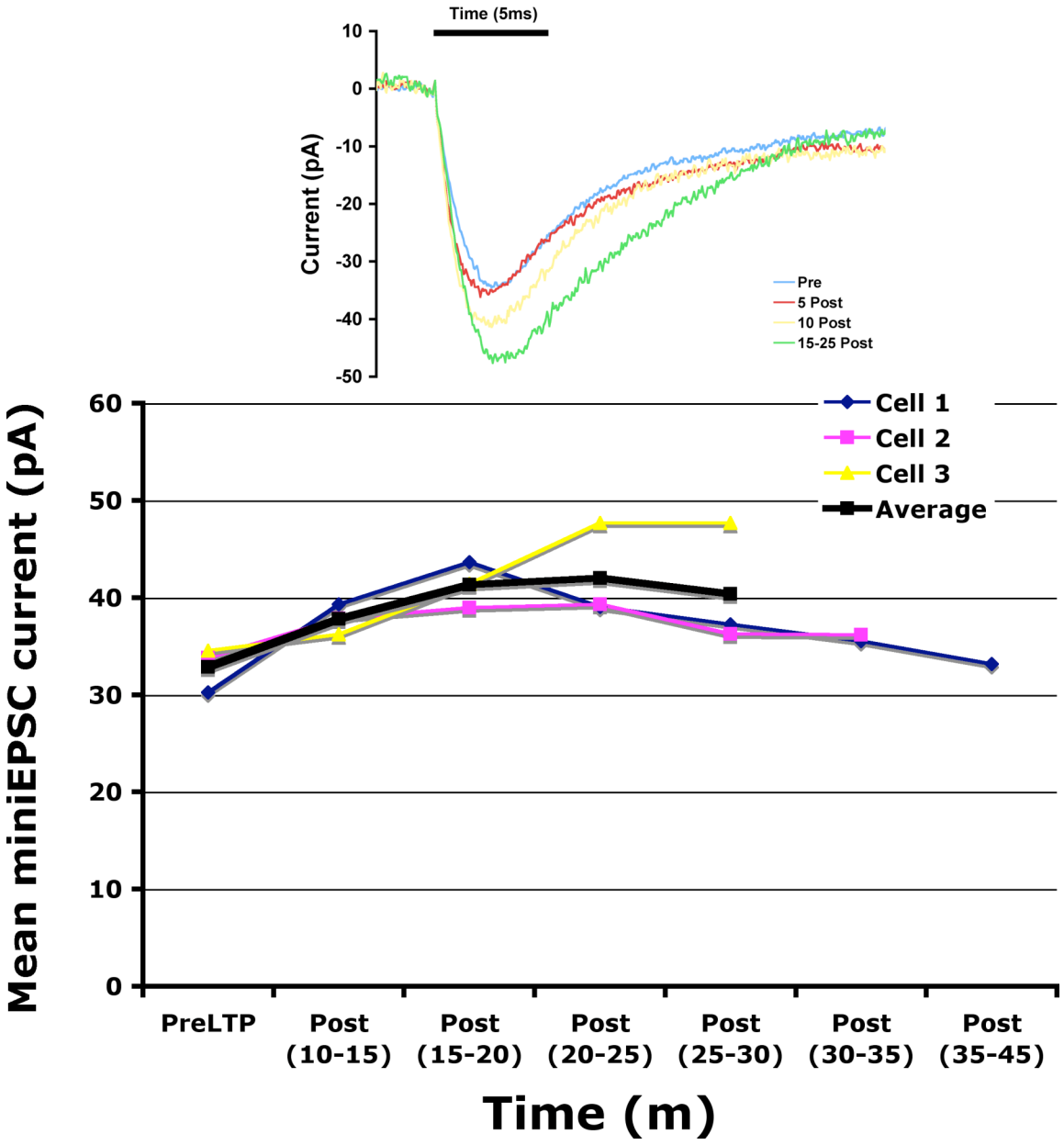

Figure 2.8 – Transient glycine application potentiates miniEPSC size. (*above*) Mean miniature EPSCs before and at 5-10 minute windows after glycine LTP induction from Cell 3. (*below*) Summary of response amplitudes of the three cells successfully held for thirty minutes or more.

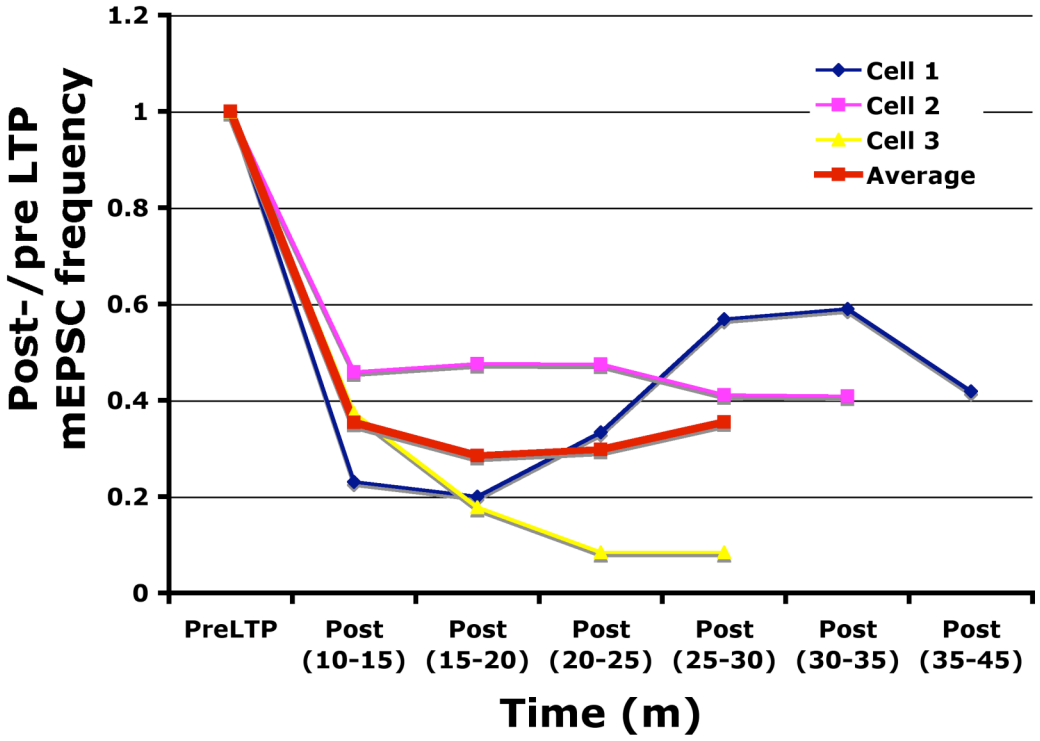

Figure 2.9 – Transient glycine application reduces miniEPSC frequency. Summary of the same cells as in Fig. 2.8

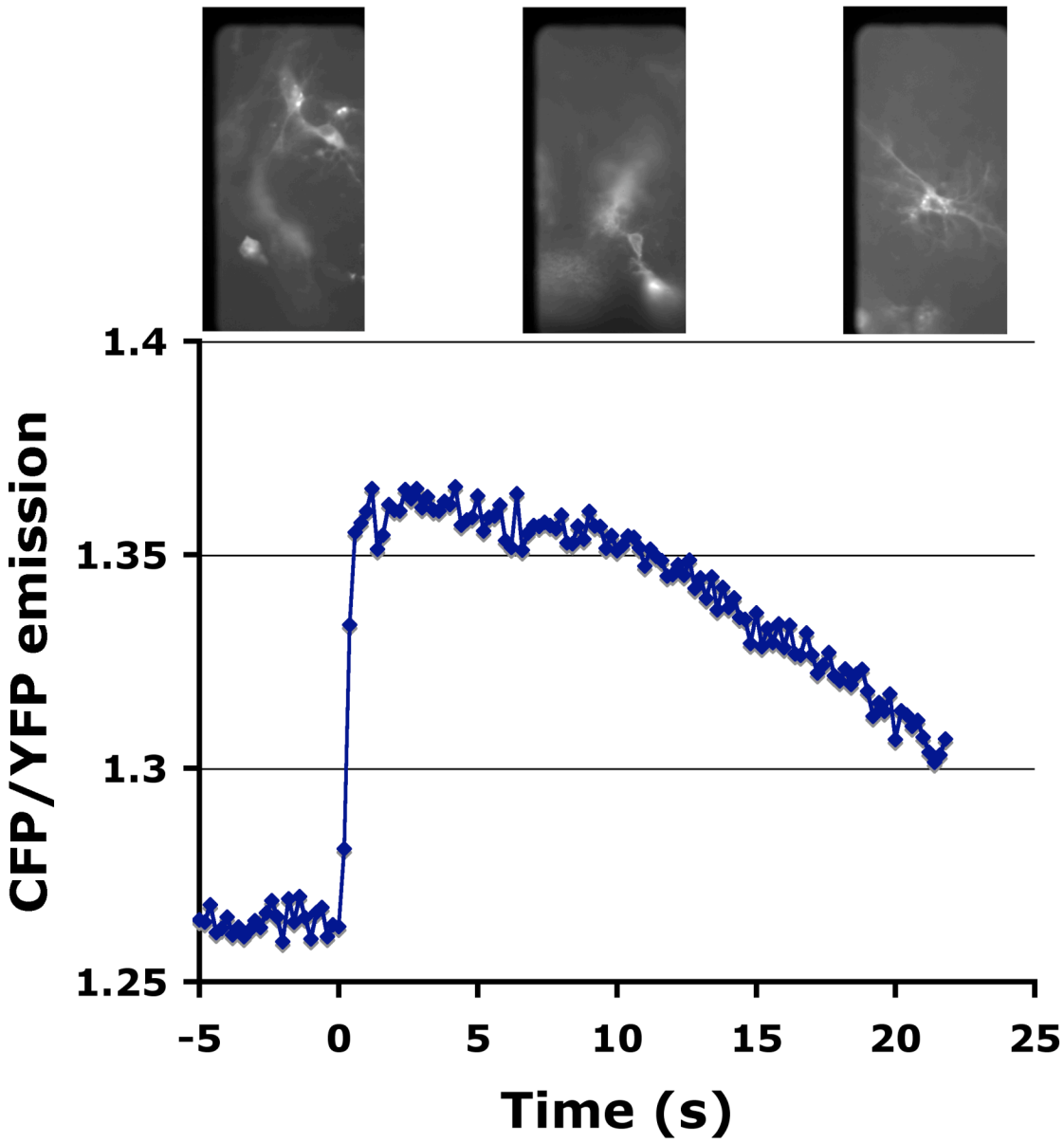

Figure 2.10 – GluSnFR$_{8N0C}$ expresses in organotypic hippocampal culture and is functional. (*above*) Three neurons expressing GluSnFR$_{8N0C}$. (*below*) The response of the rightmost neuron to puffing of Ringer's solution including 100µM glutamate.

References

1. Ramon y Cajal, S. "The Croonian Lecture: La Fine Structure des Centres Nerveux". *Proceedings of the Royal Society of London* **55**, 444-468 (1894).

2. Malenka, R. C. & Nicoll, R. A. Long-term potentiation--a decade of progress? *Science* **285**, 1870-1874 (1999).

3. Hebb, D. O. *The organization of behavior; a neuropsychological theory* (Wiley, New York, 1949).

4. Whitlock, J. R., Heynen, A. J., Shuler, M. G. & Bear, M. F. Learning induces long-term potentiation in the hippocampus. *Science* **313**, 1093-1097 (2006).

5. Malinow, R. & Tsien, R. W. Presynaptic enhancement shown by whole-cell recordings of long-term potentiation in hippocampal slices. *Nature* **346**, 177-180 (1990).

6. Chavez-Noriega, L. E. & Stevens, C. F. Increased transmitter release at excitatory synapses produced by direct activation of adenylate cyclase in rat hippocampal slices. *J Neurosci* **14**, 310-317 (1994).

7. Manabe, T., Renner, P. & Nicoll, R. A. Postsynaptic contribution to long-term potentiation revealed by the analysis of miniature synaptic currents. *Nature* **355**, 50-55 (1992).

8. Manabe, T. & Nicoll, R. A. Long-term potentiation: evidence against an increase in transmitter release probability in the CA1 region of the hippocampus. *Science* **265**, 1888-1892 (1994).

9. Bekkers, J. M. & Stevens, C. F. Presynaptic mechanism for long-term potentiation in the hippocampus. *Nature* **346**, 724-729 (1990).

10. Emptage, N. J., Reid, C. A., Fine, A. & Bliss, T. V. Optical quantal analysis reveals a presynaptic component of LTP at hippocampal Schaffer-associational synapses. *Neuron* **38**, 797-804 (2003).

11. Shi, S. H. et al. Rapid spine delivery and redistribution of AMPA receptors after synaptic NMDA receptor activation. *Science* **284**, 1811-1816 (1999).

12. Lu, W. et al. Activation of synaptic NMDA receptors induces membrane insertion of new AMPA receptors and LTP in cultured hippocampal neurons. *Neuron* **29**, 243-254 (2001).

13. Kafri, T., van Praag, H., Gage, F. H. & Verma, I. M. Lentiviral vectors: regulated gene expression. *Mol Ther* **1**, 516-521 (2000).

14. Jeromin, A., Yuan, L. L., Frick, A., Pfaffinger, P. & Johnston, D. A modified Sindbis vector for prolonged gene expression in neurons. *J Neurophysiol* **90**, 2741-2745 (2003).

15. Nguyen, P. V., Abel, T. & Kandel, E. R. Requirement of a critical period of transcription for induction of a late phase of LTP. *Science* **265**, 1104-1107 (1994).

16. Bolshakov, V. Y., Golan, H., Kandel, E. R. & Siegelbaum, S. A. Recruitment of new sites of synaptic transmission during the cAMP-dependent late phase of LTP at CA3-CA1 synapses in the hippocampus. *Neuron* **19**, 635-651 (1997).

17. Jiang, M., Deng, L. & Chen, G. High Ca(2+)-phosphate transfection efficiency enables single neuron gene analysis. *Gene Ther* **11**, 1303-1311 (2004).

18. Adesnik, H., Nicoll, R. A. & England, P. M. Photoinactivation of native AMPA receptors reveals their real-time trafficking. *Neuron* **48**, 977-985 (2005).

19. Otmakhov, N. et al. Forskolin-induced LTP in the CA1 hippocampal region is NMDA receptor dependent. *J Neurophysiol* **91**, 1955-1962 (2004).

20. Navarro-Quiroga, I., Chittajallu, R., Gallo, V. & Haydar, T. F. Long-term, selective gene expression in developing and adult hippocampal pyramidal neurons using focal in utero electroporation. *J Neurosci* **27**, 5007-5011 (2007).

21. Sastry, B. R., Goh, J. W. & Auyeung, A. Associative induction of posttetanic and long-term potentiation in CA1 neurons of rat hippocampus. *Science* **232**, 988-990 (1986).

22. Nicoll, R. A. & Schmitz, D. Synaptic plasticity at hippocampal mossy fibre synapses. *Nat Rev Neurosci* **6**, 863-876 (2005).

23. Dudek H, G. A., Greenberg *Current Protocols in Neuroscience* ME 3.11.1-3.11.6 1998).

24. Gogolla, N., Galimberti, I., DePaola, V. & Caroni, P. Preparation of organotypic hippocampal slice cultures for long-term live imaging. *Nat Protoc* **1**, 1165-1171 (2006).

Acknowledgements

The work in this chapter was primarily performed by the dissertation author. Yongling Zhu participated in many of the GluSnFR imaging experiments, recorded the data in Figure 2.2, participated in numerous discussions on experimental direction and design and put forth the majority of the effort preparing and maintaining the dissociated neuronal cultures. The image acquisition of Figure 2.10 was done with Varda Lev-Ram. Varda and John Lin assisted with electrophysiology equipment and training, but the presented traces were recorded by the dissertation author. The Sindbis cloning vectors were provided by Andreas Jeromin. Jian Xu transcribed the viral RNA and harvested the $GluSnFR_{8N0C}$ Sindbis virus.

Chapter Three

Towards a genetically-encoded optical reporter for γ-aminobutyric-acid

Abstract

Genetically-encoded optical reporters of inhibitory neurotransmitters would provide a tremendous functional complement to GluSnFR imaging. However, reporters for GABA, the primary inhibitory neurotransmitter in the brain have not yet been produced. Two strategies of PBP-based designs for a genetically-encoded GABA sensor, based of the structure of GluSnFR, are proposed. A bacterium, *Pseudomonas fluorescens,* contains a GABA periplasmic binding protein, which we tentatively identify by bioinformatics and synthesize. Linear fusions of this gene with ECFP and Citrine produce a FRET-generating protein. However, these prototypes are non-responsive to GABA. Response enhancement is attempted by creation of a variety constructs with affinity mutations, domain swaps with GltI and varied ECFP insertion points. However, all constructs remain non-functional. Future troubleshooting experiments are proposed.

Introduction

The primary inhibitory neurotransmitter in the mammalian cerebrum is GABA[1]. Inhibition via GABA release is primarily achieved by increased anionic conductances, particularly Cl^-, through activated ionotropic $GABA_A$ receptors. Throughout the brain, GABA plays a primary role in the homeostatic regulation of glutamate release through feedback inhibition[2]. Additional functional roles for GABA include shaping of tuning curves in the auditory cortex[3], multiplicative gain control in cerebral cortex[4], and control of spike routing in the hippocampus[5].

During glutamate-mediated neurotransmission, intracellular calcium levels rise in concert with neurotransmitter action, and numerous calcium dyes and genetically-encoded sensors reliably report calcium dynamics, a correlate of glutamate release. In contrast, the imaging solutions for surrogate markers of inhibitory GABA neurotransmission are poor. Quinolinium-derived dyes such as 6-methoxy-N-(3-sulfopropyl) quinolinium (SPQ) and N-[ethoxycarbonylmethyl]-6-methoxy-quinolinium bromide (MQAE) [6] generally require excitation in the near-UV, toxic loading methods, tend to leak from cells and are dim. Genetically-encoded chloride sensors, such as Clomeleon[7] and YFP-H148Q[8], are pH-sensitive, have slow binding kinetics and in the case of YFP-H148Q are non-ratiometric. Therefore, a genetically-encoded reporter of GABA concentration would provide an excellent solution to the unmet need of high-speed, spatially resolved measurements of GABA concentration and inhibition.

Given the success of GluSnFRs in glutamate imaging and the structural similarity between glutamate and GABA (Fig. 3.1), we sought to extend the GluSnFR reporter framework to GABA detection. Two general strategies were considered to make GluSnFRs selective to GABA. The first method was to identify a natural PBP for GABA and replace GltI with this GABA-selective PBP. We found an excellent candidate in PFL_0342 from *Pseudomonas fluorescens.* However, our evidence that PFL_0342 was a periplasmic binding protein specific for GABA was circumstantial and the linkers in SuperGluSnFR were already optimized for GltI. The logical alternative to finding a new PBP for GABA was to mutate the residues of

SuperGluSnFR that had direct ligand interactions to those that may confer GABA specificity.

Highly specific, nanomolar level affinities for non-native ligands have been engineered into PBPs by advanced computational techniques coupled with high-throughput bacterial screens[9]. GltI shares four critical ligand-binding residues with PFL_0342 (Fig 3.2), and GABA is a close structural homolog to glutamate. However, GltI has six additional residues that directly interact with glutamate and are not shared by PFL_0342. Since a single point mutation of a ligand interacting residue can have a profound impact on binding affinity, complementary mutations of multiple binding pocket residues would likely be needed to achieve reasonable specificity for GABA on a glutamate PBP backbone. Lacking an efficient high-throughput bacterial screen for GABA-sensitive fluorescence, this second avenue was left for future work.

Results

The first evidence of the existence of a periplasmic binding protein specific to GABA was a report by Guthrie et al, which indicated that a strain of the gram-negative bacterium *Pseudomonas fluorescens* was capable of high-affinity uptake of radiolabeled GABA[10]. This particular strain's affinity for GABA was measured with Km for GABA of 65nm, which was inhibitable by the $GABA_A$ agonist muscimol. Further investigations lead to the isolation of the binding protein by cold shock treatment. The isolated GABA binding protein had a molecular weight of 42,000 Daltons, significantly larger than the usual range of bacterial PBPs[11]. This surprisingly large mass may have been the result of post-translational modifications.

On the basis of these studies, I searched the published genome of the Pf-5 strain *P. fluorescens* for possible GABA PBP sequences[12]. Immediately adjacent to a gene identified by homology as *gabP*, a GABA permease gene of the amine–polyamine–choline transporter superfamily, was a set of four other genes with homology to the ABC transporter family. These included two putative permease genes, an ATP-binding gene and a periplasmic binding protein gene (PFL_0342) (Fig. 3.3). Although this set of four genes was transcribed in the opposite direction as *gabP*, the proximity of this cluster with *gabP* suggested that PFL_0342 might be a periplasmic binding protein for GABA.

PFL_0342 was aligned with ClustalW and manually adjusted to the sequences for the *e. coli* glutamate PBP GltI (accession #P37902), *e. coli* histidine PBP HBP (P39182), *e. coli* glutamine PBP GlnBP (P10344), the GluR0 binding core (pdb1ii5), and the glutamate binding region of rat GluR2 (M85035) (Fig 3.4). Secondary structure of HBP, GlnBP, GluR0 and GluR2 sequencing was determined by examining published crystal structures, while GltI was inferred from sequence alignment. Residues involved in critical ligand-protein interactions were noted and based crystal structure and literature reports[13]. PFL_0342 shares ligand interacting residues S90, S92, R97, T141 with the consensus, but E31, Y34, W72, Q138, L152 and V184 are significantly different from GltI and consensus resides at those critical sites. The substitution of the bulky aromatics tyrosine and tryptophan for serines 90 and 92 may provide some compensatory space filling for the smaller GABA ligand in PFL_0342.

Encouraged by the structural and ligand interacting residue similarities, the mature coding sequence of PFL_0342 was optimized for rat expression and synthesized. This replaced the GltI sequence in GluSnFR in both $pRSET_B$ and pDisplay vectors. Expression of this prototype as a purified protein yielded a fluorescent spectrum that appeared to have a small amount of FRET, perhaps limited from partial proteolysis (Fig. 3.5). When fused into pDisplay and expressed on the surface of HEK293 cells, the sensor GABASnFR0.1 appeared properly membrane targeted and also had a small but significant FRET ratio (Fig. 3.6). However, application of 100μM GABA to the cells caused no change in FRET ratio (Fig. 3.6).

Several possibilities were proposed for the lack of response. First, the chromophores may be in a poor distance and orientation for FRET. Second, the conformational change of the sensor may not cause a significant change in FRET efficiency. Third, GABA affinity of the protein may be too high, preventing the sensor from reaching the apo state with background GABA levels. Finally, PFL_0342 may not be a GABA binding protein.

To address chromophore orientation, Citrine in GabaSnFR0.1 was replaced by circularly permuted Venus at the Y145M, Q157M and D173M positions[14,15]. Only the Q157M and D173M mutants folded properly and were well targeted to the plasma membrane following transfection in HEK293 cells. The GABA-free YFP/CFP emission for both Q157M and D173M was ~2.0. However, these two properly folded mutants still showed no sign of GABA sensitivity.

One possibility for the lack of response was the location of the N- and C-terminus of the PBP relative to the two lobes of the structure. No crystal structure

exists for either GltI or PFL_0342, but they have similar structure based on sequence alignment. A Robettea fit had been performed threading GltI onto known similar crystal structures[16,17], in which the C-terminal tail appears to cross over the hinge region and interact with the N-terminal lobe, making this a type II PBP[16]. Interestingly, despite both N- and C-terminals being on the same lobe in GltI, SuperGluSnFR still shows large FRET changes. PFL_0342 has a C-terminus that is significantly truncated relative to GltI, suggesting that the its C-terminal tail may not interact in the same way with the N-terminal lobe. I reasoned that it might be possible to recover GluSnFR-like responses in the GABASnFR prototypes by adding the missing GltI tail. The I274-N302 segment of GltI was swapped with the I249-Y250 segment of PFL_0342 in the prototype GABASnFR. When expressed in HEK293 cells, this construct expressed with proper membrane targeting (Fig. 3.7). In GABA free solution the average YFP/CFP ratio was ~1.25. Bleaching of the acceptor chromophore increased CFP fluorescence by 17%, indicating a FRET efficiency of ~15%, similar to $GluSnFR_{0N0C}$. However, despite the promising initial YFP/CFP ratio, application of 100μM GABA caused no change in FRET (Fig 3.7).

The C-terminal tail's conformation may depend on interactions with of neighboring secondary structures. Therefore domain fragments likely to interact with the I274-N302 tail in GltI were determined (Fig. 3.8). Chimeric sensors were generated using PFL_0342 as the main binding protein with either the full length or 5 amino acid truncated C-terminal tail of GltI with additional interacting domain fragments E261-P273, D243-P273, or F126-V133 with D243-P273. Although G112-A125 also was adjacent to the tail, it was excluded from swapping due to the presence

of three ligand interacting residues within it. None of these six prototype sensors folded properly. Most sensor was expressed in the cytosol with an unresponsive YFP/CFP of ~0.7 (Figure 3.9).

Before attempting additional fine-tuning of chromophore location or secondary structure, I addressed the possibility that the binding protein may in the closed state at background GABA concentrations due to excessive GABA affinity. The following mutations of possible ligand interacting residues in PFL_0342 were made in the GABASnFR0.1 background: Y34A, G48A, D52E, S90A, S92A, T94A, Q138E, Q138A, T141A, L142A and V183I. All mutant constructs folded properly and expressed on the surface of HEK293 cells with GABA-free YFP/CFP ratio of ~1.0. However, no construct showed any ratio change in response to 100μM of GABA application.

Since neither the tail domain swap nor the affinity mutations led to GABA-sensitive FRET responses, I tried one additional strategy of chromophore orientation change. ECFP insertions into unstructured loops of FLIPE had led to glutamate-induced ratio changes of 100% in soluble FLI^{81}PE^{16}. Although these inserts did not fold properly when fused to pDisplay, when we inserted ECFP with superfolder mutations (sfECFP) into GluSnFR-pDisplay, proper targeting and marginal glutamate-sensitivity was achieved at some insert sites. Given this experimental validation of sfECFP insertion into PBPs, eleven sites were selected for sfECFP insertion into PFL_0342, after amino acids 37, 43, 62, 81, 120, 128, 156, 164, 206, 217 and 235. Of the insert sites tested, only inserts at 62, 81, 120 and 206 produced membrane expressed CFP and YFP fluorescence when transfected into HeLa cells. Site 120 had a

particularly impressive GABA-free YFP/CFP ratio of ~2.0, while the other three ranged from 1-1.25. However no constructs were responsive to 100μM GABA application.

Discussion

Despite the inability to show GABA-sensitive fluorescence changes with a PBP based sensor, the potential of a PBP based approach and the ultimate value to downstream applications remains high. The most pressing need to further development is to confirm whether PFL_0342 is a GABA selective PBP. The could be performed by binding assays using radiolabeled GABA. A non-radioactive alternative method to determine the PBP's affinity for GABA is to use Biacore based measurements. Biacore measures changes in surface plasmon resonance due to ligand binding to the PBP which is immobilized on a gold film at the interface of glass and buffer[18]. Although the GABA ligand is quite small compared to the substrate, the conformational change in the PBP associated with ligand binding should cause an easily detectable change in the surface plasmon resonance (L. Looger, personal communication). If PFL_0342 does not bind GABA, then the appropriate PBP in *P. fluorescens* needs to be determined. This could be done by cloning or synthesizing all close homologs of GltI that have unknown function in the *P. fluorescens* genome, and screening these for GABA affinity. Alternatively, a library of known GABA interacting sequences from other species could be panned against the genome of *P. fluorescens*, to hunt for homologous proteins. Finally, mutant strains of *P. fluorescens* could be generated and screened for those that cannot grow with GABA as the sole

carbon and nitrogen source. Mutant proteins involved in GABA harvesting could then be determined.

Once GABA-specific binding in a PBP has been conclusively demonstrated, screening based on linker variation between PBP and FPs and sfECFP insertion should be renewed with vigor. Given the large number of PBPs that have been successfully made into biosensors[16], sufficient screening should produce a reasonable GABA sensor if a true GABA-specific PBP is used as the scaffold. A higher throughput screening method would ease the difficulty of sifting through numerous variants. A possible method would be to screen fluorescence changes of soluble sensor before and after ligand application in crude bacterial lysates, with positive hits validated in mammalian surface displayed constructs.

An improved screening process would be essential for determining the combination of binding pocket mutations needed to shift the affinity of SuperGluSnFR to GABA. Given the structural similarity of GABA and glutamate and the known ligand interacting residues of GltI, computational modeling may not be necessary to restrict the search space of potential affinity mutations. But even with knowledge of key residues, a combination of changes at six or more sites may be required to achieve high GABA affinity. Therefore a successful screen will likely require a screen with throughput of thousands of mutants. Furthermore, even small changes in the allosteric interactions between the binding pocket and the fluorescent proteins could completely eliminate the advantages of the finely tuned SuperGluSnFR construct.

Once a successful two-chromophore FRET sensor is generated, single FP insertions should be screened to attempt to make a single wavelength sensor. Although

a single FP would be more difficult to calibrate for quantitative measurements and would be more susceptible to drift due to subject motion or FP bleach, it would simplify two-photon excitation and perhaps allow simultaneous interrogation of two different classes of neuronal input, such as GABA and glutamate. Even without quantitative calibration, high-speed, spatially resolved measurement of excitation and inhibition in a neural circuit would be tremendously powerful in assessing the dynamic interplay between these two modes of neuronal communication.

Materials and Methods

Sensor construction

The 753 nucleotide sequence of PFL_0342 was retrieved from the NCBI GenBank database from the NC_004129 locus, region 395343-396095. This sequence was codon optimized for mammalian expression based on NCBI GenBank codon usage tables, resulting in 14 silent mutations to the native *P. fluorescens* sequence. The optimized coding fragment was custom synthesized (Epoch Biolabs), PCR amplified using Phusion polymerase and digested with *SphI* and *SacI* (NEB). GluSnFR0.02:pRSET$_B$ and GluSnFR$_{8N5C}$:pDisplay vectors were digested with *SphI* and *SacI*, treated with CIP (NEB) and the GltI PBP-free section retained after gel electrophoresis. The full length PFL_0342 digest was ligated to the digested vectors to make the bacterial expression vector GABASnFR0.1:pRSET$_B$ and the mammalian surface expression vector GABASnFR0.1:pDisplay.

GABASnFR affinity mutations were performed by overlap PCR. Two PCR fragments of PFL_0342 were generated for each mutation. A N-terminal or C-terminal primer was paired with a primer of opposite direction that primed over the mutation site. Each amplified fragment had the desired mutation plus ~25 nucleotides of overlap with the other fragment. These two fragments were mixed and PCR amplified with flanking N- and C-terminal primers to create the full length PFL_0342 mutant. This was digested with *SphI* and *SacI* and inserted into the GABASnFR0.1:pDisplay scaffold.

Superfolding ECFP insertions were also made by overlap extension PCR. PFL_0342 fragments of before and after the insertion site were made by pairing

PFL_0342 forward or reverse terminal primers with opposite direction primers that could hybridize both PFL_0342 at the insertion point and the N- or C-terminal of sfECFP. These PCRs generated pairs of PFL_0342 fragments with sfECFP priming overhangs that were mixed with sfECFP and amplified with the flanking forward and reverse PFL_0342 primers to generate the full length PFL_0342 with sfECFP insertion. These were digested with *BglII* and *SacI* and ligated into the GABASnFR0.1 scaffold at those cut sites, replacing the linear fusion of ECFP and PFL_0342. This primer technique was also used to make the sequence swaps between PFL_0342 and GltI via overlap extension PCR. Rather than generate overhangs of PFL_0342 that could prime sfECFP, they primed the appropriate section of GltI. The full-length hybrid fragments were then digested by *SphI* and *SacI* and ligated into the digested GABASnFR0.1:pDisplay vector.

Sensor Characterization

Soluble GABASnFR0.1 was generated and purified as described for GluSnFR in Chapter One. *In vitro* fluorescence assays were also performed as described in Chapter One. To test GABA sensitivity for surface expressed GABASnFR prototypes, DNA encoding the sensor prototypes was transfected into HEK293 or HeLa cells plated on 18mm glass coverslips using Fugene HD (Roche). 48 hours after transfection, cells were visualized with a Xenon arc lamp with 10% ND transmission filters on a Zeiss Axiovert 200M microscope through a 40x oil objective and with a Roper 512 BFT cooled CCD camera. The extracellular buffer was standard HBSS (Invitrogen).

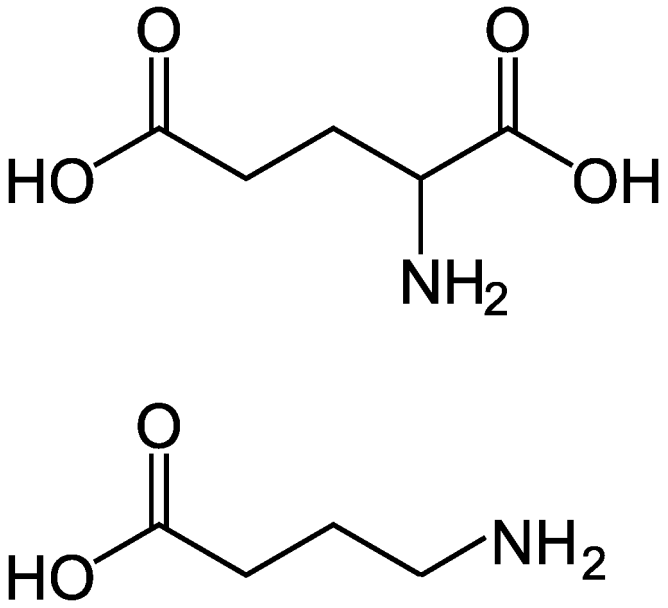

Figure 3.1 – Structural homology of glutamate (*above*) and GABA (*below*)

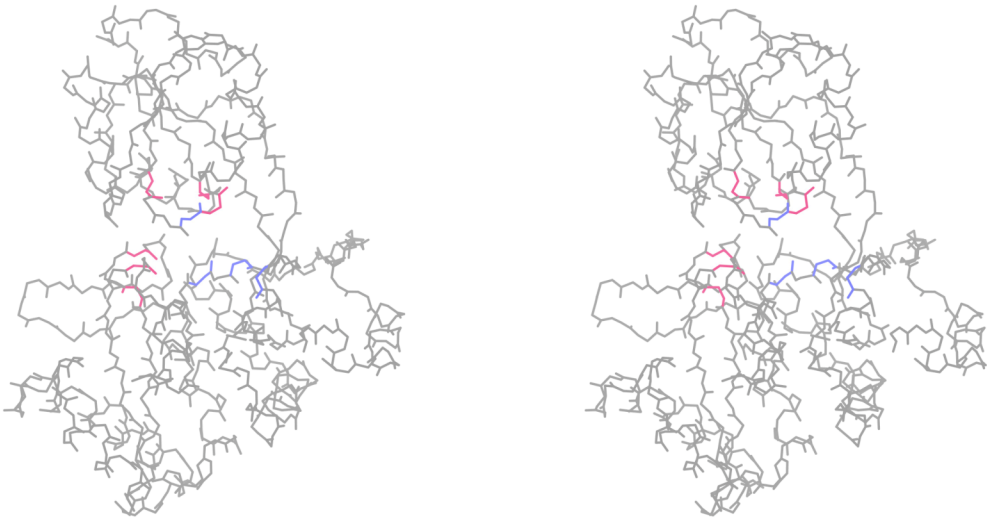

Figure 3.2 – Robetta fit of GltI backbone onto similar PBP structures. (*blue*) Ligand interacting residues conserved between GltI and PFL_0342. (*pink*) Ligand interacting residues not conserved between GltI and PFL_0342. Cross-eye stereo view.

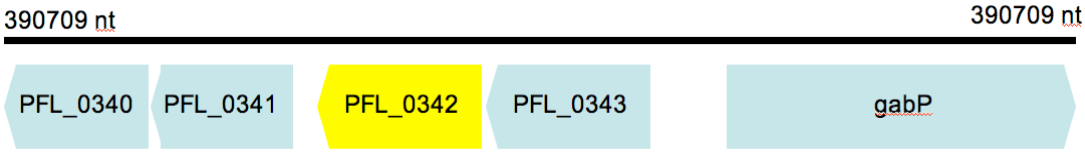

Figure 3.3 – Genomic neighborhood of putative GABA PBP in *Pseudomonas fluorescens*. gabP is GABA permease. PFL_0340 and PFL_341 are putative amino acid ABC transporter permease genes. PFL_0342 is the putative GABA periplasmic binding protein. PFL_0343 is a putative amino acid ABC transporter ATP-binding protein.

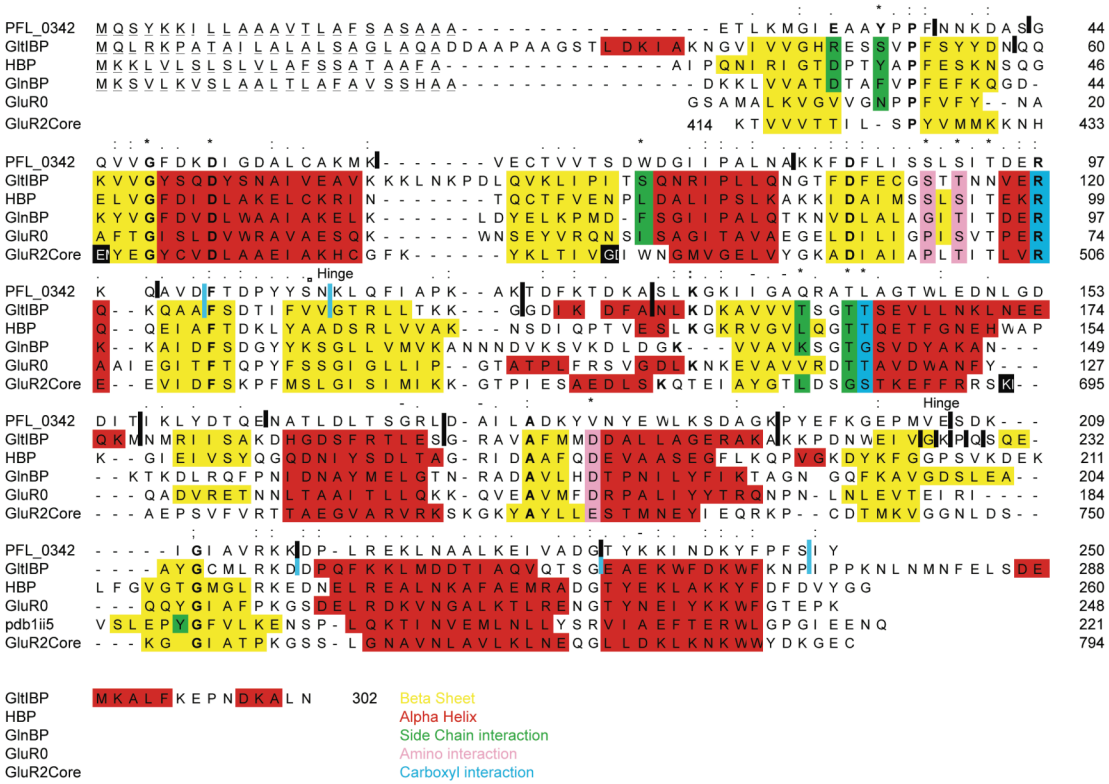

Figure 3.4 – Sequence alignment of PFL_0342 and amino acid binding proteins. Black lines indicate insertion points for sfCFP. Cyan lines indicate crossover sites of Gab GltI domain swaps. Periods and colons indicate areas of increasing similarity. Asterisks indicate sites of PFL_0342 affinity mutations. Underlines indicate the predicted signal peptide. Numbers indicate distance in amino acids from the start of the full transcript.

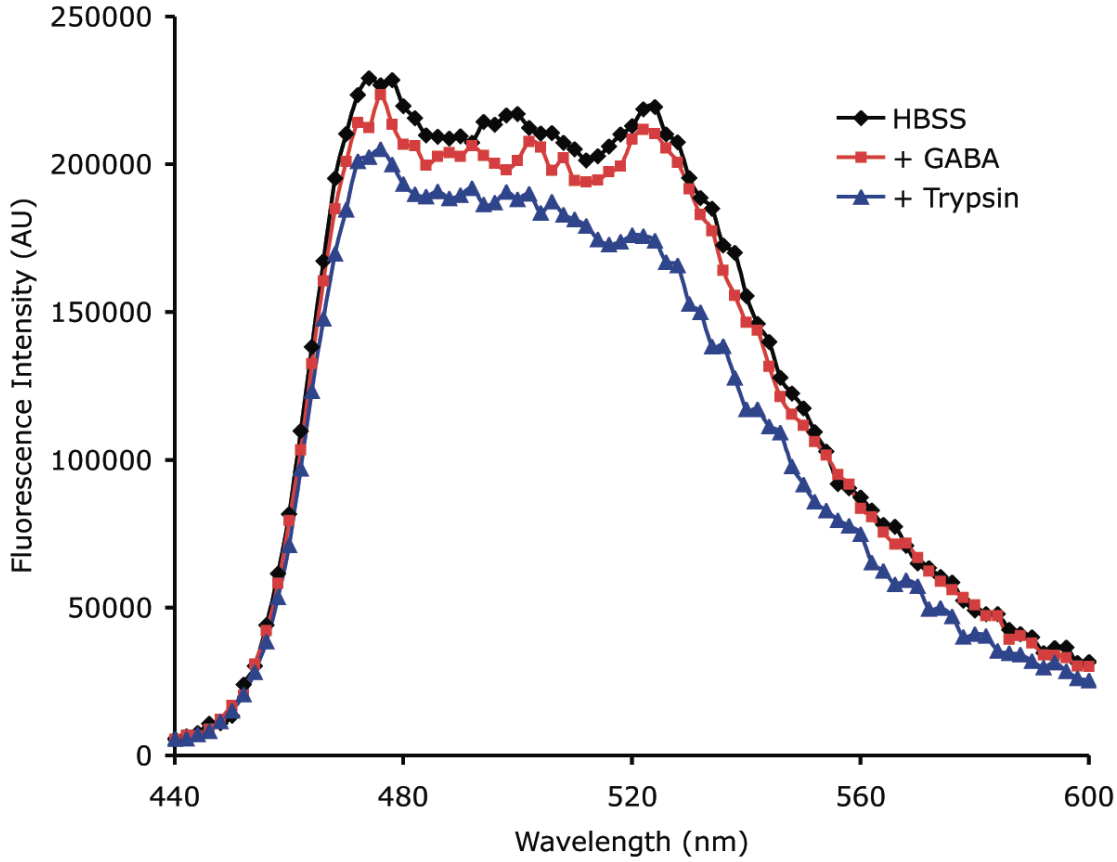

Figure 3.5 – Emission spectra of *in vitro* purified GABASnFR0.1. Spectra were unchanged after addition of 100µM GABA to cuvette. After 10 minutes of Trypsin digestion, FRET fluorescence was slightly reduced. Excitation was at 420nm.

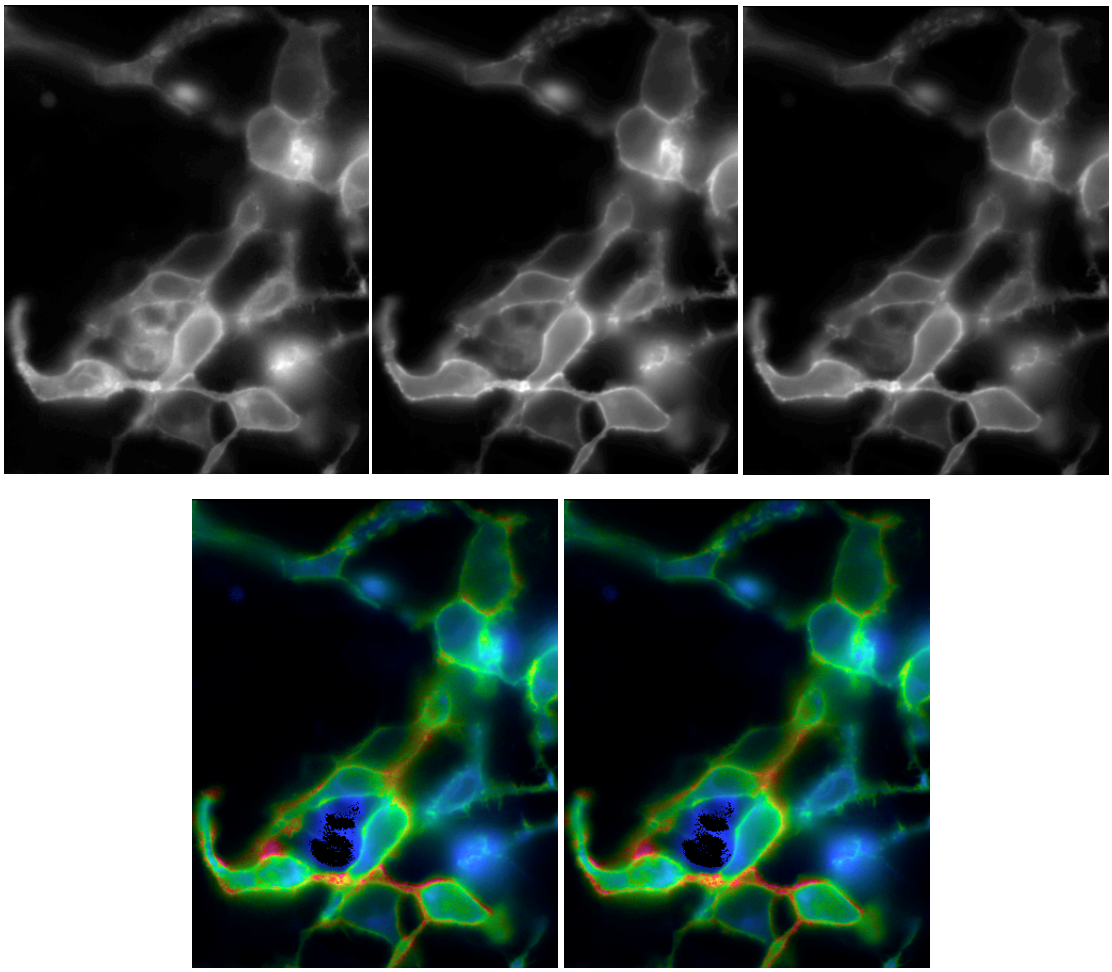

Figure 3.6 – GABASnFR0.1 expressed in HEK293 cells. Emission of CFP (*top left*), YFP direct (*top middle*) and YFP FRET (*top right*). YFP/CFP ratiometric image in 0μM (*bottom left*) and 10μM GABA (*bottom right*). Color ratio from blue to red is equal to 0.5-2.0 YFP/CFP

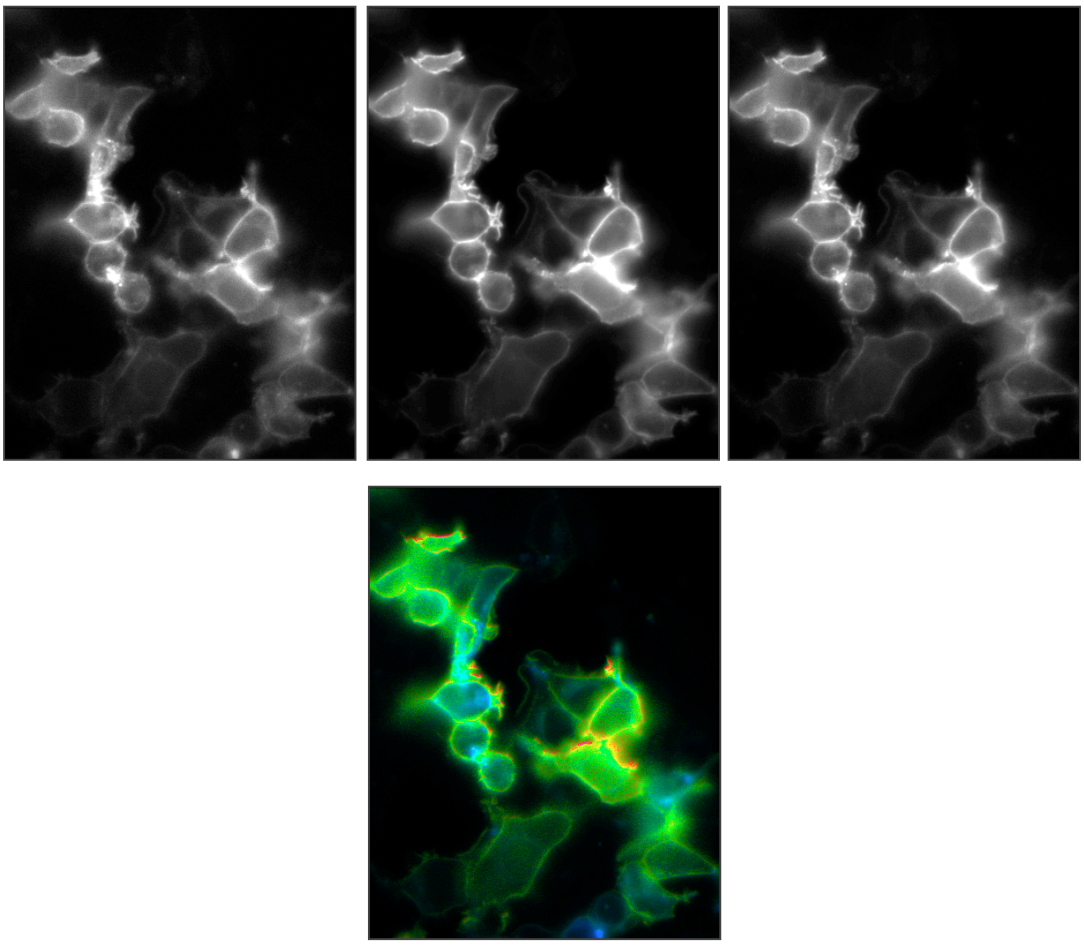

Figure 3.7 – GABASnFR0.1 with the GltI C-terminal tail from I274-N302 expressed in HEK293 cells. Emission of CFP (*top left*), YFP direct (*top middle*) and YFP FRET (*top right*). YFP/CFP ratiometric image in 0µM GABA (*bottom*). Color ratio from blue to red is equal to 0.5-2.0 YFP/CFP

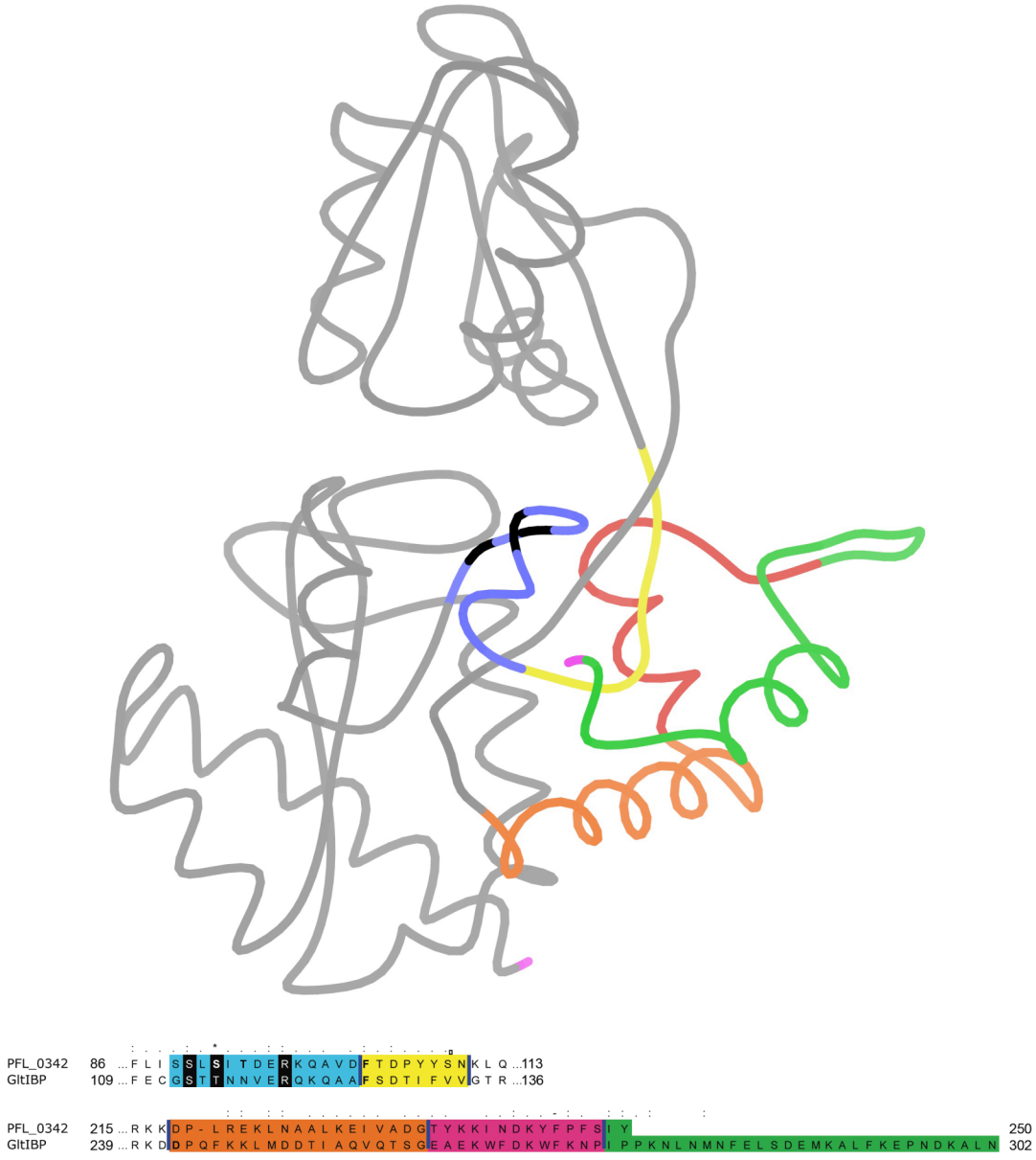

Figure 3.8 – Chimeric domain swaps between PFL_0342 and GltI. (*above*) Robetta fit of GltI. Colored sections indicate domains interacting with the C-terminal tail (*green*). All colored sections, except *blue*, were swapped with PFL_0342. *Blue* was left unswapped due to ligand binding residues within *black*.

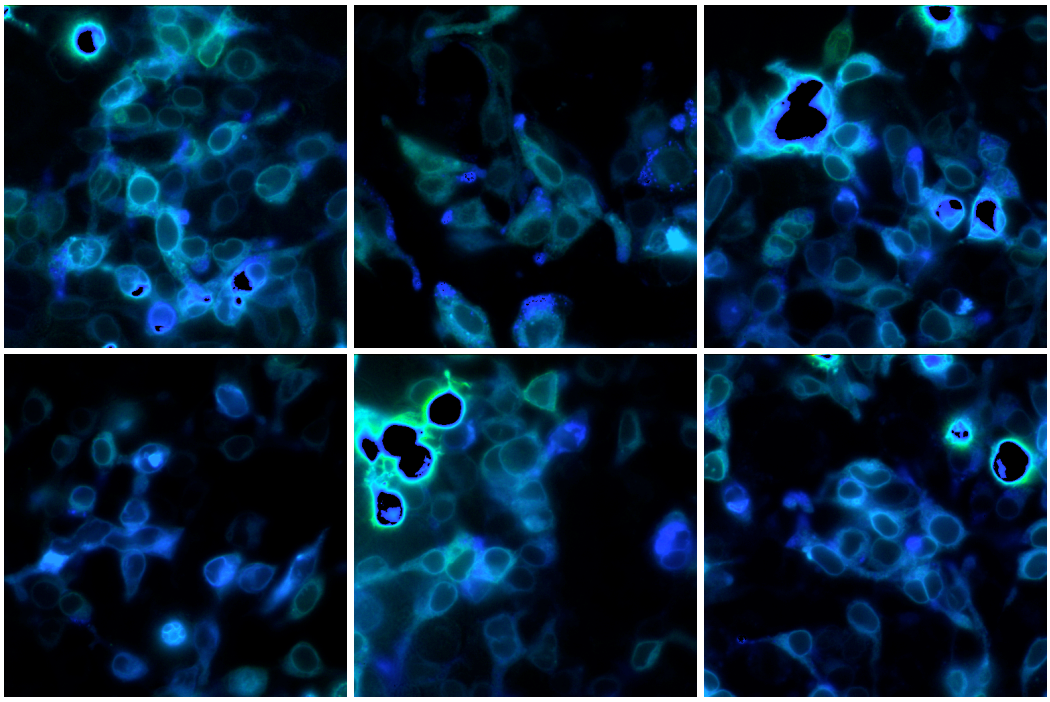

Figure 3.9 - Chimeric GABASnFR prototypes. Sensors include the full length 274I-302N (*top*) or the five amino acid truncated 274I-N297 tail from GltI (*bottom*). They also include GltI fragments E261-P273 (*left*), D243-P273 (*middle*), or F126-V133 with D243-P273 (*right*). Color ratio from blue to red is equal to 0.5-2.0 YFP/CFP

References

1. Roberts, E. GABA: The road to neurotransmitter status. In: *Benzodiazepine/GABA Receptors and Chloride Channels: Structural and Functional Properties*, R.W. Olsen and J.C. Venter, editors, pp. 1-39. New York: Alan R. Liss, Inc., 1986a.

2. Eccles, J. C. *The neurophysiological basis of mind; the principles of neurophysiology* (Clarendon Press, Oxford, 1953).

3. Fujita, I. & Konishi, M. The role of GABAergic inhibition in processing of interaural time difference in the owl's auditory system. *J Neurosci* **11**, 722-739 (1991).

4. Mitchell, S. J. & Silver, R. A. Shunting inhibition modulates neuronal gain during synaptic excitation. *Neuron* **38**, 433-445 (2003).

5. Pouille, F. & Scanziani, M. Routing of spike series by dynamic circuits in the hippocampus. *Nature* **162**, 717-723 (2004).

6. Verkman, A. S. Development and biological applications of chloride-sensitive fluorescent indicators. *The American Journal of Physiology*, C375-C308 (1990).

7. Augustine, G. J. & Neher, E. Calcium requirements for secretion in bovine chromaffin cells. *J Physiol (Lond)* **450**, 247-271 (1992).

8. Jayaraman, S., Teitler, L., Skalski, B. & Verkman, A. S. Long-wavelength iodide-sensitive fluorescent indicators for measurement of functional CFTR expression in cells. *Am J Physiol* **277**, C1008-18 (1999).

9. Looger, L. L., Dwyer, M. A., Smith, J. J. & Hellinga, H. W. Computational design of receptor and sensor proteins with novel functions. *Nature* **423**, 185-190 (2003).

10. Guthrie, G. D. & Nicholson-Guthrie, C. S. gamma-Aminobutyric acid uptake by a bacterial system with neurotransmitter binding characteristics. *Proc Natl Acad Sci U S A* **86**, 7378-7381 (1989).

11. Guthrie, G. D., Nicholson-Guthrie, C. S. & Leary, H. L. J. A bacterial high-affinity GABA binding protein: isolation and characterization. *Biochem Biophys Res Commun* **268**, 65-68 (2000).

12. Paulsen, I. T. et al. Complete genome sequence of the plant commensal Pseudomonas fluorescens Pf-5. *Nat Biotechnol* **23**, 873-878 (2005).

13. de Lorimier, R. M. et al. Construction of a fluorescent biosensor family. *Protein Sci* **11**, 2655-2675 (2002).

14. Baird, G. S., Zacharias, D. A. & Tsien, R. Y. Circular permutation and receptor insertion within green fluorescent proteins. *Proc Natl Acad Sci U S A* **96**, 11241-11246 (1999).

15. Nagai, T., Yamada, S., Tominaga, T., Ichikawa, M. & Miyawaki, A. Expanded dynamic range of fluorescent indicators for Ca(2+) by circularly permuted yellow fluorescent proteins. *Proc Natl Acad Sci U S A* 10554-10559 (2004).

16. Deuschle, K. et al. Construction and optimization of a family of genetically encoded metabolite sensors by semirational protein engineering. *Protein Sci* **14**, 2304-2314 (2005).

17. Kim, D. E., Chivian, D. & Baker, D. Protein structure prediction and analysis using the Robetta server. *Nucleic Acids Res* **32**, W526-31 (2004).

18. Malmqvist, M. Biospecific interaction analysis using biosensor technology. *Nature* **361**, 186-187 (1993).

Acknowledgements

The dissertation author designed and performed all experiments in Chapter Three. The Robetta fit of the GltI PBP was provided by Loren Looger.

Chapter Four

Development and application of pH-sensitive red fluorescent proteins to neuronal and astrocyte communication

Abstract

We attempt to visualize spontaneous vesicular glutamate release from astrocytes with GluSnFRs. We use a genetically-encoded sensor of vesicle fusion, synaptopHluorin, which reports changes in vesicle pH via a change in fluorescence intensity, to observe and localize spontaneous exocytosis in astrocytes. However, this sensor is limited to a GFP wavelength that is incompatible with simultaneous imaging with CFP/YFP FRET reporters. With the goal of simultaneous glutamate and vesicle fusion imaging, we develop a red-shifted variant of pHluorin, synaptopHluorange, which is spectrally orthogonal to GluSnFR. SynaptopHluorange is targeted to appropriate subcellular compartments when expressed in neurons and astrocytes. It also strongly responds to changes in intravesicular pH. However, synaptopHluorange expression appears to interfere with vesicle fusion machinery, preventing its use as an exocytosis sensor. Various improvements and optimizations to synaptopHluorange are made and further troubleshooting possibilities are discussed.

Introduction

The release of a single vesicle of neurotransmitter may be considered as the unitary bit of information transmission in the brain. Measuring the release of a synaptic vesicle by sensing its contents, as with GluSnFR imaging, has several benefits. Each vesicle has thousands of neurotransmitters, each which may transduce an optical response. Furthermore, measurement with a neurotransmitter-specific sensor identifies the vesicle contents, and thus the class of signal, excitatory, inhibitory or modulatory. However, there are cases where a vesicle fusion-specific sensor is

more useful. These include when the contents of the vesicle are already known or irrelevant, when spillover of neurotransmitter makes identification of specific synaptic sources unclear, when the location of vesicle release apparatus is unclear, and when the signal to noise ratio of GluSnFRs are insufficient to resolve responses. Vesicle fusion sensors also remove the possible confound of buffering of neurotransmitter by the sensor, although they introduce possible perturbation of the presynaptic release apparatus. If the experimental goal requires simply recording the flow of synaptic 'bits' of information, vesicle fusion sensors may be the most appropriate optical technique.

A common method for visualizing synaptic vesicle release has been by the destaining rate of vesicles filled with the fluorescent styryl dye FM1-43[1,2]. During a long train of electrical stimulation in the presence of FM1-43, vesicles are loaded with dye and become fluorescent. Subsequent depolarization and exocytosis in the absence of free extracellular FM1-43 causes the release of dye from the vesicle and a reduction in fluorescence. Disadvantages of this technique include diffuse background staining of extrasynaptic structures, the great difficulty of dye application in slice or *in vivo* preparations, required preloading with electrical stimulation or high potassium buffer, exocytosis measured as a decrease rather than increase in fluorescence, and possible perturbation of membrane fluid dynamics by intercalation of the dye.

Several limitations of this technique were resolved by the development of a genetically-encoded alternative. This was first demonstrated by tethering the pH-sensitive GFP mutant, ecliptic-pHluorin, to the interior of synaptic vesicles by genetic fusion to VAMP[3]. This construct is known as synaptopHluorin (SpH). Prior to

membrane fusion, intravesicular pH is near 5.5, making the pHluorin non-fluorescent. Following application of a high KCl solution or electrical stimulation, synaptic vesicles undergo membrane fusion and the previously quenched pHluorins are exposed to the extracellular buffer, with a pH of ~7.4. This causes a rapid brightening of the fluorescent protein and the cell membrane of the presynaptic terminal. In addition to ecliptic-pHluorins, where lower pH dramatically reduces the sensitivity of the 395nm excitation peak, ratiometric-pHluorins were created, where lower pH reduces the 395nm peak while increasing a 475nm excitation peak[3]. The signal to noise ratio of SpH was enhanced by the point mutations F64L and S65T, which produced superecliptic pHluorin, with increased single FP fluorescence[4].

As a genetically-encoded sensor, synaptopHluorins have allowed vesicle fusion to be visualized *in vivo*, in systems such as *Drosophila* antennal lobe[5] and mouse olfactory cortex[6]. However, their signal to noise ratio and thus their utility was limited by two factors: the level of background fluorescence, and the maximal brightness of each vesicle. VAMP-tethered proteins leave ~12% of the pHluorins on the extracellular surface of the axon. Since pHluorins expressed on the cell surface are much brighter those quenched inside vesicles, the small percentage of surface expressed pHluorins are a major source of background fluorescence[4]. An improved targeting scheme was found to be insertion of superecliptic pHluorin into a permissive site in the vesicular membrane protein synaptophysin, which lowers the surface expressed fraction by 53% (Y Zhu, J Xu, CF Stevens, SFN Abstracts 2006). Fusing a second pHluorin to the synaptophysin-pHluorin raised the maximal fluorescence increase by ~101%. This optimized construct (2p-SypH) had a 328% improvement in

ΔF/F0 over VAMP-SpH (Y Zhu, unpublished observations). 2p-SypH and VAMP-SpH were used for our studies of neurons and astrocytes.

A remaining advantage of styryl dye based imaging is the availability of multiple orthogonal colors. FM4-64 is a dye with characteristics similar to FM1-43, but with a longer wavelength, which permits their simultaneous use. These two dyes can be combined to study complex behavior of synaptic vesicles, such as the mixing of vesicle pools between synaptic boutons[7]. Bringing the multi-color advantage of styryl dyes to a genetically-encoded solution would greatly expand the potential for studying synaptic vesicle release, receptor mixing and turnover in brain slice and *in vivo*. To this end, we attempted to develop a red-shifted version of synaptopHluorin. This could be used simultaneously with green SpH, GFP or CFP/YFP-based sensors, permitting studies of synaptic activity in distinct populations of neurons simultaneously. Interrogation modalities could also be mixed, allow the observation of the relationship between vesicle release and neurotransmitter or calcium dynamics.

Astrocytes have taken an expanding role in the field of synaptogenesis, synaptic stability and neuronal communication. Astrocytes not only scavenge excess glutamate from the extracellular space, they also release glutamate in a calcium-regulated manner[8]. This release appears to be vesicular[9]. Recently, glutamate release from astrocytes was shown to modulate neuronal excitability and increase the synaptic release probability between neighboring neurons[10,11]. We attempted to directly observe glutamate release from astrocytes using GluSnFR, and to characterize its release properties. The challenges associated with localizing the sites of neurotransmitter

release in space and time provided an excellent test application for the development and use red-shifted pHluorins in conjunction with neurotransmitter imaging.

Results

We first simply checked if we could see spontaneous glutamate release from astrocytes. We transfected cultured hippocampal astrocytes with the prototype $GluSnFR_{8N0C}$:pDisplay. Astrocytes had a wide and very flat morphology with GluSnFR expressed relatively homogenously on the extracellular surface with scattered intracellular puncta (Fig. 4.1). In glutamate-free Ringer's solution, mean YFP/CFP ratios over the entire cell were 2.15, which was reversibly lowered to 1.87 by the addition of 250μM glutamate (Fig. 4.2). However, following observation of astrocytes without any exogenous stimulation, no global or localized changes in FRET ratio were resolvable above noise. Pilot experiments using total internal reflection microscopy to reduce the background fluorescence also failed to show clear, localized, spontaneous glutamate release.

A prerequisite for vesicular glutamate release is the release of vesicles. To check for spontaneous glutamate release, we transfected astrocytes with VAMP-pHluorin. Initial observation showed no obvious spontaneous changes. However, following several minutes of visual inspection through the microscope, spontaneous flashes of fluorescent puncta appeared (Fig. 4.3). Over the course of observation, significant bleaching of the membrane exposed pHluorin fraction occurred, greatly increasing the relative contrast of the exocytosing vesicles. These puncta appeared much larger and more fluorescent than single synaptic vesicle releases in cultured

neurons. The release sites were randomly distributed across the entire surface of the astrocyte (Fig. 4.4). These flashes were also observable without pre-bleaching by post-hoc subtraction of the initial astrocyte fluorescence signal. Their release and requenching kinetics were variable, but could be grouped into two broad classes. Of 58 fusion events analyzed in 30 seconds of observation, 33 events released and quickly quenched, with a time to half-decay of 3.1 seconds (Fig. 4.5), 4 remained stuck in a fluorescent state (Fig. 4.6), and 21 were excluded from analysis due to multiple events overlapping events in the same region. These two classes of release may be analogous to kiss-and-run vs. full fusion events at a central synapse[12], or may represent astrocyte-specific vesicle recycling modes. In nearly all cases, the fluorescence onset occurred faster than our camera could resolve, with 10-90% rise time in 2 frames (30Hz interlaced frame rate).

Although we demonstrated that spontaneous vesicle fusion occurs in astrocytes, the contents of the vesicles were unknown. A major limitation in our ability to resolve possible glutamate transients from the vesicle releases was the random distribution of release times and locations, which prevented trial-based averaging of the glutamate signal. Therefore, we sought to create a probe that could provide the time and location of vesicular release, and could be used simultaneously with GluSnFR. The superecliptic pHluorin used in the VAMP-pHluorin astrocyte imaging had the emission spectrum of EGFP, which would interfere with GluSnFR. However, during the diversification of fluorescent wavelength of the monomeric red fluorescent protein mRFP[13] into the mFruit family[14], several variants were found to have enhanced pH-sensitivity. In particular, precursors to mOrange had pKas in the range of pH 6.5-

7.5. These also had emission spectra that were sufficiently distinct from the Citrine component of GluSnFR (Fig. 4.7). Therefore, we tested these as fluorescent markers of vesicular release.

Synaptophysin is a four-transmembrane, vesicle-associated integral membrane protein its with N- and C-terminus located on the cytosolic side of the membrane[15]. Screening pHluorin insertions at numerous sites between transmembrane segments one and two, and between three and four by Y. Zhu and J. Xu led to an insert with synaptic targeted fluorescence, which was responsive to electrical stimulation. The permissive site was between amino acids T181 and T184. While most published reports on synaptopHluorins used a configuration similar to the VAMP fusion, superecliptic pHluorin insertion into this permissive site of synaptophysin yielded a 2.5-4x increase in puncta fluorescence ($\Delta F/F$) compared to VAMP-based constructs, due to reduced surface fluorescence (Y Zhu, J Xu, CF Stevens, SFN Abstracts 2006). Therefore, the initial synaptopHluorange prototype consisted of mOFP(74-11) inserted between T181 and T184 of synaptophysin (SFO).

Two days after transfection of SFO into DIV7 hippocampal neurons, dim orange puncta were seen along the axons of transfected cells. The fluorescence intensity was similar to autofluorescence of the astrocyte feeder layer, but was distinctly orange by eye, in contrast to the yellowish autofluorescence. The expression pattern appeared similar in morphology to SypH expressing presynaptic terminals. Puffing of Ringer's solution of pH 7.4 containing 50mM ammonium chloride (NH_4Cl) onto the cells produced a rapid, transient 5-fold increase in ($\Delta F/F$) (Fig. 4.8), consistent with the alkalinization of mOFP containing synaptic vesicles. However,

application of a 90mM KCl Ringer's solution to depolarize the neurons resulted in no change in fluorescence intensity. Delivery of 900 action potentials by field stimulation also had no effect. To address the possibility that the synaptic machinery had insufficient time to mature at DIV9, we repeated these experiments at DIV14, seven days post-transfection, which gave identical results.

Faced with the failure to detect neuronal release with a synaptophysin-based sensor, a more conventional design of mOFP fused to the C-terminus of VAMP was tested (VSFO). When transfected into neurons, membrane surface expression was higher in this construct, hence the $\Delta F/F$ upon NH_4Cl application was only 2.5-fold (Fig. 4.9). This construct also did not respond to either high KCl application or sustained field stimulation. Interleaved experiments with neurons from the same batch of cultures that were transfected with either SpH or SypH showed robust responses to electrical stimulation.

Since synaptic targeting for both SFO and VSFO appeared identical to the corresponding pHluorin-based sensor and the fluorescence response changed appropriately with intracellular alkalinization, the sensor failure was likely due to intrinsic properties of the fluorescent protein. Although SFO showed a 5-fold change in neurons upon NH_4Cl application, the slope and pKa of mOFP (Fig. 4.10) may not have been optimal for detecting electrically-evoked release. Variants of mOFP with pKas of 6.5, 7.0, and 7.5 were inserted into synaptophysin and were tested along with mOFP(74-11) on transfected HEK293 cells. The construct with the maximum dynamic range between HBSS (pH 5.5) and HBSS + NH_4Cl (pH 7.4) was mOFP-7.0.

However, SFO constructed with this mOFP variant still showed no response to electrical stimulation when expressed in hippocampal neurons.

Another possibility for the lack of response of mOFP-based constructs to electrical and chemical stimulation was the relatively fast bleach rate of mOFP relative to EGFP. Since the fluorescence rise from electrically evoked release is relatively slow, freshly dequenched mOFP from sequentially released vesicles might be quickly bleached, resulting in no aggregate increase in fluorescence. The time to bleach from 1000 to 500 photons*$mol^{-1}s^{-1}$ for EGFP is 174 seconds, while it is 9.0 seconds for mOrange[16], a 19-fold difference. Following screens for photostability, a vastly more photostable mOFP variant was found. This mOrange2 had Q64H, F99Y, E160K, and G196D mutations from mOrange and a half-bleach time of 228s (N. Shaner, P. Steinbach, unpublished observations). mOrange2-synaptophysin (SFO2) expressed in HEK293 cells was highly photostable, exhibiting a slight photoactivation and subsequent bleach during three minutes of 1Hz, 500ms illumination (Fig. 4.11). However, electrical stimulation of SFO2 expressing neurons again gave no increase in fluorescence. Astrocytes transfected with VAMP-mOrange2 showed surface fluorescence similar to SpH, but extended observations revealed no spontaneous vesicle release.

A final possibility for the lack of synaptopHluorange function was the direct interference of mOFP with vesicle release machinery. Substitution of another pH-sensitive mRFP descendent, mApple0.2, into VAMP and synaptophysin constructs yielded synaptically targeted fluorescence that was unresponsive to electrical stimulation. We hypothesize that descendents of the DsRed/mRFP protein family may

exhibit a residual tendency to dimerize or aggregate inside the synaptic vesicle, due to low vesicle pH or high protein concentration. This could crosslink essential synaptic proteins and inhibit synaptic release.

Discussion

We sought to develop red-shifted pHluorins as a tool to complement and extend fluorescent imaging techniques for neuronal and astrocyte communication. Although our attempts at using synaptopHluorange for measuring electrically-evoked synaptic release from neurons and spontaneous vesicle release from astrocytes failed, they suggest future troubleshooting experiments and applications where they may find more success. Potential problems with the fluorescence pH-sensitivity and bleach rate were examined and solved, but the possibility of fluorescent protein dimerization remains.

The average synaptic vesicle contains 70 copies of VAMP and 32 of synaptophysin[17]. The average interior volume of a vesicle is 19.86e-21 L[17], giving the interior concentration of VAMP as ~6mM and synaptophysin as ~3mM. In vesicles over-expressing VAMP-pHluorange or synaptophysin-pHluorange, the concentrations could be significantly higher. Furthermore, these proteins are tethered to the membrane and thus confined to the interior vesicle surface, further increasing their effective concentration. mRFP-derived fluorescent proteins have a large number of surface-exposed, positively-charged lysines and arginines, making an enhanced dimerization at low-pH unlikely. However, dimerization tendencies at millimolar fluorescent protein concentrations have not been tested (R. Campbell, personal

communication). Given the extreme packing conditions inside a synaptic vesicle, one might expect that green synaptopHluorins also dimerize, aggregate or interfere with synaptic release. There is anecdotal evidence of this, as terminals with the greatest absolute change in fluorescence to electrical stimulation typically have only a moderate level of expression (Y. Zhu, personal communication). With mRFP derivatives, interference may be significantly worse due to their specific pattern of surface charges or orientation.

An important clue to the mode of synaptopHluorange failure is to determine if SFO2 or VSFO2 expression is dominant negative for synaptic release. To test this, SypH and SFO2 or VSFO2 should be cotransfected into neuronal cultures. This will result in a sparse labeling of cells with a mixture of orange and green synaptopHluorins in different ratios. Electrical stimulation of coexpressing cells should demonstrate whether orange synaptopHluorin expression blocks synaptic release. The release efficiency could be compared with the green vs. orange ratio of presynaptic terminals to determine if the release block is a graded phenomenon and if orange pHluorin-tagged vesicles can be rescued by substitution or dilution with functional green pHluorin-tagged synaptic proteins. Predominantly green cells could provide an internal positive control for release.

To test the degree to which mOrange2 and other mRFP derivatives exhibit pH or concentration-dependent dimerization, analytical equilibrium centrifugation could be performed on purified FPs at pH 5.5 and at pH 7.4[18,19]. One difficulty with this analysis is that the precise buffer composition of the vesicle lumen is uncertain. Salt or protein concentrations may have a significant impact dimerization tendency. Also,

concentration gradients reaching tens of millimolar of fluorescent protein may be difficult to achieve.

Although a primary goal of this project was to validate mOrange2-based pHluorins in a biologically relevant system, the quantitative measurement of glutamate release from astrocytes remains a research interest. If orange pHluorins remain non-functional, there are other mechanisms for determining timing of astrocyte secretory-vesicle release. One very popular method has been to load astrocyte vesicles with acridine orange (AO)[9,20]. Release of the vesicle causes a rapid dequenching of AO and a burst of green fluorescence. However, this dye stains acidic lysosomal and endosomal vesicles, which can also undergo exocytosis. It also exhibits a metachromicity[21], which makes spectral segregation from EGFP or GluSnFR difficult. An approach which avoids these difficulties is the use of the red dye FM4-64 to observe vesicle turnover[22]. This gives sufficient spectral segregation from GluSnFR, but retains the negative aspects of styryl dye labeling.

Orange pHluorins may yet prove to be useful molecular tags when not confined within tightly packed synaptic vesicles. Trafficking of specific membrane receptors into and out of the plasma membrane plays a crucial role numerous cellular processes, including regulation of synaptic strength[23], pain perception[24], cell motility[25], and cell fate determination[26]. Receptors of different types can be genetically labeled with distinct fluorescent tags, but these rarely discriminate between surface expressed and intracellular receptor localization. To understand the dynamics of receptor exo- and endocytosis, a tag that changes its fluorescence depending on its subcellular localization would be ideal. In the case of synaptic strength, activity-

dependent changes in surface expression of GluR1 and GluR2 subunits can dramatically shift postsynaptic ion selectivity and current amplitude[27]. Recently, the pH-dependent fluorescence of green pHluorins have been used to monitor changes in surface expressed AMPA receptor subtypes, exploiting the differential pH between cell surface and secretory vesicles[28]. Using orange pHluorins in conjunction with green could facilitate comparisons of the functional expression of two populations of receptor subtypes.

Materials and Methods

Sensor construction

DNA for the mRFP derivatives mOFP(74-11), mOFP6.5, mOFP7.0, mOFP7.5, mOrange, mOrange2 and mApple0.2 were obtained from N. Shaner in pBAD bacterial expression vectors. To make single FP synaptophysin-pHluoranges, a pCDNA3 mammalian expression vector containing the coding sequence of mouse synaptophysin (NM_009305) with an *EcoRV* restriction site inserted between the third and fourth transmembrane domain was obtained from J. Xu. To generate the *EcoRV* site, the amino acid sequence from synaptophysin residue 181 was changed from TGNT to TDIT. Blunt-end, full-length OFP fragments were generated by PCR with *pfu* polymerase (Promega) with primers that reconstituted a single *EcoRV* site at the N-terminal end of the insert following blunt-end ligation into the *EcoRV*-digested synaptophysin vector. Double FP insertions were made by digesting the resulting vector with *EcoRV* and inserting the OFP fragment again. OFP tagged VAMP constructs were made by replacement of the pHluorin in a VAMP-pHluorin pCDNA3 vector from J. Xu. The VAMP-pHluorin vector was digested with *KpnI* and *EcoRI* and OFP PCR fragments with compatible cohesive ends were ligated in.

Tissue Preparation

Neuronal cultures were prepared and transfected as described in Chapter One. Astrocytes were harvested by dissection and dissociation of hippocampus from P0-P1 rats. Following dissociation, 400,000 hippocampal cells were placed in 25cm^2 plastic tissue-culture flasks containing 10mL of 10FCS astrocyte feeding media. 10FCS consisted of MEM (Gibco 51200-020), 10% fetal calf serum (Gibco 26140-028), 2%

glucose, 0.5% N2 supplement (Gibco 17502-014) and 0.5% pen/strep antibiotic solution (Gibco 15070-014). Astrocytes adhered to the flask floor and continued division till the flask was confluent at two weeks post-seeding. Media was replaced every three days. To remove contaminating neurons, flasks were sealed and placed in a culture shaker at 37^{o}C overnight. Following media exchange, a purified layer of astrocytes remained. These were seeded onto poly-D-lysine coated glass coverslips at 10,000 cells per 18mm coverslip. Two days after plating, cells were transfected with GluSnFR$_{8N0C}$, or pHluorin constructs. Astrocytes were imaged 3-7 days post-transfection.

Neuronal and Astrocyte Imaging

All experiments were performed at room temperature and all fluorescence analysis was background subtracted. Most imaging of spontaneous astrocyte vesicle release and electrical stimulation of GluSnFR or pHluorin-expressing neurons was performed with the same optical setup as the neuronal imaging described in Chapter One. A DualView FITC/Dil filter set (EX: 480/20, 545/14; EM: 515/30, 585/40; Optical Insights) was used for syanptopHluroin and synaptopHluorange imaging. Spontaneous astrocyte vesicle release was typically visualized through a 50% neutral density excitation filter. Bath solution was a Ringer's solution with 2mM $CaCl_2$, 1.3mM $MgCl_2$.

All tests of synaptopHluorange variants in HEK293 cells were imaged on a Zeiss Axiovert 200M microscope through a 40x oil objective with a cooled CCD camera (Roper Scientific), controlled by Metafluor 6.1 Software (Universal Imaging).

Filter sets were EM: 540/25, EX: 595/50, and 560 dichroic (Chroma). Bath solutions were Hank's Buffered Salt Solution of pH 7.4 or acidified with HCl to pH 5.5.

TIRF imaging of GluSnFR was acquired using a through-the-lens Olympus IX71 TIRF microscope with an Apo 100x 1.65NA lens. Illumination was provided by a 488 ion laser (Melles Griot) and images acquired with a Cascade 512B CCD camera (Photometrics). Data streams were recorded and analyzed in Metafluor.

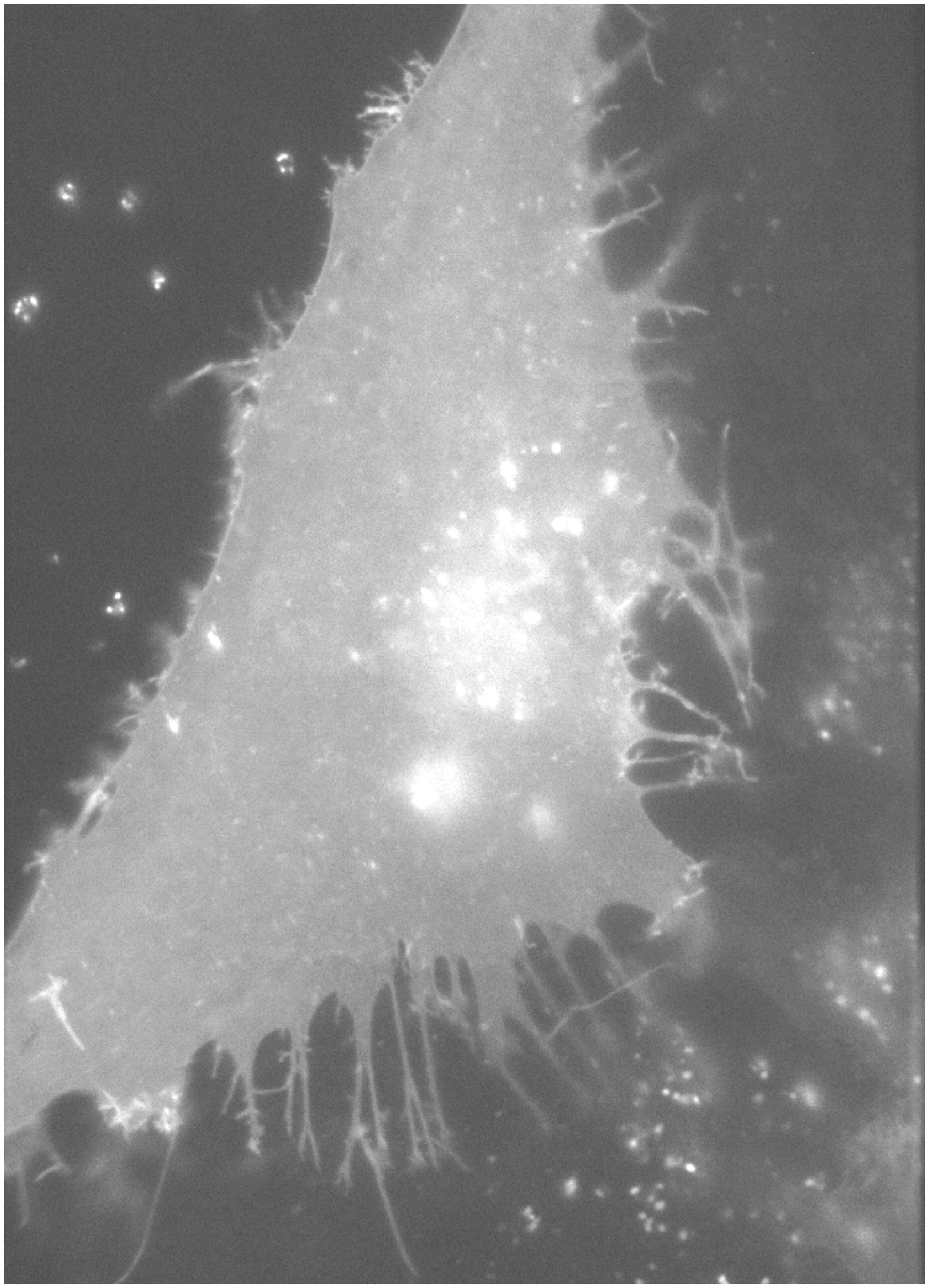

Figure 4.1 – YFP FRET emission of a $GluSnFR_{8N0C}$ transfected cultured hippocampal astrocyte.

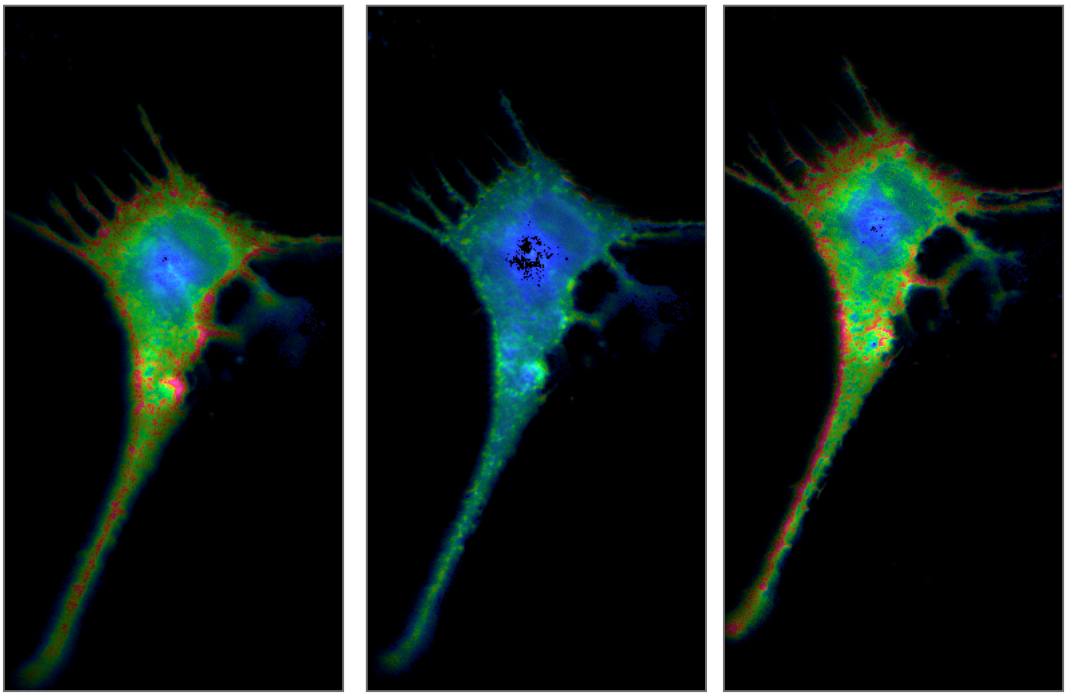

Figure 4.2 – YFP/CFP emission ratio change of $GluSnFR_{8N0C}$ transfected astrocytes. Buffer is Ringer's before glutamate application (*left*), during 100µM glutamate application (*center*), and after glutamate washout (*right*). Color scale is from 0.5 blue to 2.0 red.

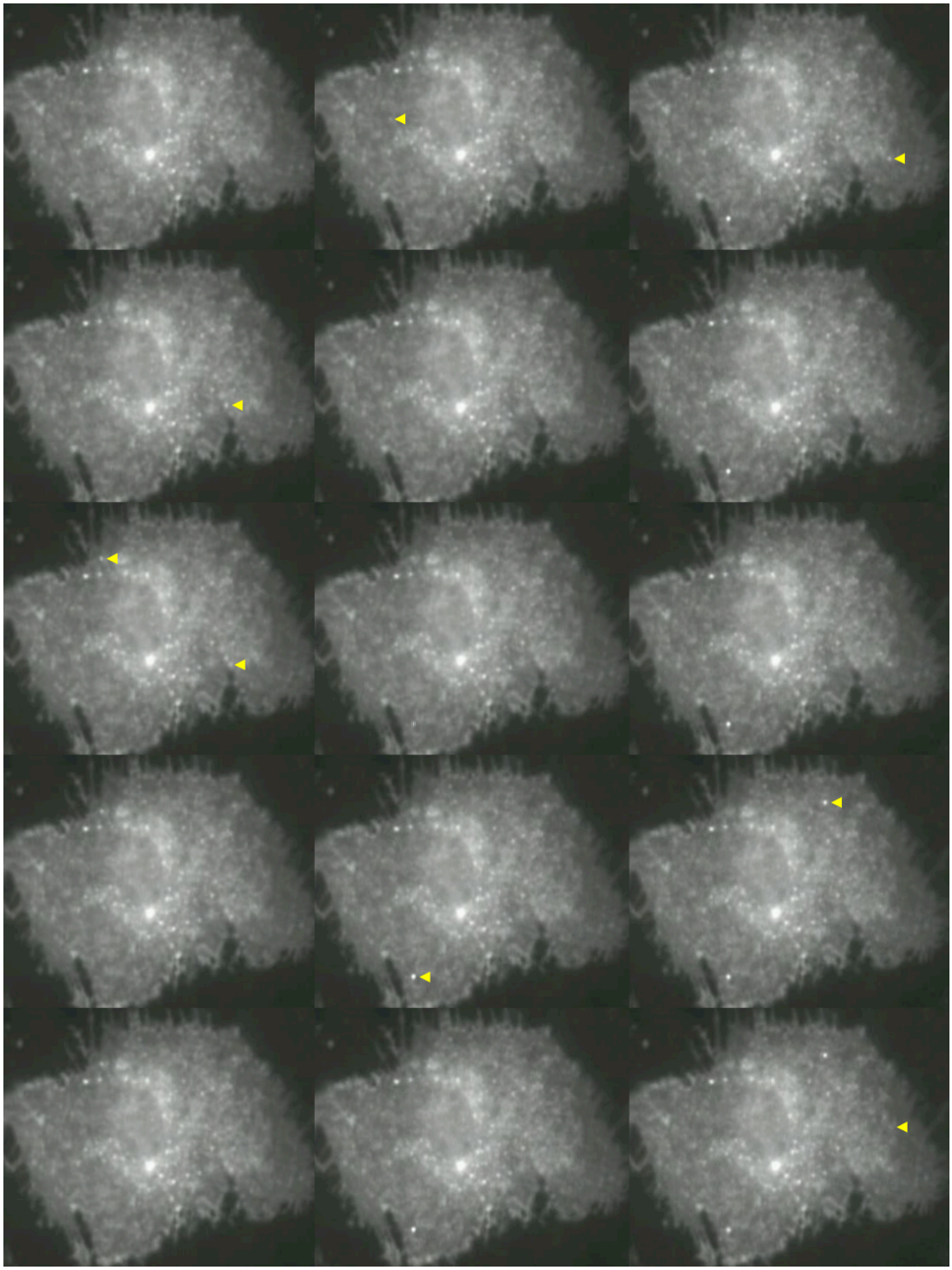

Figure 4.3 – Vesicle fusion events in VAMP-pHluorin expressing astrocyte. Frames spaced 150ms apart, viewed downwards from top left to bottom right. Yellow arrows indicate new fusion events.

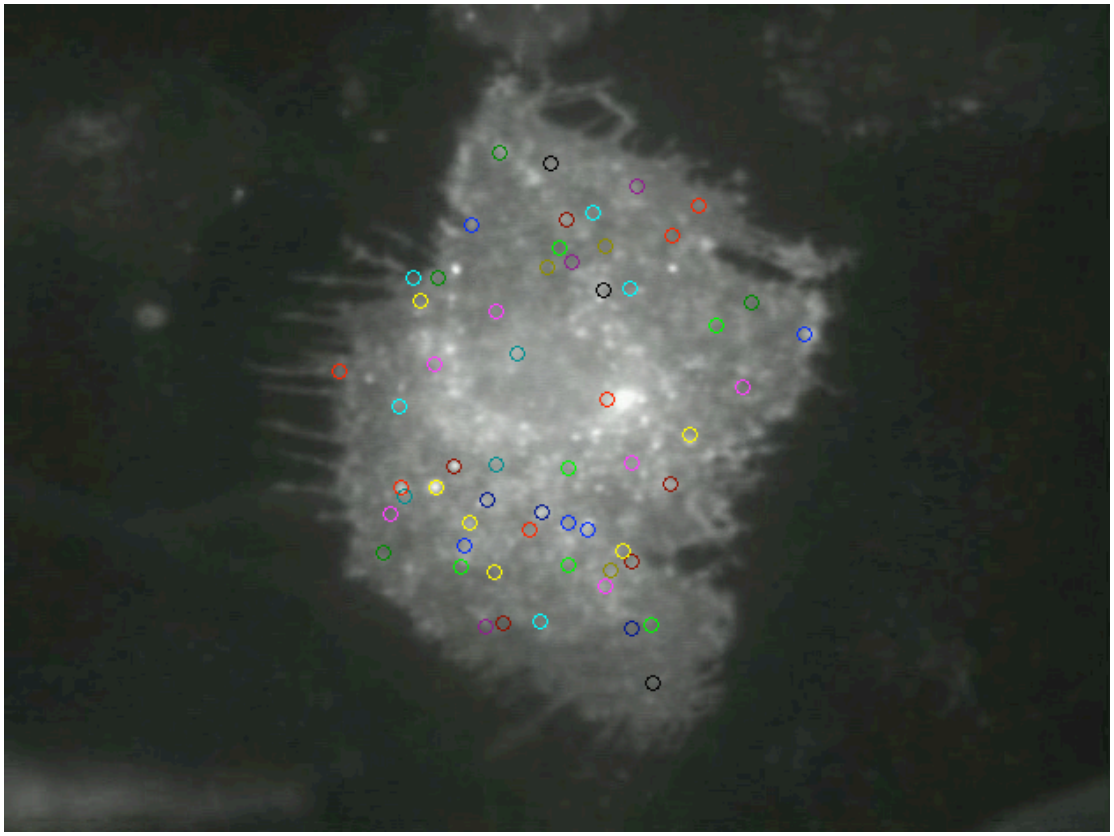

Figure 4.4 – Locations of spontaneous vesicle release during a 30-second observation period of a VAMP-pHluorin expressing astrocyte.

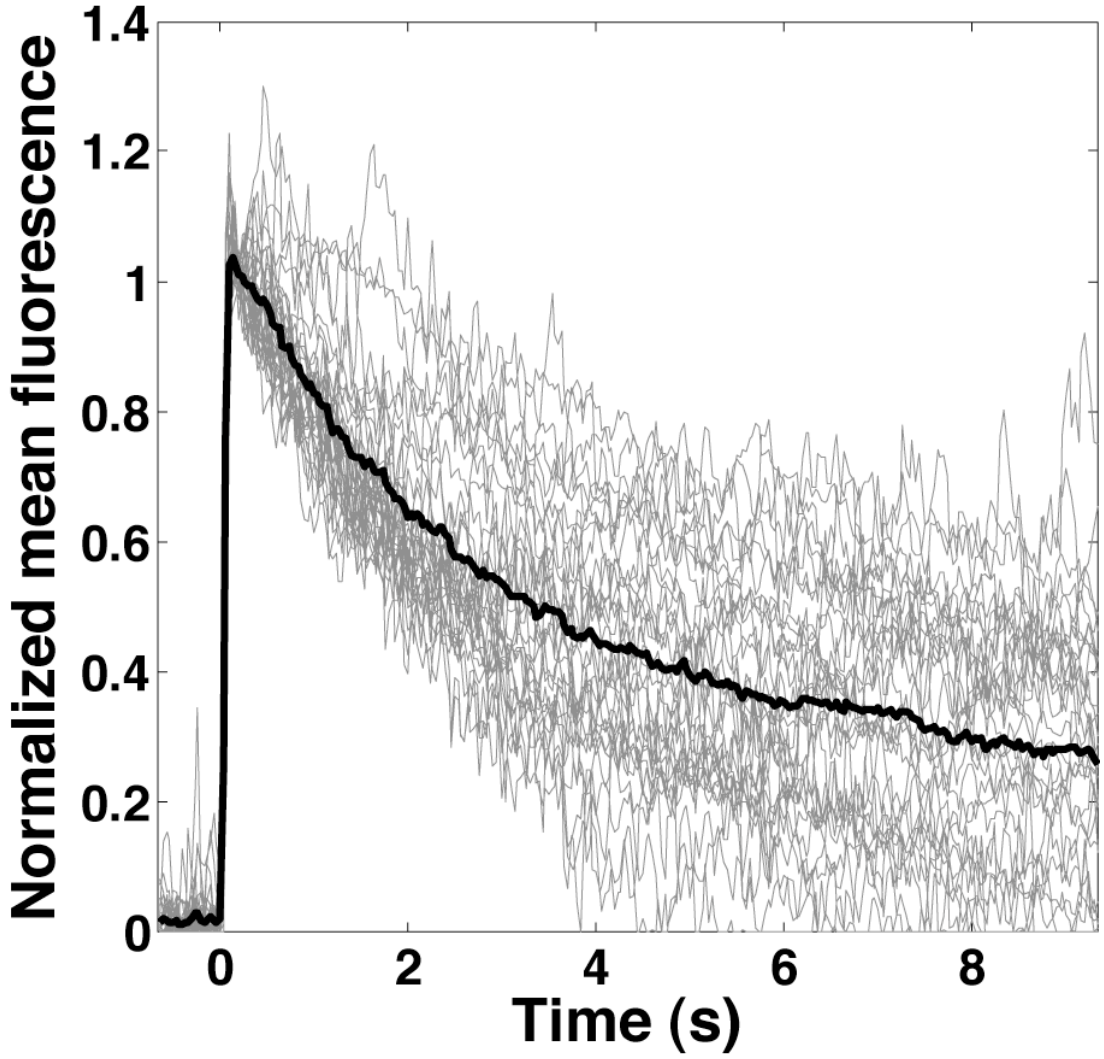

Figure 4.5 – Timecourse of fluorescence decay of typical SpH vesicle release events in astrocytes. Gray traces are individual events, while the mean response is in thick black. Responses are background subtracted and normalized, but not corrected for bleaching

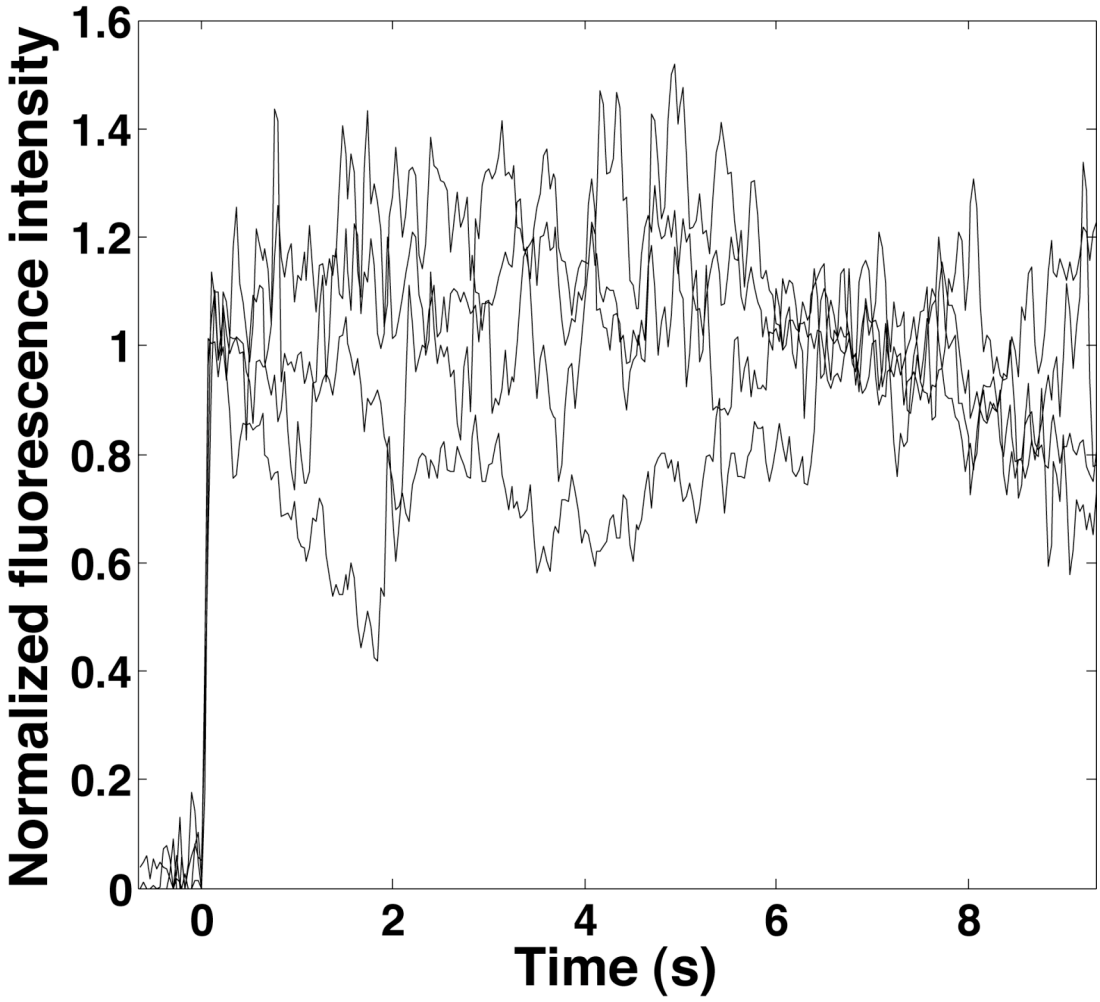

Figure 4.6 – Lack of fluorescence decay of stuck-on SpH vesicle release events in astrocytes. Each line is an individual event.

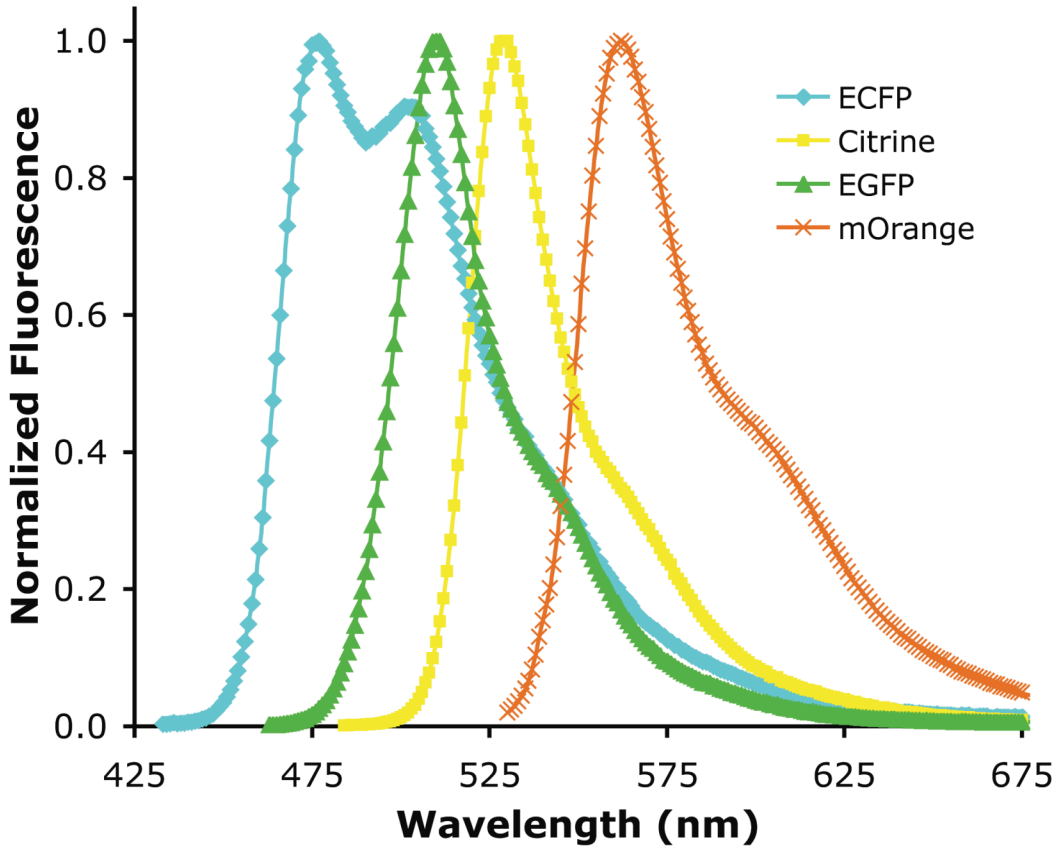

Figure 4.7 – Emission spectra of GluSnFR components, EGFP, and mOrange.

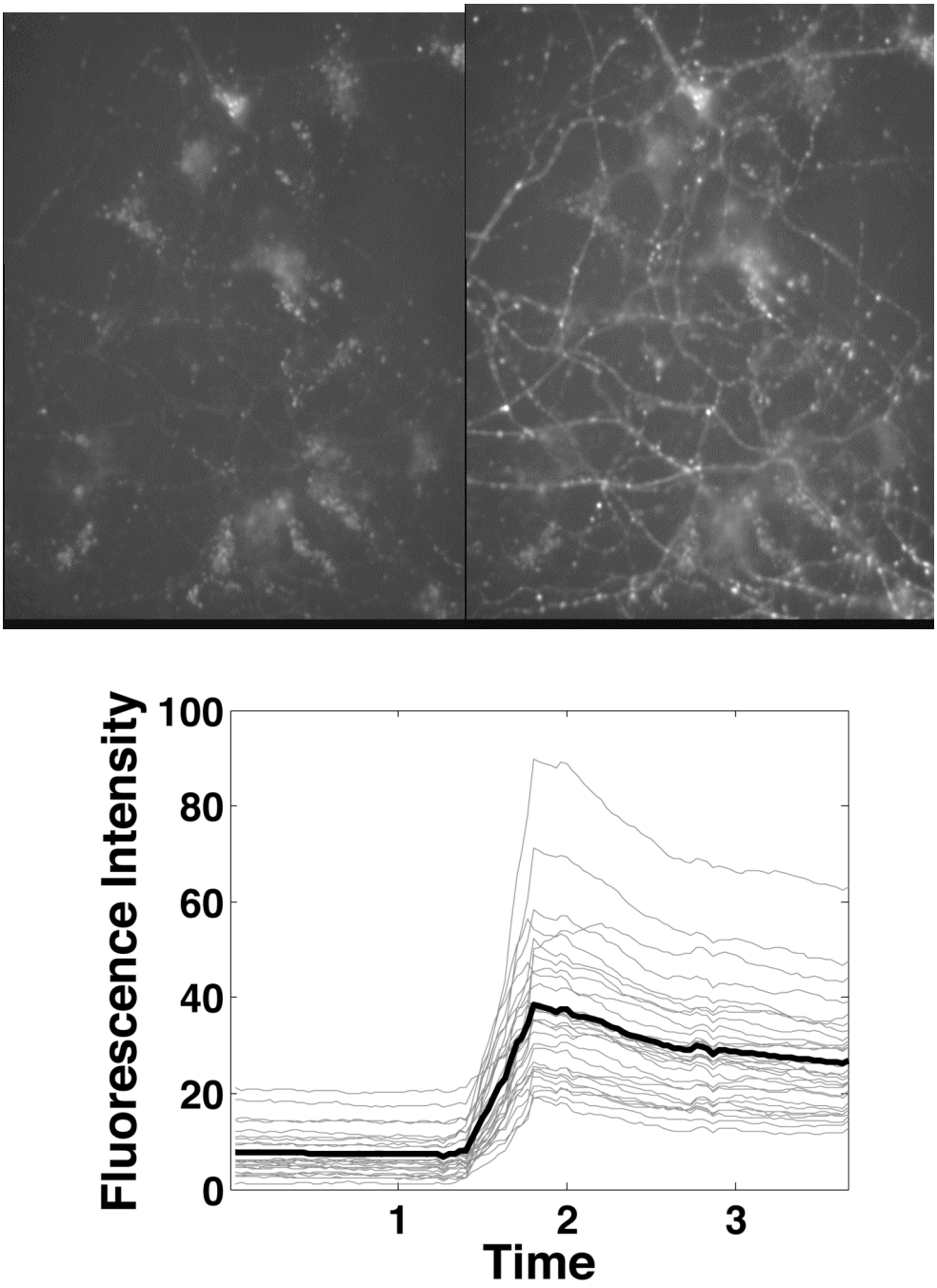

Figure 4.8 – Response of SFO transfected neurons to intracellular alkalinization. Orange fluorescence in Ringer's solution before (*left*) and during 50mM NH_4Cl (pH 7.4) perfusion (*right*). Fluorescence change of selected punctua from perfusion (*bottom*). Individual punctua in gray, average in thick black.

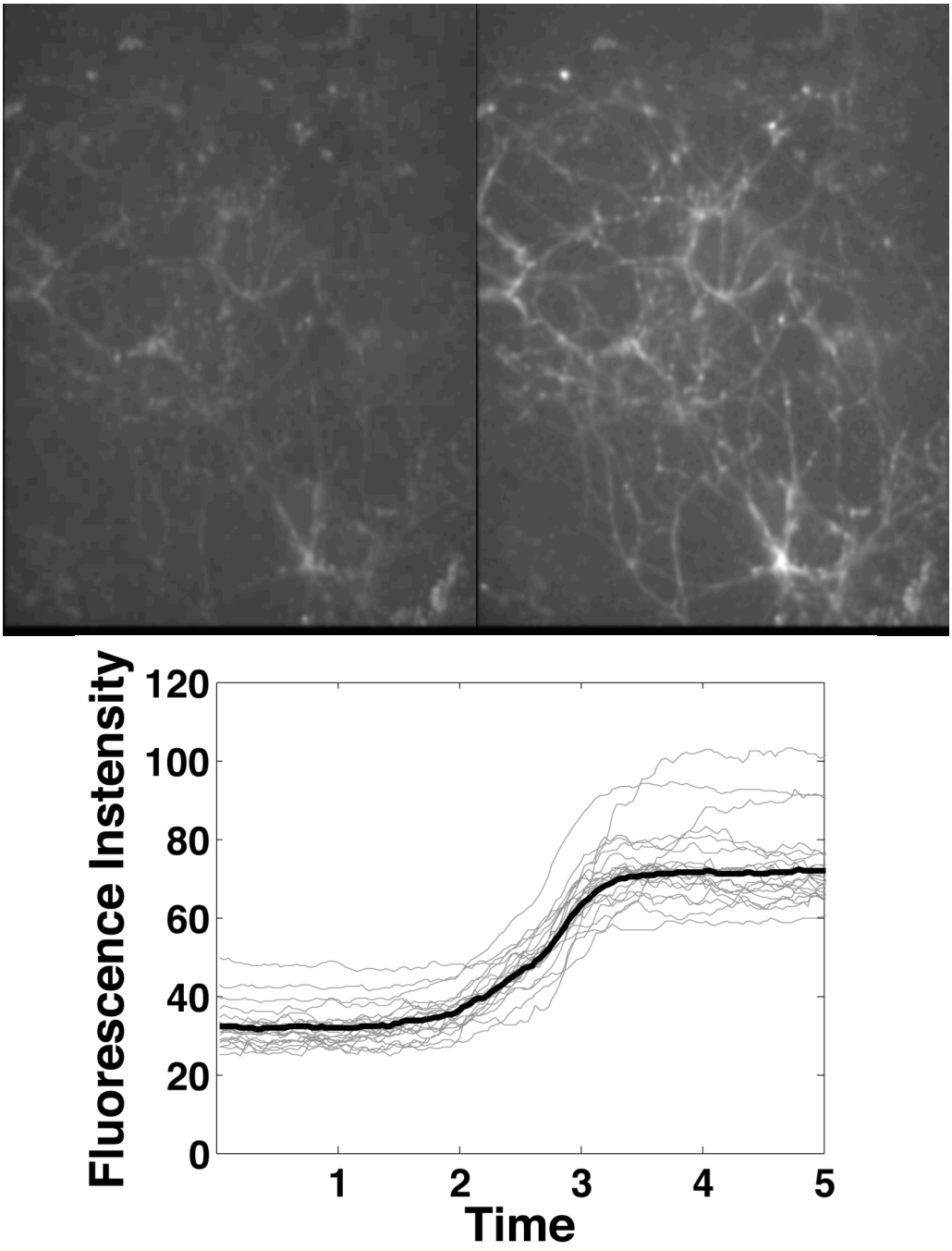

Figure 4.9 – Response of VSFO transfected neurons to intracellular alkalinization. Orange fluorescence in Ringer's solution before (*left*) and during 50mM NH_4Cl (pH 7.4) perfusion (*right*). Fluorescence change of selected puncta from perfusion (*bottom*). Individual puncta in gray, average in thick black.

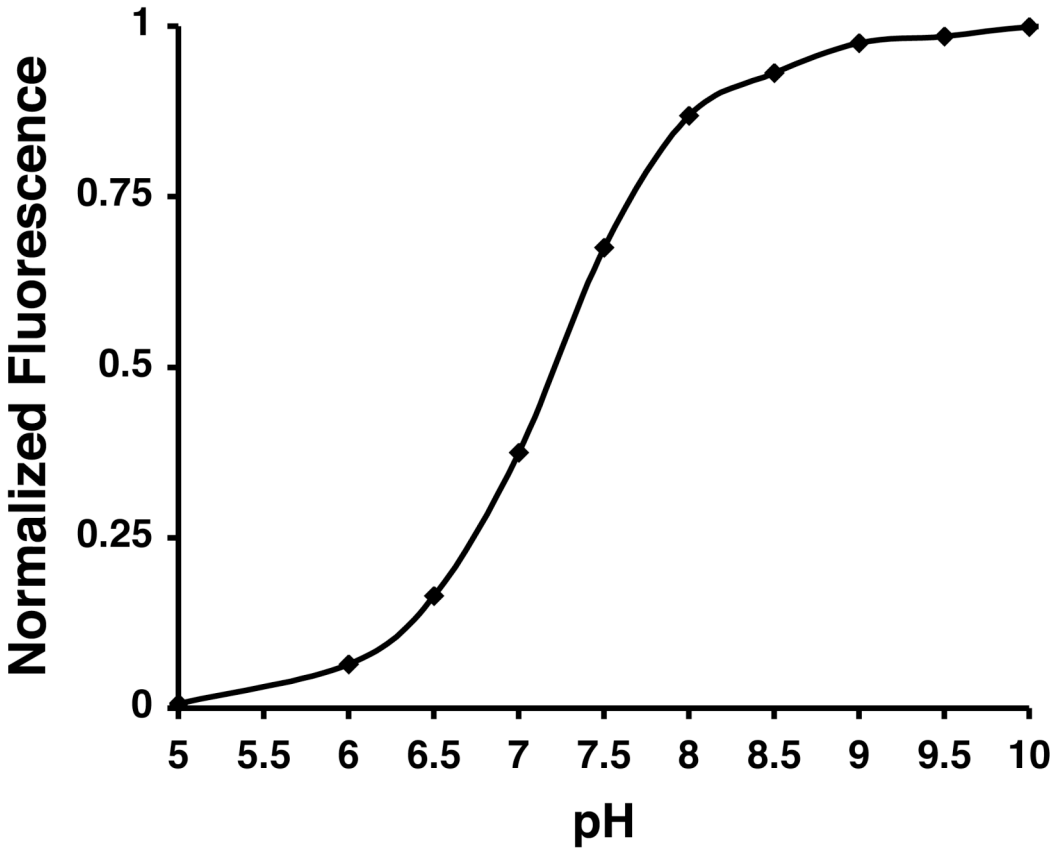

Figure 4.10 – The emission intensity of mOFP is strongly pH-dependent. The pKa of mOFP is pH 7.2.

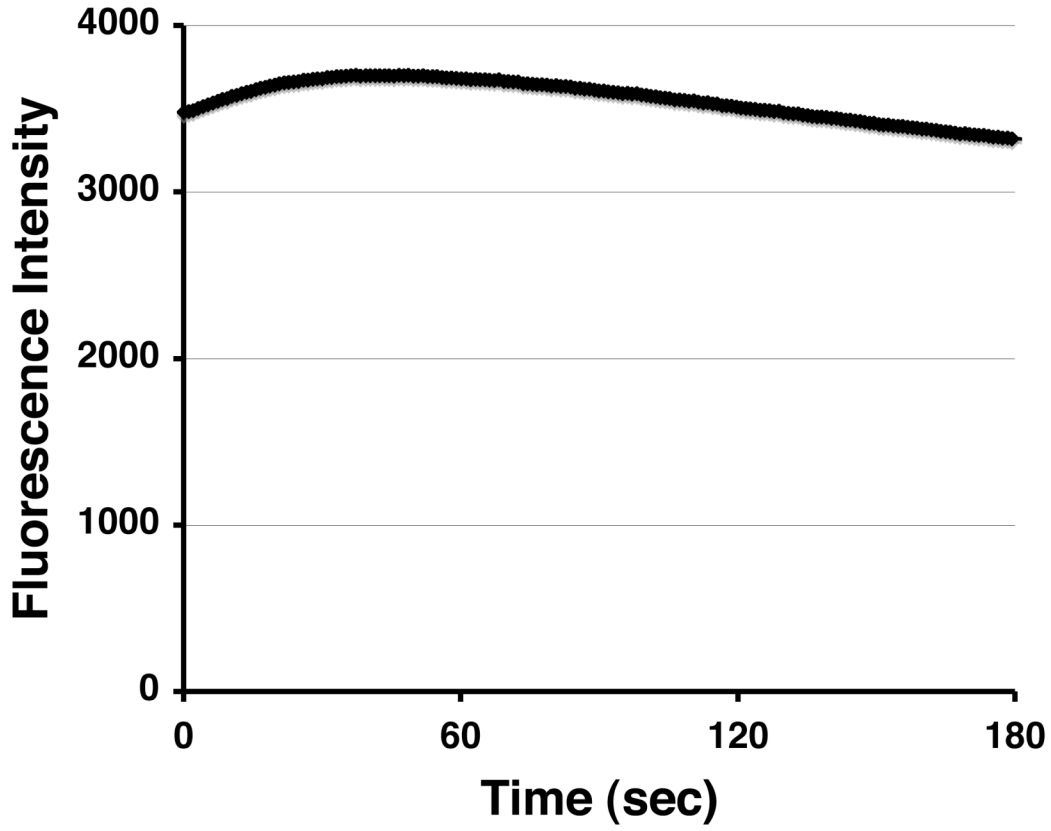

Figure 4.11 – mOrange2-synaptophysin exhibits high photostability. Images were acquired every second, with a 500ms exposure, no neutral density filters and xenon lamp.

References

1. Betz, W. J. & Bewick, G. S. Optical analysis of synaptic vesicle recycling at the frog neuromuscular junction. *Science* **255**, 200-203 (1992).

2. Ryan, T. A. et al. The kinetics of synaptic vesicle recycling measured at single presynaptic boutons. *Neuron* **11**, 713-724 (1993).

3. Miesenbock, G., De Angelis, D. A. & Rothman, J. E. Visualizing secretion and synaptic transmission with pH-sensitive green fluorescent proteins. *Nature* **394**, 192-195 (1998).

4. Sankaranarayanan, S., De Angelis, D., Rothman, J. E. & Ryan, T. A. The use of pHluorins for optical measurements of presynaptic activity. *Biophys J* **79**, 2199-2208 (2000).

5. Ng, M. et al. Transmission of olfactory information between three populations of neurons in the antennal lobe of the fly. *Neuron* **36**, 463-474 (2002).

6. Li, Z. et al. Synaptic vesicle recycling studied in transgenic mice expressing synaptopHluorin. *Proc Natl Acad Sci U S A* **102**, 6131-6136 (2005).

7. Darcy, K. J., Staras, K., Collinson, L. M. & Goda, Y. Constitutive sharing of recycling synaptic vesicles between presynaptic boutons. *Nat Neurosci* **9**, 315-321 (2006).

8. Araque, A., Parpura, V., Sanzgiri, R. P. & Haydon, P. G. Tripartite synapses: glia, the unacknowledged partner. *Trends Neurosci* **22**, 208-215 (1999).

9. Bezzi, P. et al. Astrocytes contain a vesicular compartment that is competent for regulated exocytosis of glutamate. *Nat Neurosci* **7**, 613-620 (2004).

10. Jourdain, P. et al. Glutamate exocytosis from astrocytes controls synaptic strength. *Nat Neurosci* **10**, 331-339 (2007).

11. Perea, G. & Araque, A. Astrocytes potentiate transmitter release at single hippocampal synapses. *Science* **317**, 1083-1086 (2007).

12. Gandhi, S. P. & Stevens, C. F. Three modes of synaptic vesicular recycling revealed by single-vesicle imaging. *Nature* **423**, 607-613 (2003).

13. Campbell, R. E. et al. A monomeric red fluorescent protein. *Proc Natl Acad Sci U S A* 7877-7882 (2002).

14. Shaner, N. C. et al. Improved monomeric red, orange and yellow fluorescent proteins derived from Discosoma sp. red fluorescent protein. *Nat.Biotechnol.* 1567-1572 (2004).

15. Jahn, R. & Sudhof, T. C. Synaptic vesicles and exocytosis. *Annu Rev Neurosci* **17**, 219-246 (1994).

16. Shaner, N. C., Steinbach, P. A. & Tsien, R. Y. A guide to choosing fluorescent proteins. *Nat Methods* **2**, 905-909 (2005).

17. Takamori, S. et al. Molecular anatomy of a trafficking organelle. *Cell* **127**, 831-846 (2006).

18. Laue, T. M. & Stafford, W. F. I. I. I. Modern applications of analytical ultracentrifugation. *Annual Review of Biophysics and Biomolecular Structure* **28**, 75-100 (1999).

19. Baird, G. S., Zacharias, D. A. & Tsien, R. Y. Biochemistry, mutagenesis, and oligomerization of dsRed, a red fluorescent protein from coral. *Proc Natl Acad Sci U S A* **97**, 11984-11989 (2000).

20. Zoccarato, F., Cavallini, L. & Alexandre, A. The pH-sensitive dye acridine orange as a tool to monitor exocytosis/endocytosis in synaptosomes. *J Neurochem* **72**, 625-633 (1999).

21. Wolf, M. K. & Aronson, S. B. Growth fluorescence and metachromasy of cells cultured in the presence of acridine orange. *J Histochem Cytochem* **9**, 22-29 (1961).

22. Nadrigny, F. et al. Systematic colocalization errors between acridine orange and EGFP in astrocyte vesicular organelles. *Biophys J* **93**, 969-980 (2007).

23. Bredt, D. S. & Nicoll, R. A. AMPA receptor trafficking at excitatory synapses. *Neuron* **40**, 361-379 (2003).

24. Guan, J. S. et al. Interaction with vesicle luminal protachykinin regulates surface expression of delta-opioid receptors and opioid analgesia. *Cell* **122**, 619-631 (2005).

25. Nishimura, T. & Kaibuchi, K. Numb controls integrin endocytosis for directional cell migration with aPKC and PAR-3. *Dev Cell* **13**, 15-28 (2007).

26. Santolini, E. et al. Numb is an endocytic protein. *J Cell Biol* **151**, 1345-1352 (2000).

27. Liu, S. Q. & Cull-Candy, S. G. Synaptic activity at calcium-permeable AMPA receptors induces a switch in receptor subtype. *Nature* **405**, 454-458 (2000).

28. Kopec, C. D., Li, B., Wei, W., Boehm, J. & Malinow, R. Glutamate receptor exocytosis and spine enlargement during chemically induced long-term potentiation. *J Neurosci* **26**, 2000-2009 (2006).

Acknowledgements

The work performed in Chapter Four was primarily done by the dissertation author. Nathan Shaner performed all the mutagenesis on the fluorescent proteins and participated in troubleshooting discussions. Jian Xu and Yongling Zhu provided the green SypH and precursor cloning plasmids. Yongling participated in many of the functional imaging experiments and in numerous troubleshooting discussions. She also put forth the majority of the effort in preparing and maintaining the neuronal cultures.

Appendix One

List of Primers

Ref #	Primer Name	Nucleotide sequence
AH1	SphI-GltI-A	GGCCGGGCATGCATGCAATTACGTAAACCTGCC
AH2	SacI-GltI-B	GCCGAGCTCTTAGTTCAGTGCCTTGTCATTCGG
AH3	BamHI-GltI-A	CGGGATCCATGCAATTACGTAAACCTGCC
AH4	EcoRI-GltI-B	GGAATTCTTAGTTCAGTGCCTTGTCATTCGG
AH5	GltISt-A	CGTAAACCTGCCACAGCAATCC
AH6	GltISt-B	GGATTGCTGTGGCAGGTTTACG
AH7	GltIEnd-A	GAACCGAATGACAAGGCACTG
AH8	GltIEnd-B	CAGTGCCTTGTCATTCGGTTC
AH9	BamSphGluB-A	CGGGATCCTGCATGCatgtcgcacaaacgcatgttcac
AH10	EcoSacGluB-B	GGAATTCTGAGCTCAACTCGTCCAGGAAGGAGAGGTC
AH11	SphI-GltI-A2	GGCCGGGCATGCTTATGCAATTACGTAAACCTGCC
AH12	SacI-GltI-B2	GCCGAGCTCTTTGTTCAGTGCCTTGTCATTCGG
AH13	SphIGltI-AX	CGTGACCGCCGCCCGCATGCGTATGCAATTACGTAAACC
AH14	GltI-SacI-AX	GACAAGGCACTGAACAAAGAGCTCATGGTGAGC
AH15	BamHI-ECFP-A	GCGGATCCCATGGTGAGCAAGGGCGAGGAG
AH16	ECFP-SphI-B2	cggcatgccttgtacagctcgtccatgcc
AH17	SphI-GltIM-A	GAAGCATGCTCGGAGATGACGCCGCCCCGGCAGCGGG
AH18	SphGluBm2-A	CCGGGCATGCTCGGATGTGGTGATTCAAGCGGTGGCG
AH19	SacGluBm-B	GCCGAGCTCGCTTGCGTCGAGGAAGGAGAG
AH20	BamSphIGltIM-A	CGGGATCCTGGCATGCTCGGAGATGACGCCGCCCCGG
AH21	EcoSacGltIMX-B	GGAATTCTGAGCTCTTAGTTCAGTGCCTTGTCATTCGG
AH22	GltIM-R47K-A	GTGATTGTCGTCGGTCACAAGGAATCTTCAGTGCCTTTCTC
AH23	GltIM-R47K-B	GAGAAAGGCACTGAAGATTCCTTGTGACCGACGACAATCAC
AH24	GltIM-R47A-A	GTGATTGTCGTCGGTCACGCCGAATCTTCAGTGCCTTTCTC
AH25	GltIM-R47A-B	GAGAAAGGCACTGAAGATTCGGCGTGACCGACGACAATCAC
AH26	GltIM-R47E-A	GTGATTGTCGTCGGTCACGAGGAATCTTCAGTGCCTTTCTC
AH27	GltIM-R47E-B	GAGAAAGGCACTGAAGATTCCTCGTGACCGACGACAATCAC
AH28	GltIM-R47D-A	GTGATTGTCGTCGGTCACGATGAATCTTCAGTGCCTTTCTC
AH29	GltIM-R47D-B	GAGAAAGGCACTGAAGATTCATCGTGACCGACGACAATCAC
AH30	GltIM-E48R-A	GTGATTGTCGTCGGTCACCGTCGCTCTTCAGTGCCTTTCTC
AH31	GltIM-E48R-B	GAGAAAGGCACTGAAGAGCGACGGTGACCGACGACAATCAC
AH32	GltIM-E48K-A	GTGATTGTCGTCGGTCACCGTAAGTCTTCAGTGCCTTTCTC
AH33	GltIM-E48K-B	GAGAAAGGCACTGAAGACTTACGGTGACCGACGACAATCAC
AH34	GltIM-E48A-A	GTGATTGTCGTCGGTCACCGTGCCTCTTCAGTGCCTTTCTC
AH35	GltIM-E48A-B	GAGAAAGGCACTGAAGAGGCACGGTGACCGACGACAATCAC
AH36	GltIM-E48D-A	GTGATTGTCGTCGGTCACCGTGATTCTTCAGTGCCTTTCTC
AH37	GltIM-E48D-B	GAGAAAGGCACTGAAGAATCACGGTGACCGACGACAATCAC
AH38	GltIM-T93A-A	GTGGTTCTACCGCCAACAACGTCGAACGCC
AH39	GltIM-T93A-B	GGCGTTCGACGTTGTTGGCGGTAGAACCAC
AH40	GltIM-d8-B	GGAATTCTGAGCTCTTTGAACAGTGCTTTCATTTCG
AH41	GltIM-d17-B	GGAATTCTGAGCTCCAGTTCGAAATTCATGTTCAGG
AH42	GltIM-d23-B	GGAATTCTGAGCTCCAGGTTTTTCGGCGGAATTGG
AH43	GltIM-d31-B	GGAATTCTGAGCTCTTTGAACCACTTATCAAACCATTTTTC
AH44	EcoSacGltIM-B	GGAATTCTGAGCTCTTTGTTCAGTGCCTTGTCATTCGG
AH45	Bgl2BamHIECFP	AGCAGATCTGACGATAAGGATCCCATGGTG
AH46	CitrinePstI	TTTTCTGCAGCTTGTACAGCTCGTCCATGCC
AH47	GltIm-SeqA	GATGACGCCGCCCCGGCAGC
AH48	GltIm-SeqB	GCTGCCGGGGCGGCGTCATC
AH49	BglII-EK-BamHI	GTCGAGATCTGGGTACGACGATGACGATAAGGATCC

AH50	BglII-loop-BamHI	GATCTGTACGACGATAGATCTGACGATAAGGATCC
AH51	TorAlead_Nde1_B	ggaattccatatgcgcagtcgcacgtcgcggc
AH52	StrpEcoRIYFP-B	GgaattcTTAGCCGCCAAACTGCGGATGACGCCACGCCTTGTACA GCTCGTCCATGCCGAG
AH53	SphXmaGltIm-A	AACATgcatgcccgggGATGACGCCGCCCCGGCAGCG
AH54	GltISac2PSacI-B	TATAATgagctcTTTGTTccgcggCTTGTCATTCGGTTCTTTGAA C
AH55	GltISac2SacI-B	TATAATgagctcTTTGTccgcggCCTTGTCATTCGGTTCTTTGAA C
AH56	GltI-A6G-A	GACGCCGCCCCGGgAGCGGGCAGTACTC
AH57	GltI-Sac2-A	GCACTGTTCAAAGAACCGcggGACAAGGCACTGAAC
AH58	TorA1	agatatacatatgaacaataacgatctctttcaggcatcacgtcg gcgttttctggcacaactcggcggcttaaccgtcgccgggatgc
AH59	TorA2	cttaaccgtcgccgggatgctggggccgtcattgttaacgccgcg acgtgcgactgcggcgcaagcggcggatcccatggtgagcaaggg
AH60	ECFPtrunk_B	ccatatgcatgcgggcggcggtcac
AH61	GLTIM_MID_A	CGTGGTCGGTACGCGCCTGTTG
AH62	GLTIM_MID_B	CTACGGCTTTGTCTTTCAGGTTGGC
AH63	GLTIM-T8-A	CGGGATCCTGGCATGCTCAGTACTCTGGACAAAATCGCC
AH64	GLTIM-T16-A	CGGGATCCTGGCATGCTCAACGGTGTGATTGTCGTCGGTC
AH65	NR1_1-A	gcacgcgcaagcatgaacagatg
AH66	NR1_2-B	gagccgtgtcgcttattggcc
AH67	NR1_3-A	cagccgcaatgctgaacatgac
AH68	NR1_4-A	tgatctgtacggggcctaatgac
AH69	NR1_5-A	tggtgtgggctggtttcgccatg
AH70	NR1_6-A	agatcgcctacaagcgacacaag
AH71	NR2aSt-A	tgaacattgcggtgctgctggg
AH72	NR2aSt-B	cagatttcgaagttcgcgttctg
AH73	NR2aEnd-A	taccatgtactctacccccagg
AH74	NR2aEnd-B	ctaggcattttcttgtacactcg
AH75	GluR6St-B	tggggccagattccacatattc
AH76	GluR6End-A	gcacacatttaacgacagaagg
AH77	EGFPSt-B	gtcgccgtccagctcgaccagg
AH78	XSac593	AGGTCTATATAAGCAGAACTCTCTGGCTAACTAGAG
AH79	XSac680	AGCTTGGTACCGAACTCGGATCCACTAGTAAC
AH80	XSph1281	AAGACAATAGCAGGCGTGCTGGGGATGCGG
AH81	XSph2897	TCGCCGTCGGGCTTGCTCGCCTTGAG
AH82	XSph3657-3729	GCTGACTAATTGAGATGCTTGCTTTGCATACTTCTGC
AH83	VenusXPstI207-A	CTGGGCTACGGCCTTCAGTGCTTCGCCCGC
AH84	VenusXPstI207-B	GCGGGCGAAGCACTGAAGGCCGTAGCCCAG
AH85	CitrineNS_EcoRI-B	ccggccGAATTCcttgtacagctcgtccatgcc
AH86	HindIII5UTRNR1-A	caagAAGCTTcttgcggccgccaccatggtg
AH87	SigNR1-BamHI-B	ttaattGGATCCgcgaaggagcaggaaaaaagc
AH88	EcoRI-NR1TM4	ccggaaGAATTCtttgagaacatggcaggggtc
AH89	cpFP_KpnI_A	ggaggtaccggtggatctatggtgagcaagggcgagg
AH90	cpFP_KpnI_B	ACCGGTACCTCCCTTGTACAGCTCGTCCATGCC
AH91	BamHI-SacI-Y145M	TAAGGATCCCGAGCTCATGAACAGCCACAACGTCTATATCAC
AH92	N144-PstI_EcoR_B	GGTTGAATTCCTGCAGGTTGTACTCCAGCTTGTGCCC
AH93	BamHI-SacI-Q157M	TAAGGATCCCGAGCTCATGAAGAACGGCATCAAGGCCTTC
AH94	K156-PstI_EcoR_B	GGTTGAATTCCTGCAGCTTGTCGGCGGTGATATAGAC
AH95	BamHI-SacI-D173M	TAAGGATCCCGAGCTCATGGGCGGCGTGCAGCTCGCC
AH96	E172-PstI_EcoR_B	GGTTGAATTCCTGCAGCTCGATGTTGTGGCGGATCTT
AH97	BamHI-SacI-L195M	TAAGGATCCCGAGCTCATGCCCGACAACCACTACCTGAG
AH98	L194-PstI_EcoR_B	GGTTGAATTCCTGCAGCAGCACGGGGCCGTCGCC
AH99	GltIM_T3-A	CGGGATCCTGGCATGCTCGCCCCGGCAGCGGGCAG
AH100	GltIM_T6-A	CGGGATCCTGGCATGCTCGCGGGCAGTACTCTGGAC

AH101	GltIM_T11-A	CGGGATCCTGGCATGCTCCTGGACAAAATCGCCAAAAACG
AH102	GltIM_d2-B	GGAATTCTGAGCTCTGCCTTGTCATTCGGTTCTTTG
AH103	GltIM_d5-B	GGAATTCTGAGCTCATTCGGTTCTTTGAACAGTGC
AH104	pDisplay_B	CTGCGTGTCCTGGCCCACAGC
AH105	BamNR14sigBgl-A	cgGGATCCatgagcaccatgcacctgctgacattcgccctgcttt tttcctgctccttcgccAGATCTaacc
AH106	BamNR14sigBgl-B	ggttAGATCTggcgaaggagcaggaaaaaagcagggcgaatgtca gcaggtgcatggtgctcatGGATCCcg
AH107	PstI-NR14TM4-A	caagCTGCAGgttcggtatcaggaatgcgac
AH108	PstIXNRTM4-B	gatggtactgCTCCAGgttcttcctccacacg
AH109	PstIXNRTM4-A	gaagaacCTGGAGcagtaccatcccactg
AH110	NotI-NR14TM4-B	aagaaGCGGCCGCtcacaccacggtgctgaccg
AH111	BamHI-BglII-Y145M	TAAGGATCCCAGATCTATGAACAGCCACAACGTCTATATCAC
AH112	N144-SphI_EcoR_B	GGTTGAATTCGCATGCCGTTGTACTCCAGCTTGTGCCC
AH113	BamHI-BglII-Q157M	TAAGGATCCCAGATCTATGAAGAACGGCATCAAGGCCTTC
AH114	K156-SphI_EcoR_B	GGTTGAATTCGCATGCCCTTGTCGGCGGTGATATAGAC
AH115	BamHI-BglII-D173M	TAAGGATCCCAGATCTATGGGCGGCGTGCAGCTCGCC
AH116	E172-SphI_EcoR_B	GGTTGAATTCGCATGCCCTCGATGTTGTGGCGGATCTT
AH117	BamHI-BglII-L195M	TAAGGATCCCAGATCTATGCCCGACAACCACTACCTGAG
AH118	L194-SphI_EcoR_B	GGTTGAATTCGCATGCCCAGCACGGGGCCGTCGCC
AH119	SacI-ECFP-A	ACAAAGAGCTCatggtgagcaagggcgaggag
AH120	BamSigBglECFP-A	cgGGATCCatgagcaccatgcacctgctgacattcgccctgcttt tttcctgctccttcgccAGATGTatggtgagcaagggcgaggag
AH121	pDisplay_B2	CAACAGATGGCTGGCAACTAGAAGGC
AH122	BamSigBglECFPA2	cgGGATCCatgagcaccatgcacctgctgacattcgccctgcttt tttcctgctccttcgccAGATCTatggtgagcaagggcgaggag
AH123	GltIM_T7-A	CGGGATCCTGGCATGCTCGGCAGTACTCTGGACAAAATCG
AH124	GltIM_T9-A	CGGGATCCTGGCATGCTCACTCTGGACAAAATCGCCAAAAAC
AH125	GltIM-S73T-A	CTGATTCCGATTACATCACAAAACCGTATTCCACTG
AH126	GltIM-S73T-B	CAGTGGAATACGGTTTTGTGATGTAATCGGAATCAG
AH127	PdisPDZb1	GCGGCCGCCTAcaccacggtagacacagaACGTGGCTTCTTCTGC CAAAGCATG
AH128	PdisPDZb2	GCGGCCGCCTAcacatcagactcACGTGGCTTCTTCTGC CAAAGCATG
AH129	PdisPDZb3	GCGGCCGCCTAgactctggtggtACGTGGCTTCTTCTGC CAAAGCATG
AH130	PdisPDZb4	GCGGCCGCCTAcagggtggaagaACGTGGCTTCTTCTGC CAAAGCATG
AH131	PdisPDZb5	GCGGCCGCCTAcacgtagtactcACGTGGCTTCTTCTGC CAAAGCATG
AH132	AgeNotBam-A	accggtgggggcggccgca
AH133	AgeNotBam-B	gatctgcggccgcccccaccggt
AH134	PstSac2Asc-A	gGggcgcgccGccgcggga
AH135	PstSac2Asc-B	tcccgcggCggcgcgccCctgca
AH136	PdsPDZbNR14	atcttGCGGCCGCCTAcaccacggtgctgaccgagggatctgaga gACGTGGCTTCTTCTGCCAAAGCATG
AH137	PdsPDZbNR2A	atcttGCGGCCGCCTAaacatcagattcgatactaggcattttct tACGTGGCTTCTTCTGCCAAAGCATG
AH138	PdsPDZbNlgn1	atcttGCGGCCGCCTAtaccctggttgttgaatgtgaatgggggt gACGTGGCTTCTTCTGCCAAAGCATG
AH139	PdsPDZbMGR5	atcttGCGGCCGCCTAcaacgatgaagaactctgcgtgtaatctc tACGTGGCTTCTTCTGCCAAAGCATG
AH140	PdsPDZbNxn1	atcttGCGGCCGCCTAgacataatactccttatccttgttcttct tACGTGGCTTCTTCTGCCAAAGCATG
AH141	BamSigBglECFPA3	cgGGATCCatgagcaccatgcacctgctgacattcgccctgcttt tttcctgctccttcgccAGATCTatggtgagcaagggcgaggag

AH142	FPpHlourin_A	ctagccaccatggtgagcaagggcgaggagctg
AH143	FPpHlourin_B	tcgagctccaccggtcttgtacagctcgtccatgccgag
AH144	GltI+3_SacI_B	AAAATTgagctcGGTTCCTCCtttgttcagtgccttgtcattcgg
AH145	GltI+6_SacI_B	AAAATTgagctcAGATCCACCGGTTCCTCCtttgttcagtgccttgtcattcgg
AH146	OFP-EcoRV_B	taatGATATCagctccaacggttttcttaagctcgtccatgccg
AH147	EcoRV-OFP_A	attaGATATCctagccaccatggtgagcaagggcgaggag
AH148	Hind3-V2_A	ctgctgAAGCTTatgtcggctaccgctgccac
AH149	V2-ssgsKpn_B	ACCGGTACCTCCGCTCCCACCagtgctgaagtaaacgatgatg
AH150	OFP-EcoRI_B	ggccggGAATTCttacttaagctcgtccatgccgcc
AH151	OFP-BamHI_B	ggccggGGATCCgctgctctccttaagctcgtccatgccgcc
AH152	BglII-CFP_A	ataaAGATCTatggtgagcaagggcgaggag
AH153	CFPt-SphI_B	tccgaGCATGCgggcggcggtcacgaactc
AH154	CFPtp-SphI_B	tccgaGCATGCgaggggcggcggtcacgaactc
AH155	CFPtpp-SphI_B	tccgaGCATGCgaggaggggcggcggtcacgaactc
AH156	CFP-SphI_B	tccgaGCATGCgcttgtacagctcgtccatgcc
AH157	CFPt3p-SphI_B	tccgaGCATGCgaggaggtggggcggcggtcacgaactc
AH158	CFPt4p-SphI_B	tccgaGCATGCgaggaggtggtggggcggcggtcacgaactc
AH159	CFPt5p-SphI_B	tccgaGCATGCgaggaggtggtggaggggcggcggtcacgaactc
AH160	CFPt6p-SphI_B	tccgaGCATGCgaggaggtggtggaggtggggcggcggtcacgaactc
AH161	pCSC-SC_1456_A	CCAAGGAAGCTTTAGACAAGATAG
AH162	pCSC-SC_3052_A	agatcgcctggagacgccatcc
AH163	pCSC-SC_3210_B	CAGCATTGGTAGCTGCTGTGTTGC
AH164	mOFP-649_A	CAACGAGGACTACACCATCGTGG
AH165	mOFP-66_B	CCGTTCACGGAGCCCTCCATG
AH166	pSinRep5_A	AGCATAGTACATTTCATCTG
AH167	pSinRep5_B	TTCCTCGGAAGTACATCGAG
AH168	GltI_SphI_B	aaccaaGCATGCgTTTGTTCAGTGCCTTGTCATTCGG
AH169	CyPet-QC1	gaggagctgttcGGcgggAtCgtgcccatcctggtcgagctggaGggcgacgtaaac
AH170	CyPet-QC2	cacgacttcttcaagtccgTGatgcccgaaggctacgtccagg
AH171	CyPet-QC3	ggcccacttcaagGCccgccacaacatcACCgacggcagcgtgc
AH172	CyPet-QC4	catcggcgacggccccgtgAtCctgcccgacaaccactacctg
AH173	YPet-QC1	ggcaagctgaccctgaagctgCTGtgcaccaccggcaagctgc
AH174	YPet-QC2	ctacctgagctaccagtccgccctgTTcaaagaccccaacgag
AH175	YPet-QC3	gctggagttcCtgaccgccgccgggatcactGAGggcatgAacgagctgtac
AH176	YPet-PstI_B	TTTTCTGCAGcttgtacagctcgtTcatgcc
AH177	mSynApp_B	tcgagctccaccggtCTTGTACAGCTCGTCGATGCC
AH178	KpnI_mApp_A	ttaattGGTACCggtggatctATGGTGAGCAAGGGCGAGGAG
AH179	mApp-EcoRI_B	aattaaGAATTCTTACTTGTACAGCTCGTCGATGCC
AH180	SacI-YPet_A	ACAAAGAGCTCatgtctaaaggtgaagaattattc
AH181	YPet2-PstI_B	TTTTCTGCAGtttgtacaattcatTcataccC
AH182	BglII-CyPet_A	CCGGCCAGATCTatgtctaaaggtgaagaattattcggc
AH183	CyPet_SphI_B	TACTGAGCATGCgtttgtacaattcatccataccatg
AH184	CyPetT_Sph_B	TACTGAGCATGCgagcagcagtaacaaattcgagcaagac
AH185	AgeI-FP_A	aattaaACCGGTgtgagcaagggcgaggagctgttc
AH186	YFP-AgeI_B	agtcagACCGGTcttgtacagctcgtccatgccgag
AH187	SynCAM+Bgl_A	ggcactgatccccAGATCTacaggtgatggacag
AH188	SynCAM+Bgl_B	ctgtccatcacctgtAGATCTggggatcagtgcc
AH189	YFP-BglII_B	ttggttAGATCTcttgtacagctcgtccatgccgagagtg
AH190	pCS6NLGN-Bgl	gaatttactcatgagGtctcagtagaggaac
AH191	pCS6NLGN+Bgl	gtactctctcaaaagttgAGATCTgatgatgtagacccattgg
AH192	YFP-BglII_B2	ttggttAGATCTGCTACTGCCGCCGCTACTcttgtacagctcgtccatgccgag

AH193	AgeI-GSFR_A	AAGGAAagatctTATGCTGGGGCCCAGCCGGCC
AH194	YFP-AgeI_B2	agtcagACCGGTGCTACTGCCGCCGCTACTcttgtacagctcgtccatgccgag
AH195	SacI_YFP-5Nt_A	aattaaGAGCTCgaggagctgttcaccggggtgg
AH196	mSynApp_B2	tcgagctccaccactgcttccaccggtCTTGTACAGCTCGTCGATGCC
AH197	EcoRV-OFP_A2	attaGATATCctagccaccggaggtagtagcggaggtatggtgagcaagggcgaggag
AH198	PSD95-KpnIQC-A	gactcgGAATTGGGGGAggtaccAGCGGCGGAAGCGGCGGG
AH199	PSD95-KpnIQC-B	CCCGCCGCTTCCGCCGCTggtaccTCCCCCAATTCcgagtc
AH200	KpnI_ECFP_A	acacacggtaccAGCGGCGGAAGCGGCGGGatggtgagcaagggcgaggagctg
AH201	D3_B	ccagctccggggcactggagctcatg
AH202	D3_A	cgcatgcatgaccaactgacagaagagc
AH203	NotI_cpV_B	gtgtgtGCGGCCGCttactcgatgttgtggcggatcttg
AH204	Bgl2_GltIm_A	aaccaaAGATCTGATGACGCCGCCCCGGCAGCGG
AH205	GltI_Kpn_B	ttggttggtaccATTGTCGTAATAAGAGAAAGGCACTG
AH206	GltI81-AgeI_B	ttaattaccggtattgtcgtaataagagaaaggcactgaag
AH207	ECFP228_NheI_B	ttggttgctagcggcggcggtcacgaactccagc
AH208	ECFP232_NheI_B	ttggttgctagcgcgagtgatcccggcggcggtc
AH209	NheI_GltI82_A	aattaagctagccagcaaaaagtggtgggttactcgcaggattac
AH210	AgeI_ECFP	aattaaaccggtatggtgagcaagggcgaggagc
AH211	NotI_PCDNA3	AACCAAGCGGCCGCGACTCTAGATCATAATCAGCC
AH212	CitPDZbNR14	TTCCTTGAATTCCTACACCACGGTGCTGACCGAGGGATCTGAGAGCTCGATGTTGTGGCGGATCTTGAAG
AH213	CitPDZbNR2A	TTCCTTGAATTCCTAAACATCAGATTCGATACTAGGCATTTTCTTCTCGATGTTGTGGCGGATCTTGAAG
AH214	CitPDZbNlgn1	TTCCTTGAATTCCTATACCCTGGTTGTTGAATGTGAATGGGGGTGCTCGATGTTGTGGCGGATCTTGAAG
AH215	CitPDZbMGR5	TTCCTTGAATTCCTACAACGATGAAGAACTCTGCGTGTAATCTCTCTCGATGTTGTGGCGGATCTTGAAG
AH216	CitPDZbNxn1	TTCCTTGAATTCCTAGACATAATACTCCTTATCCTTGTTCTTCTTCTCGATGTTGTGGCGGATCTTGAAG
AH217	OFP-EcoRI_B2	ggccggGAATTCttacttgtacagctcgtccatgccgcc
AH218	OFP-EcoRV_B2	taatgatatcagctccaacggtcttgtacagctcgtccatgccgc
AH219	pDisplay_B2	CAACAGATGGCTGGCAACTAGAAG
AH220	GLTIM_MID_B2	CCGTGATCTTTGGCGCTGATG
AH221	SFO-Or2_A	ctagccaccatgggaagcaagggcgaggagaataac
AH222	SFO-Or2_B	tcgagctccaccggtcttgtacagctcgtccatgccgc
AH223	AgeI-Or2_A	aattaaACCGGTGGAAGCAAGGGCGAGGAGAATAACATGGCC
AH224	mOr2-AgeI_B	attttaACCGGTCTTGTACAGCTCGTCCATGCCGCC
AH225	Kpn_pHfp_A	ggaggtaccggtggatctatggtgAGTAAAGGAGAAGAACTTTTCACTGGAG
AH226	EcoRI_pHfp_B	ggccggGAATTCTTAACCGGTTTTGTATAGTTCATCCATG
AH227	tdTxPstI	gatcagcgtgccgtcctgaagggaggagtcctggg
AH228	mOr2xPstI	gatgaactcgccgtcctgaagggaggagtcctggg
AH229	XmaIpDisp_A	ctgtacaagCCCGGGgtcgacgaacaaaaactcatctcag
AH230	FPXmaIPDisp_B	gtcgacCCCGGGcttgtacagctcgtccatgcc
AH231	Gab_Y34A_A	CATCGAAGCAGCCgcCCCACCTTTCAAC
AH232	Gab_Y34A_B	GTTGAAAGGTGGGgcGGCTGCTTCGATG
AH233	Gab_G48A_A	CCAGGTCGTGGcCTTCGACAAGGAC
AH234	Gab_G48A_B	GTCCTTGTCGAAGgCCACGACCTGG
AH235	Gab_G52E_A	GCTTCGACAAGGAgATCGGCGACGC
AH236	Gab_G52E_B	GCGTCGCCGATcTCCTTGTCGAAGC
AH237	Gab_W72A_A	GGTCACCTCCGACgcGACGGCATCATTC
AH238	Gab_W72A_B	GAATGATGCCGTCgcGTCGGAGGTGACC

AH239	Gab_S90A_A	CTTCCTGATCTCCgCCCTGTCAATCACC
AH240	Gab_S90A_B	GGTGATTGACAGGGcGGAGATCAGGAAG
AH241	Gab_S92A_A	GATCTCCTCCCTGgCAATCACCGATGAG
AH242	Gab_S92A_B	CTCATCGGTGATTGcCAGGGAGGAGATC
AH243	Gab_T94A_A	CTCCCTGTCAATCgCCGATGAGCGCAAG
AH244	Gab_T94A_B	CTTGCGCTCATCGGcGATTGACAGGGAG
AH245	Gab_Q138E_A	CATCGGCGCCgAGCGGGCTACC
AH246	Gab_Q138E_B	GGTAGCCCGCTcGGCGCCGATG
AH247	Gab_Q138A_A	CATCGGCGCCgcGCGGGCTACC
AH248	Gab_Q138A_B	GGTAGCCCGCgcGGCGCCGATG
AH249	Gab_T141A_A	CCAGCGGGCTgCCCTGGCCGG
AH250	Gab_T141A_B	CCGGCCAGGGcAGCCCGCTGG
AH251	Gab_L142A_A	GCGGGCTACCgcGGCCGGTACCTG
AH252	Gab_L142A_B	CAGGTACCGGCCgcGGTAGCCCGC
AH253	Gab_V183I_A	GCCGACAAGTACGcCAACTACGAGTGGC
AH254	Gab_V183I_B	GCCACTCGTAGTTGgCGTACTTGTCGGC
AH255	pDisplay_B2	CAACAGATGGCTGGCAACTAGAAGGC
AH256	SacI-FP-A	acaaaGAGCTCatggtgagcaagggcgaggag
AH257	EBFP-S30R-R	ggcatcgccctcgccctcgccCCTcacgctgaacttgtggccgtt tac
AH258	EBFP-Y39N-F	GGCGAGGGCGATGCCACCAACGGCAAGCTGACCCTGAAGTTC
AH259	GabGlt_B	cggcggaattggatttttGAAGTACTTGTCGTTGATCTTC
AH260	GabGlt_A	aaaaatccaattccgccg
AH261	Glt261_A	TGAAGCGGAAAAATGGTTTG
AH262	GabGlu261_B	CAAACCATTTTTCCGCTTCACCGGAGGTCTGCACC
AH263	Glt243_A	GATCCGCAGTTCAAAAAGC
AH264	GabGlu243_B	GCTTTTTGAACTGCGGATCATCTTTACGCAACATACAACCG
AH265	GltGab126-133_A	TTCTCTGACACTATTTTCGTGGTCaagctCcagttcatcgc
AH266	GltGab126-133_B	GACCACGAAAATAGTGTCAGAGAAgtccacGgcctgc
AH267	GabGlt36_A	GAGACCCTGAAGATGGGCATCGAAGCAGCCTACCCAccTttcaac aacaaggacg
AH268	GabGlt72_B	ccagtcggaCGGAATCAGTTTTACCTGC
AH269	GabGlt72_A	GATTCCGtccgactggCAAAACCGTATTCCACTGC
AH270	GabGlt94_B	ggtgatTgacagAGAACCACATTCAAAATCGAAAG
AH271	GabGlt94_A	GGTTCTctgtcAatcaccGTCGAACGCCAAAAACAG
AH272	GabGlt120_B	cagggtAgcccgctgGgcGACTACGGCTTTGTCTTTC
AH273	GabGlt120_A	gcCcagcgggcTaccctgTCTGAAGTTTTGCTCAACAAAC
AH274	GabGlt166_B	gttgacgtaCATAAAGGCAACGGCACG
AH275	GabGlt166_A	GTTGCCTTTATGtacgtcaacGCTCTGCTGGCCG
AH276	Glt142_FP_B	ctcgcccttgctcaccatACCCTTTTTGGTCAACAGG
AH277	Glt143_FP_A	gccgccgggatcactGGCGATATCAAAGATTTTGCC
AH278	Glt149_FP_B	ctcgcccttgctcaccatGGCAAAATCTTTGATATCGCC
AH279	Glt150_FP_A	gccgccgggatcactAACCTGAAAGACAAAGCCG
AH280	Glt177_FP_B	ctcgcccttgctcaccatCATTTTTTGCTCTTCATTCAGTTTG
AH281	Glt178_FP_A	gccgccgggatcactAATATGCGCATCATCAGCG
AH282	Glt196_FP_B	ctcgcccttgctcaccatGCTTTCCAGGGTGCG
AH283	Glt196_FP_A	gccgccgggatcactGGTCGTGCCGTTGC
AH284	Glt216_FP_B	ctcgcccttgctcaccatCGCTTTCGCACGTTCAC
AH285	Glt217_FP_A	gccgccgggatcactAAGAAACCAGACAACTGGG
AH286	Glt225_FP_B	ctcgcccttgctcaccatGACGATTTCCCAGTTGTCTG
AH287	Glt226_FP_A	gccgccgggatcactGGCAAGCCGCAGTC
AH288	Glt226_FP_B	ctcgcccttgctcaccatGCCGACGATTTCCCAG
AH289	Glt227_FP_A	gccgccgggatcactAAGCCGCAGTCTCAGG
AH290	Glt227_FP_B	ctcgcccttgctcaccatCTTGCCGACGATTTCCC
AH291	Glt228_FP_A	gccgccgggatcactCCGCAGTCTCAGGAGG
AH292	Glt228_FP_B	ctcgcccttgctcaccatCGGCTTGCCGACG

AH293	Glt229_FP_A	gccgccgggatcactCAGTCTCAGGAGGCCTAC
AH294	Glt229_FP_B	ctcgcccttgctcaccatCTGCGGCTTGCCGAC
AH295	Glt230_FP_A	gccgccgggatcactTCTCAGGAGGCCTACG
AH296	FP_A	atggtgagcaagggcgaggag
AH297	FP232_B	agtgatcccggcggcggt
AH298	Glt_S95T_A	GATTCCGATTACCaCACAAAACCGTATTCCAC
AH299	Glt_S95T_B	GTGGAATACGGTTTTGTGtGGTAATCGGAATC
AH300	GabGlu261_B	CAAACCATTTTTCCGCTTCgccgtcggccacg
AH301	GabGlu243_B	GCTTTTTGAACTGCGGATCtttcttgcgcacggc
AH302	BamHI_GltIm	aattaaggatccgGATGACGCCGCCCCG
AH303	Glt58_FP_B	ctcgcccttgctcaccatATTGTCGTAATAAGAGAAAGGCAC
AH304	Glt59_FP_A	gccgccgggatcactCAGCAAAAAGTGGTGGGTTAC
AH305	Gab37_FP_B	CTCGCCCTTGCTCACCATGAAAGGTGGGTAGGCTGCTTC
AH306	Gab38_FP_A	GCCGCCGGGATCACTAACAACAAGGACGCCAGCG
AH307	Gab43_FP_B	CTCGCCCTTGCTCACCATGCTGGCGTCCTTGTTGTTG
AH308	Gab44_FP_A	GCCGCCGGGATCACTGGCCAGGTCGTGGGC
AH309	Gab62_FP_B	CTCGCCCTTGCTCACCATTTTCATCTTGGCGCACAGGG
AH310	Gab63_FP_A	GCCGCCGGGATCACTGTCGAGTGCACCGTGGTC
AH311	Gab81_FP_B	CTCGCCCTTGCTCACCATGGCGTTCAGGGCCGG
AH312	Gab82_FP_A	GCCGCCGGGATCACTAAGAAGTTCGACTTCCTGATCTCC
AH313	Gab120_FP_B	CTCGCCCTTGCTCACCATCTTGGCCTTGGGGGCGATG
AH314	Gab121_FP_A	GCCGCCGGGATCACTACCGACTTCAAGACCGACAAGG
AH315	Gab128_FP_B	CTCGCCCTTGCTCACCATGGCCTTGTCGGTCTTGAAGTC
AH316	Gab129_FP_A	GCCGCCGGGATCACTTCACTCAAGGGCAAGATCATCGG
AH317	Gab156_FP_B	CTCGCCCTTGCTCACCATGGTGATGTCGTCGCCCAG
AH318	Gab157_FP_A	GCCGCCGGGATCACTATCAAGCTCTACGACACCCAG
AH319	Gab164_FP_B	CTCGCCCTTGCTCACCATTTCCTGGGTGTCGTAGAGCTTG
AH320	Gab165_FP_A	GCCGCCGGGATCACTAACGCTTACCTGGACCTGAC
AH321	Gab206_FP_B	CTCGCCCTTGCTCACCATTTCCACCATTGGCTCGCC
AH322	Gab207_FP_A	GCCGCCGGGATCACTAGCGACAAGATCGGGATTGC
AH323	Gab217_FP_B	CTCGCCCTTGCTCACCATTTTCTTGCGCACGGCAATC
AH324	Gab218_FP_A	GCCGCCGGGATCACTGATCCACTGCGCGAGAAGC
AH325	Gab235_FP_B	CTCGCCCTTGCTCACCATGCCGTCGGCCACGATTTC
AH326	Gab236_FP_A	GCCGCCGGGATCACTACCTACAAGAAGATCAACGACAAG
AH327	Gab175_FP_B	CTCGCCCTTGCTCACCATCAGGCGGCCGGAGG
AH328	Gab176_FP_A	GCCGCCGGGATCACTGACGCCATCCTGGCCG
AH329	Gab195_FP_B	CTCGCCCTTGCTCACCATCTTGCCGGCGTCGCTC
AH330	Gab196_FP_A	GCCGCCGGGATCACTCCTTATGAGTTCAAGGGCGAGC
AH331	pDispETQV_B	ttaattGCGGCCGCCTAcacctgtgtttcACGTGGCTTCTTCTGCC
AH332	pDispVSNL_B	ttaattGCGGCCGCCTAcagattagacacACGTGGCTTCTTCTGCC
AH333	Bgl2_Gab_A	aattaaAGATCTgagaccctgaagatgggcatcg
AH334	Gab_SacI_B	ttaattGAGCTCatagatgctgaacgggaagtacttgtc

GluSnFR Linker Optimization Screen Primers

Ref #	**Sequence**
Glt0	aattaaGCATGCtcGATGACGCCGCCCCGGC
Glt1	aattaaGCATGCtcGACGCCGCCCCGGCAGC
Glt2	aattaaGCATGCtcGCCGCCCCGGCAGCGGG
Glt3	aattaaGCATGCtcGCCCCGGCAGCGGGCAG
Glt4	aattaaGCATGCtcCCGGCAGCGGGCAGTACTCTG
Glt5	aattaaGCATGCtcGCAGCGGGCAGTACTCTGGACAAAATC
Glt6	aattaaGCATGCtcGCGGGCAGTACTCTGGACAAAATCGC
Glt7	aattaaGCATGCtcGGCAGTACTCTGGACAAAATCGCCAAAAACG
Glt8	aattaaGCATGCtcAGTACTCTGGACAAAATCGCCAAAAACGGTG

Glt9	aattaaGCATGCtcACTCTGGACAAAATCGCCAAAAACGGTGTG
Glt10	aattaaGCATGCtcCTGGACAAAATCGCCAAAAACGGTGTGATTGTC
Glt11	aattaaGCATGCtcGACAAAATCGCCAAAAACGGTGTGATTGTCGTC
Glt12	aattaaGCATGCtcAAAATCGCCAAAAACGGTGTGATTGTCGTCG
Glt13	aattaaGCATGCtcATCGCCAAAAACGGTGTGATTGTCGTCG
Glt14	aattaaGCATGCtcGCCAAAAACGGTGTGATTGTCGTCGGTC
Glt15	aattaaGCATGCtcAAAAACGGTGTGATTGTCGTCGGTCACC
GltA	ttaattGAGCTCTTTGTTCAGTGCCTTGTCATTCGGTTCTTTGAACAG
GltB	ttaattGAGCTCGTTCAGTGCCTTGTCATTCGGTTCTTTGAACAG
GltC	ttaattGAGCTCCAGTGCCTTGTCATTCGGTTCTTTGAACAGTGC
GltD	ttaattGAGCTCTGCCTTGTCATTCGGTTCTTTGAACAGTGC
GltE	ttaattGAGCTCCTTGTCATTCGGTTCTTTGAACAGTGCTTTCATTTCG
GltF	ttaattGAGCTCGTCATTCGGTTCTTTGAACAGTGCTTTCATTTCGTC
GltG	ttaattGAGCTCATTCGGTTCTTTGAACAGTGCTTTCATTTCGTCTG
GltH	ttaattGAGCTCCGGTTCTTTGAACAGTGCTTTCATTTCGTCTGAC
GltI	ttaattGAGCTCTTCTTTGAACAGTGCTTTCATTTCGTCTGACAGTTCG
GltJ	ttaattGAGCTCTTTGAACAGTGCTTTCATTTCGTCTGACAGTTCG
GltK	ttaattGAGCTCGAACAGTGCTTTCATTTCGTCTGACAGTTCGAAATTC
GltL	ttaattGAGCTCCAGTGCTTTCATTTCGTCTGACAGTTCGAAATTCATG

GABASnFR linker optimization screen primers

Gab+2	aattaaGCATGCtcGCCGCCGAGACCCTGAAGATGG
Gab+1	aattaaGCATGCtcGCCGAGACCCTGAAGATGGGCATC
Gab0	aattaaGCATGCtcGAGACCCTGAAGATGGGCATCGAAGC
Gab1	aattaaGCATGCtcACCCTGAAGATGGGCATCGAAGCAG
Gab2	aattaaGCATGCtcCTGAAGATGGGCATCGAAGCAGCCTAC
Gab3	aattaaGCATGCtcAAGATGGGCATCGAAGCAGCCTACC
Gab4	aattaaGCATGCtcATGGGCATCGAAGCAGCCTACCC
Gab5	aattaaGCATGCtcGGCATCGAAGCAGCCTACCCACC
Gab6	aattaaGCATGCtcATCGAAGCAGCCTACCCACCtTTCAAC
Gab7	aattaaGCATGCtcGAAGCAGCCTACCCACCtTTCAACAACAAG
Gab8	aattaaGCATGCtcGCAGCCTACCCACCtTTCAACAACAAGG
Gab9	aattaaGCATGCtcGCCTACCCACCtTTCAACAACAAGGACG
Gab10	aattaaGCATGCtcTACCCACCtTTCAACAACAAGGACGCC
Gab11	aattaaGCATGCtcCCACCtTTCAACAACAAGGACGCCAGC
Gab12	aattaaGCATGCtcCCtTTCAACAACAAGGACGCCAGCGG
Gab13	aattaaGCATGCtcTTCAACAACAAGGACGCCAGCGGC
GabA	ttaattGAGCTCgccATAGATGCTGAAgGGGAAGTACTTGTCGTTGATC
GabB	ttaattGAGCTCATAGATGCTGAAgGGGAAGTACTTGTCGTTGATC
GabC	ttaattGAGCTCGATGCTGAAgGGGAAGTACTTGTCGTTGATCTTC
GabD	ttaattGAGCTCGCTGAAgGGGAAGTACTTGTCGTTGATCTTCTTG
GabE	ttaattGAGCTCGAAgGGGAAGTACTTGTCGTTGATCTTCTTGTAGG
GabF	ttaattGAGCTCgGGGAAGTACTTGTCGTTGATCTTCTTGTAGGTG
GabG	ttaattGAGCTCGAAGTACTTGTCGTTGATCTTCTTGTAGGTGCCG
GabH	ttaattGAGCTCGTACTTGTCGTTGATCTTCTTGTAGGTGCCGTC
GabI	ttaattGAGCTCCTTGTCGTTGATCTTCTTGTAGGTGCCGTCG
GabJ	ttaattGAGCTCGTCGTTGATCTTCTTGTAGGTGCCGTCGG
GabK	ttaattGAGCTCGTTGATCTTCTTGTAGGTGCCGTCGGC
GabL	ttaattGAGCTCGATCTTCTTGTAGGTGCCGTCGGCC
Gab_Mid_A	AAGTTCGACTTCCTGATCTCCTC
Gab_Mid_B	CGTAGAGCTTGATGGTGATGTCG